

Characterization of Desmin Disease Mutants and their Association with α B-Crystallin in Desminopathy

Sarika Sharma

Doctoral Thesis

German Cancer Research Centre, University Hospital of Heidelberg

Dissertation

submitted to the
Combined Faculties for the Natural Sciences
and for Mathematics
of the Ruperto-Carola University of Heidelberg, Germany
for the degree of
Doctor of Natural Sciences

Presented by: Sarika Sharma, MSc Biotechnology

Born in: Patna, India

Oral-examination: October 2010

Characterization of Desmin Disease Mutants and their Association with α B-Crystallin in Desminopathy

Referees: Prof. Dr. Harald Herrmann-Lerdon
PD Dr. Karsten Rippe

Acknowledgments

To Tatjana, Dr. Norbert Mücke, Michaela and Dr. Karsten Richter, for readily sharing their technical expertise and immensely helping me in the field of protein biochemical methods, analytical ultracentrifugation analyses, cell culture and microscopy techniques, respectively.

To past and present B065 colleagues (Doro, Michaela, Thorsten, Helga, Julia, Tatjana, Tanja, Ulrike, Pavle, Moni Z., Stephi, Moni M., Katharina, Petra, Bettina, Rolf), as well as to members of B060 and B140, for providing a congenial working atmosphere “on the same floor” that made lab-life “fun”.

To Pavle and Dr. Gloria Conover, for taking out their “precious” time to go through my thesis, as well as for those fruitful discussions that lead to the generation of novel ideas.

To Prof. Roy Quinlan and his lab-members, for cooperating closely on the “desmin- α B-crystallin” project, as well as for their generous supply of the α B-crystallin protein.

To Prof. Rüdiger Hell, Prof. Peter Lichter and Dr. Karsten Rippe, for readily accepting to be my examiners.

To Prof. Harald Bär, for closely supervising my thesis through all these years, and for encouraging me to give talks at various conferences, and also for his genuine feedback on various manuscripts.

To Prof. Harald Herrmann, for readily accepting me as a doctoral student in his lab, for encouraging me to participate actively in meetings and seminars, and above all for his constant support such that I could finish my thesis in a “decent” time-frame.

To Jochen, Irene and Alfred, for all their kindness and compassion.

Abstract

Mutations in intermediate filaments (IFs) and associated proteins have been shown to cause a number of diseases in humans, ranging from blistering skin diseases to premature aging, as well as from cataract to cardiomyopathies. Desminopathy, a disease caused by dysfunctional mutations in type III muscle-specific IF protein desmin, constitutes a distinct sub-group of myofibrillar myopathies (MFM) manifesting as skeletal and / or cardiac myopathy. Mutations in the chaperone α B-crystallin, that supposedly maintains cytoskeletal integrity, have also been identified to cause MFM. Intracytoplasmic aggregates in desminopathy uniformly comprise aberrantly folded desmin that, among other proteins, recruits α B-crystallin. Currently, the molecular basis of sequential events that lead to such aggregates in the myocyte of patients harboring desmin mutations is not well understood. Thus, to unravel the molecular basis of desminopathy, we have investigated the interdependence between filament alterations arising from desmin mutations and their functional consequences in terms of interaction with the small heat shock protein α B-crystallin.

We have systematically characterized various mutants spanning the non- α -helical amino-terminal “head”, central α -helical “rod” and non- α -helical carboxy-terminal “tail” domain of desmin. We show by *in vitro* characterization of the five head mutants, that two mutant variants residing in the conserved nonapeptide motif “SSYRRTFGG” of desmin - DesS13F and DesR16C - interfere with assembly by forming filamentous aggregates. Consistent with *in vitro* data, both mutants fail to generate a *bona fide* filament system in cells lacking a type III IF cytoskeleton. In cells expressing vimentin or desmin, both mutants fail to integrate into the endogenous filament network and severely affect its cellular localization. The novel desminopathy-causing mutant DesL377 Δ 22fs apparently interacts with wild-type desmin at dimer, tetramer and higher level of filament organization *in vitro*, but leads to a disruption of the IF cytoskeleton in cells. This mutant is not detectable in the myotubes of a heterozygous carrier even upon proteasome inhibition. Two – DesR454W and DesK449T - out of the six tail mutants form abnormal filaments during *in vitro* assembly and correspondingly generate aberrant filaments in cells devoid of type III IF protein cytoskeleton. The desmin fragment Des(ESA) Δ C244, resembling almost “first-half” of a desmin molecule, has deleterious effects on filament assembly *in vitro* as well as in transfected cells. It exhibits nucleoplasmic aggregates in two of the four investigated cell lines.

With respect to characterizing the association of desmin disease mutants with α B-crystallin, data from yeast two-hybrid analyses, electron microscopy (EM), cosedimentation assay and viscometry distinctly suggest that the tail domain of desmin is pivotal in modulating its binding to α B-crystallin. We show that α B-crystallin binds to wild-type desmin filament under optimized buffer condition, but its binding to C-terminal deletion variants is either diminished or abolished. We speculate that this occurs due to differences in hydrophobic surface properties and exposed residues of wild-type desmin and its deletion variants. Des Δ RDG is devoid of the conserved

tripeptide motif “RDG”, yet it binds to α B-crystallin with similar strength as desmin wild-type. Thus, we propose that the prerequisite for binding of α B-crystallin to desmin is the 3-dimensional desmin protein conformation, which can be altered due to a mutation, and not the linear amino acid sequence involving conserved motifs *per se*. The two tail mutants – DesI451M and DesR454W - reveal weaker and stronger binding, respectively, to α B-crystallin as compared to wild-type protein. With respect to kinetics of binding, unlike desmin wild-type, DesR454W binds to α B-crystallin at all stages of assembly, and this probably results from its “open” filament structure both alone and in an equimolar mixture with wild-type desmin. Data from R454W and wild-type desmin transfection in 3T3 cells corroborate the *in vitro* data, showing that DesR454W binds ~50% more cytosolic α B-crystallin than desmin wild-type. Hence, our data suggest that mutations in desmin cause toxic gain-of-function, whereby the desmin mutants show enhanced binding to α B-crystallin. A plausible explanation for aggregate formation in desminopathy could be such modified protein-protein interactions.

In summary, our data demonstrate the impact of desmin mutations not only on its structural property, but also on its molecular interaction with α B-crystallin. This adds to our understanding of the molecular basis of desminopathy as we show for the first time that subtle alterations in the nanoarchitecture of desmin filament are sufficient to induce aberrant interaction with an associated protein α B-crystallin. Such a modification might eventually contribute to the pathogenesis of desminopathy.

Keywords: cytoskeleton, intermediate filament, desmin, mutations, myofibrillar myopathy, desminopathy, small heat shock protein, α B-crystallin, assembly, electron microscopy, transfection, cosedimentation, viscometry.

Zusammenfassung

Mutationen von Intermediärfilamenten und den mit ihnen assoziierten Proteinen können beim Menschen eine Reihe von Krankheiten verursachen, deren Spektrum von bullösen Hauterkrankungen über vorzeitiges Altern und Katarakt bis zu Kardionmyopathien reicht. Die Desminopathie, eine Krankheit, die durch dysfunktionale Mutationen im muskelspezifischen Typ-III-Intermediärfilamentprotein Desmin verursacht wird, ist die Ursache für eine spezifischen Untergruppe von myofibrillären Myopathien (MFM), die sich als skelettmuskuläre oder als kardiale Myopathien manifestieren. Mutationen in dem Chaperon α B-Crystallin, das vermutlich zur zytoskelettalen Integrität beiträgt, wurden ebenfalls als Ursache für MFM erkannt. Intrazytoplasmatische Aggregate, die bei der Desminopathie auftreten, bestehen einheitlich aus irregulär gefaltetem Desmin, an das sich neben anderen Proteinen auch α B-Crystallin anlagert. Zurzeit verstehen wir nicht die molekulare Grundlage der konsekutiven Ereignisse, die zur Bildung dieser Aggregate in den Myozyten von Patienten mit Desmin-Mutationen führen. Um die molekulare Grundlage der Desminopathie zu entschlüsseln, haben wir deshalb die gegenseitige Abhängigkeit von Filament-Veränderungen durch Desminmutationen und ihre funktionellen Folgen im Sinne der Interaktion mit dem kleinen Hitzeschockprotein α B-Crystallin untersucht.

Wir haben systematisch eine Reihe von Desminmutanten charakterisiert, die Veränderungen verteilt über die ganzen Länge des Desminmoleküls aufwiesen: von der nicht- α -helikalen, amino-terminalen Kopfdomäne über die zentrale, α -helikale und Stabdomäne bis hin zur nicht- α -helikalen, carboxy-terminalen Schwanzdomäne. Wir zeigten durch *in vitro* Charakterisierung der fünf Kopfmутanten, dass zwei Varianten (DesS13F und DesR16C), die in dem konservierten Nonapeptid-Motiv „SSYRRTFGG“ des Desmins liegen, den Filamentaufbau durch das Bilden von Aggregaten stören. Übereinstimmend mit den *in vitro* – Daten schaffen es beide Mutanten nicht, in Zellen ohne ein Typ-III IF-Zytoskelett ein echtes Filamentsystem zu erzeugen. In Zellen, die ein Desmin- oder Vimentinzytoskelett exprimieren, schaffen es beide Mutanten nicht, sich in das Zytoskelett zu integrieren und beeinträchtigen seine zelluläre Lokalisation wesentlich. Der neue, Desminopathie-verursachende Mutant DesL377 Δ 22fs interagiert mit Wildtyp-Desmin auf Dimer-, Tetramer- und höheren Ebenen der Filamentbildung *in vitro*, aber er zerreißt das IF-Zytoskelett in Zellen. Dieser Mutant ist in den Myotuben eines heterozygoten Trägers selbst beim Einsatz von Proteasom-inhibitoren nicht nachweisbar. Zwei von sechs Schwanzmutanten - DesR454W und DesK449T – bilden anormale Filamente bei *in vitro* – Filamentaufbau und erzeugen dementsprechend in Zellen, die kein Typ-III IF-Protein-Zytoskelett aufweisen, irreguläre Filamente. Das Desminfragment Des(ESA) Δ C244, das an die „erste Hälfte“ eines Desminmoleküls erinnert, hat zerstörerische Effekte auf den Filamentaufbau sowohl *in vitro* als auch in transfizierten Zellen, bei denen zwei der vier untersuchten Zelllinien Kern-Zytoplasma-Aggregate aufwiesen.

Bezüglich der Beziehung zwischen Desminmutanten und α B-Crystallin weisen Daten aus Hefe-Zwei-Hybrid-Analysen, Elektronenmikroskopie (EM), Kosedimentationsuntersuchung und Viskometrie deutlich darauf hin, dass die Schwanzdomäne des Desmins entscheidend für die Modulation seiner Bindung an α B-Crystallin ist. Wir konnten demonstrieren, dass sich α B-Crystallin an Wildtyp-Desminfilamente unter optimierten Pufferbedingungen bindet, aber seine Bindung an C-terminale Deletionsvarianten ist entweder vermindert oder aufgehoben. Wir vermuten, dass das an den Unterschieden in den hydrophoben Oberflächeneigenschaften des Wildtyp-Desmins und seiner Deletionsvarianten liegt. Dem Des Δ RDG fehlt das konservierte Tripeptid-Motiv „RDG“. Trotzdem bindet es an α B-Crystallin mit einer ähnlichen Effizienz wie Wildtyp-Desmin. Deshalb folgern wir, dass die dreidimensionale Desminproteinkonformation, die durch Mutationen verändert werden kann, und nicht die lineare Aminosäuresequenz mit ihren konservierten Motiven an sich eine Voraussetzung für die Bindung von α B-Crystallin an Desmin ist. Zwei Schwanzmutanten – DesI451M und DesR454W – zeigen im Vergleich zum Wildtyp-Protein schwächere bzw. stärkere Bindung an α B-Crystallin. Bezüglich der Bindungskinetik bindet sich DesR454W, anderes als der Desmin Wildtyp, in allen Stadien des Filamentaufbaus an α B-Crystallin, was vermutlich an seiner „offenen“ Filamentstruktur sowohl alleine als auch in equimolarer Mischung mit Wildtyp-Desmin liegt. Zelluläre Daten aus R454W- und Wildtyp-Desmin-Transfektionen von 3T3-Zellen bestätigen die *in vitro* – Daten, indem sie zeigen, dass DesR454W ~50% mehr zytosolisches α B-Crystallin bindet als der Desmin Wildtyp. Daher legen unsere Daten nahe, dass Desmin-Mutationen eine toxische Funktionsverstärkung verursachen, durch die die Desminmutanten eine verstärkte Bindung an α B-Crystallin aufweisen. Diese modifizierten Protein-Protein-Interaktionen können eine plausible Erklärung für die Aggregatbildung in Desminopathien sein.

Zusammengefasst zeigen unsere Daten die Auswirkung von Mutationen des Desmins sowohl auf seine strukturellen Eigenschaften als auch auf seine molekularen Interaktionen mit α B-Crystallin. Das trägt zu unserem Verständnis der molekularen Mechanismen der Desminopathien bei, da wir zeigen konnten, dass subtile Veränderungen in der Nanostruktur des Desminfilaments ausreichen, um abweichende Interaktionen mit dem assoziierten Protein α B-Crystallin in der Zelle zu induzieren. Dies könnte zur Pathogenese der Desminopathie beitragen.

Schlüsselwörter: Zytoskelett, Intermediärfilament, Desmin, Mutationen, Myofibrilläre Myopathie, Desminopathie, kleine Hitzeschockproteine, α B-Crystallin, Filamentaufbau, Elektronenmikroskopie, Transfektion, Kosedimentation, Viskometrie.

My contributions to the field

PEER-REVIEWED PUBLICATIONS & MANUSCRIPTS

1. Bär H., Schopferer M., **Sharma S.**, Hochstein B., Mücke N., Herrmann H. & Willenbacher N. (2010) Mutations in desmin's carboxy-terminal "tail" domain severely modify filament and network mechanics. *J Mol Biol*, 397 (5): 1188-1198.
2. **Sharma S.**, Mücke N., Katus HA., Herrmann H. & Bär H. (2009) Disease mutations in the "head" domain of the extra-sarcomeric protein desmin distinctly alter its assembly and network-forming properties. *J Mol Med*, 87 (12): 1207-1219.
3. Bär H., **Sharma S.**, Kleiner H., Mücke N., Zentgraf H., Katus HA., Aebi U. & Herrmann H. (2009) Interference of amino-terminal desmin fragments with desmin filament formation. *Cell Motil Cytoskeleton*, 66 (11): 986-999.
4. Schopferer M., Bär H., Hochstein B., **Sharma S.**, Mücke N., Herrmann H. & Willenbacher N: Desmin and Vimentin Intermediate Filament Networks: Their Viscoelastic Properties Investigated by Mechanical Rheometry. *J Mol Biol*, 388 (1): 133-143.
5. Carmignac V., **Sharma S.**, Cuisset JM., Fischer., Maurage C., Serreri C., Serria M., Stoltenburg G., Leturcq F., Herrmann H., Arbogast S., Bär H. & Ferreira A. Lack of desmin in humans due to a homozygous DES deletion causes recessive Emery-Dreifuss myopathy with lethal cardio-myopathy (*Manuscript in preparation*).
6. **Sharma S.**, Mücke N., Perng MD., Herrmann H., Quinlan RA. & Bär H. Desminopathy mutations influence the interaction of desmin with α B-crystallin (*Manuscript in preparation*).

INVITED ORAL PRESENTATIONS

- Mar 2009** 19th Congress of German Society for Muscle Diseases, Darmstadt. *In vitro* and *in vivo* characterization of human desmin disease mutations.
- Sep 2007** 5th meeting of the intermediate filament network, Grey College, Durham. Influence of deletions and mutations in the head domain of desmin on assembly competence and network formation.

POSTER PRESENTATIONS

- Dec 2009** 49th Annual Meeting of American Society for Cell Biology, San Diego. Towards a molecular understanding of the association of desmin and nebulin (Co-author: Dr. GM Conover).
- Sep 2009** European Society of Cardiology, Barcelona. Molecular mechanism of desminopathy: Analyzing the interaction of desmin and its disease variants with α B-crystallin.
- Sep 2008** Gordon Research Conferences, Magdalen College, Oxford. Molecular mechanism of desminopathy: Analyzing the interaction of desmin with α B-crystallin.
- Oct 2007** Special Helmholtz workshop on Cell and Molecular Biology, Heidelberg. Influence of deletions and mutations in the head domain of desmin on assembly competence and network formation.
- Aug 2006** Gordon Research Conferences, Salve Regina University, Rhode Island. Characterization of desmin disease mutations with regard to assembly competence and network formation.

Contents

I Introduction

Intermediate Filaments	3
1.1 Three distinct filamentous networks in a cell	3
1.2 Cytoplasmic and nuclear IFs	3
1.2.1 Structure of IF proteins	3
1.2.2 Classes and assembly groups of IF proteins	5
1.2.3 In vitro assembly of IF proteins	6
1.3 Desmin and its role in myocyte architecture	7
1.4 Desminopathy as a subtype of myofibrillar myopathy	8
1.4.1 Current state of knowledge on desmin disease mutations	9
Small Heat Shock Proteins	11
2.1 General features of small heat shock proteins	11
2.2 Structure and assembly of sHsps	11
2.3 Chaperoning function of sHsps	12
2.4 Implications of sHsps in human diseases and therapy	13
2.5 α B-crystallin and its role in desmin related myopathy	13
Motivation, objectives & chronology of result presentation	15
3.1 Motivation	15
3.2 Objectives	15
3.3 Chronology of result presentation	16
Characterization of mutations in the head, rod and tail domain of desmin	19
4.1 Assembly and network-forming properties of desmin head mutants are modified to various extents	21
4.1.1 In vitro analyses of head domain desmin disease mutants	21
4.1.2 Filament formation behaviour of desmin head mutants in cells	30
4.2 A novel homozygous mutation L377 Δ 22fs leads to the total absence of desmin in humans	35
4.2.1 DesL377 Δ 22fs apparently interacts with wild-type desmin at dimeric and tetrameric stages in vitro	35
4.2.2 Analysis of DesL377 Δ 22fs alone and in equimolar mixture with wild-type desmin during in vitro assembly	37
4.2.3 Disrupted IF cytoskeleton is observed in cells expressing DesL377 Δ 22fs	38
4.2.4 Mutant protein DesL377 Δ 22fs is not detectable in myotubes of heterozygous mother even after inhibiting the proteasome	38

4.3	The truncated desmin variant Des(ESA) Δ C244 has deleterious effects on filament assembly	40
4.4	The majority of desmin tail mutants exhibit undisturbed filament morphology both in vitro and in cell lines	43
	Interaction of desmin with α B-crystallin	47
5.1	α B-crystallin is the major binding partner of desmin by yeast two-hybrid analysis	49
5.2	Oligomers of α B-crystallin sediment at 17 S as a complex comprising \sim 22 subunits	52
5.3	Binding properties of α B-crystallin to desmin under different buffer conditions	54
5.4	Binding of α B-crystallin to desmin is enhanced by lowering the pH and ionic strength of "Tris-NaCl" buffer system and on increasing the assembly temperature"	59
5.4.1	Effect of temperature on binding of α B-crystallin to desmin	61
5.5	The C-terminal domain of desmin modulates the binding of α B-crystallin to desmin filaments	62
5.6	Binding of α B-crystallin to desmin is influenced by the desmin filament architecture	66
5.7	Desminopathy mutations influence the interaction of desmin with α B-crystallin	70
	Discussion	77
6.1	Modification of desmin filament properties by mutations	78
6.1.1	Impact of disease mutations in the head domain of desmin on assembly and network-forming properties	78
6.1.2	DesL377 Δ 22fs and loss of desmin expression in humans	80
6.1.3	Desmin tail mutants and filament property	81
6.2	Desmin "crosstalks" with the small heat shock protein α B-crystallin	82
6.2.1	Interaction of desmin filaments with α B-crystallin	82
6.2.2	Domain of desmin modulating interaction with α B-crystallin	83
6.2.3	Evidence for binding of α B-crystallin to multiple desmin domains	84
6.2.4	Desminopathy mutants show altered interaction with α B-crystallin	85
6.2.5	Defining the mechanism of chaperone action of sHsps	87
	Conclusion and Outlook	89
	<i>In vitro</i> analyses	93
8.1	Cloning and mutagenesis	93
8.2	Inclusion body and protein purification	94
8.2.1	Inclusion body purification	94
8.2.2	Desmin protein purification with ion exchanger	95
8.3	Protein dialysis	96
8.4	Protein assembly for EM and viscometry	96
8.5	Cosedimentation assay and gel quantification	97
8.6	Analytical ultracentrifuge	98
8.7	Oxidative cross-linking	99
	Analyses in cells	101

9.1	Cell lines and cell culture	101
9.2	Transfection and staining	101
9.3	Microscopy and image processing	102
9.4	Proteasome-inhibition in myoblasts	102
	<i>Bibliography</i>	105
	<i>Appendix</i>	i
	<i>Supplementary</i>	vii

Part I
Introduction

Intermediate Filaments

1.1 Three distinct filamentous networks in a cell

Eukaryotic cytoskeleton represents an elaborate infrastructure formed by the integration of three distinct filamentous networks, a large group of associated proteins, and cross-bridging factors. The three interconnected network-forming systems are tubulin-based microtubules (MTs), intermediate filaments (IFs) and actin-based microfilaments (MFs; also known as F-actin). Whereas microtubules contribute predominantly to intracellular trafficking, actin microfilaments have evolved to play a major role in cell polarity, contraction and cell motility. On the other hand, IFs not only provide crucial structural support to the cytoplasm and nucleus of metazoan cells, but also participate as regulators of signalling pathways in a cell-type-specific manner [FUCHS & YANG 1999, HERRMANN & AEBI 2004, KIM & COULOMBE 2007].

1.2 Cytoplasmic and nuclear IFs

IFs derive their name from their average filament diameter of ~10-12 nm which is intermediate to the thin actin (~5-8 nm) and thick myosin filaments (~20-25 nm). Holtzer and colleagues discovered these intermediate structures in the late 1960s upon analysis of metaphase myocytes that stained negative for actin and myosin [ISHIKAWA et al. 1968]. The three distinct systems can be distinguished by electron microscopy (EM) or immunofluorescence microscopy in myogenic and other cultured cells [FRANKE et al. 1978]. In contrast to the evolutionarily highly conserved actins and tubulins, IF protein superfamily comprises members that occasionally share as little as 20% sequence identity [FUCHS & WEBER 1994]. This implies that different IFs have distinct physical and biochemical properties. Most metazoans exhibit two principally different yet parallel IF systems: (i) an extended cytoplasmic filament array coupled to plasma membrane-associated junctional complexes such as desmosomes and hemidesmosomes in epithelial cells, costameres in striated muscle, and intercalated discs in cardiac muscle. These IFs interconnect the plasma membrane to the nuclear envelope via linker as well as nuclear membrane proteins, such as plectin and nesprin-3 α . (ii) A membrane- and chromatin-bound meshwork-like lamina made of nuclear IF proteins, the lamins [WICHE 1998, GREEN et al. 2005, HERRMANN et al. 2007].

1.2.1 Structure of IF proteins

Members of the IF superfamily share some essential structural features despite their diverse amino acid sequences. IF proteins exhibit a tripartite structure: a central α -helical “rod” domain is flanked by a non- α -helical amino-terminal “head” and a carboxy-terminal “tail” domain [GEISLER et al. 1982]. The rod domain of cytoplasmic IF proteins is ~310 amino acids (aa) / ~45 nm in length. In case of lamins (nuclear IFs), the rod is 356 aa / ~53 nm long due to insertion of 42 aa in helical domain IB. The rod comprises

FIGURE 1 Molecular scheme of desmin and structural model for IF proteins

(a) Molecular scheme of IF protein desmin. Non- α -helical head and tail domains flank the central α -helical rod domain. The rod consists of pre-coil domain (PCD), coil 1A, coil 1B, coil 2A and coil 2B. Linker segments are indicated as L1, L12 and L2 [Adapted from SHARMA et al. 2009]. (b) Modeling of human vimentin and lamin A dimers also reveals four coil segments. Left-handed coiled-coil segments are shown in green. Regions that are predicted to form nearly parallel α -helical bundles as well as the so-called stutter (stu) region in the heptad repeat pattern are represented in yellow. Non- α -helical linkers L1, L12 and L2 are shown in grey. The non- α -helical head and tail domains are colored blue and red, respectively. Parts of the coiled coils of vimentin and lamin A have been solved by x-ray crystallography. The immunoglobulin fold domain in the tail of lamin A is depicted as red arrows. The values in brackets refer to the number of amino acids in respective domain. Scale bar: 5 nm. NLS, nuclear localization signal [Source: HERRMANN et al. 2007].

Both head and tail domains vary in size and amino acid composition from one IF type to another. Length variations are common in the tail, where predicted sizes range from 15 residues in keratin K19 to up to 1300 residues in nestin. In general, the head and tail domains appear to be poorly ordered structures on their own and these domains apparently get structured only upon formation of higher order oligomers [HERRMANN & AEBI 2004]. Posttranslational modifications are mostly found in the head and the tail domains [FUCHS & WEBER 1994]. Moreover, within the head domain, a nonapeptide motif “SSYRRXFGG” is evolutionarily highly conserved within IF proteins like desmin and vimentin that are able to form “co-polymers” [HERRMANN et al. 1992, SCHAFFELD et al. 2001]. IF proteins are difficult to crystallize due to their insolubility in buffers of physiological ionic strength and pH, lack of suitable assembly inhibitors as well as their assembly-prone character [STRELKOV et al. 2001]. Thus, there is as yet no “atomic-level” information for the structure of an entire IF dimer.

1.2.2 Classes and assembly groups of IF proteins

On basis of primary amino acid sequence identity within α -helical domain, IF proteins are classified into six groups (TABLE 1; [FUCHS & WEBER 1994]). The cytoskeletal IF proteins are grouped into four sequence homology classes (SHCs), also known as types I-IV. Keratins constitute the sole members of type I and type II classes. Sharing >70% sequence identity among themselves, vimentin, desmin, glial fibrillary acidic protein (GFAP) and peripherin are designated as type III. Low-, middle-, and high-MW neurofilament (NFL, NFM, NFH) proteins, α -internexin and syncoilin have been grouped separately as type IV, sharing ~50% sequence identity with their closest type III relative. In 1986, Ueli and coworkers unveiled a meshwork of 10 nm filaments beneath the nuclear envelope by EM and sequence analyses disclosed the relation of these nuclear lamins to the IF superfamily [AEBI et al. 1986]. Lamins constitute type V IF because their rod domain is structurally different from other four classes and all lamins possess a nuclear localization signal. Early vertebrate embryos possess only B-type lamins, whereas somatic cells additionally synthesize A-type lamins. The two distantly related beaded lens filament proteins filensin and phakinin, initially grouped as orphans, are categorized separately as type VI IF proteins. Remarkably, comparison of the gene structures of lamin- and cytoplasmic IF-encoding genes suggests that all IF proteins are derived from a lamin-like progenitor [DÖRING & STICK 1990].

Based on their abilities to copolymerize, the IF proteins are further subdivided into three assembly groups (TABLE 1; [HERRMANN & AEBI 2000]). Members of different assembly groups segregate into separate networks due to distinct domains within the α -helical segments of their IF polypeptides. Group 1 consists of acidic (type I) and basic (type II) cytokeratins which are obligate heteropolymers, i.e., at least one type I and one type II keratin are required to form heteropolymeric keratin IFs. Group 2 comprises muscle, mesenchymal or neuronal type III and type IV IF proteins. This group of IF proteins can form both homo- and heteropolymers. For example, vimentin can co-assemble with desmin, GFAP or peripherin (all type III), or with NFL-, NFM-, NFH-subunits as well as α -internexin (all type IV). Vimentin,

TABLE 1 Sequence homology classes, members, assembly groups and diseases of IF proteins

Sequence homology class: • Member (distribution)	Assembly group	Example of IF disease
SHC I and II: • Acidic keratins (epithelia, hair) • Neutral/basic keratins(epithelia, hair)	1	Epidermolysis bullosa simplex, epidermolytic hyperkeratosis, liver and hair disorders
SHC III: • Desmin (muscle) • Vimentin (mesenchyma) • GFAP (glial cells) • Peripherin (neurons)	2	• Desminopathy • Cataract • Alexander disease • Amyotrophic lateral sclerosis (ALS)
SHC IV: • NFL, NFM, NFH (neurons) • α -internexin (neurons) • Synemin (muscle) • Nestin (pluripotent cells)	2	• Charcot-Marie-Tooth disease, Parkinson, ALS • ? • ? • ?
SHC V: • A-type lamins (all metazoan cells) • B-type lamins (all metazoan cells)	3	• Hutchinson-Gilford progeria syndrome, Emery-Dreifuss muscular dystrophy • Acquired partial lipodystrophy
SHC VI: • Bfsp1 / filensin (eye lens) • Bfsp2 / phakinin / CP49 (eye lens)	?	• Autosomal dominant cataract • Autosomal recessive cataract

[Adapted from ERIKSSON et al. 2009, OMARY 2009]

for instance, is transiently co-expressed with desmin in myocytes during development and it has been experimentally shown to co-assemble with desmin at all stages of *in vitro* assembly [GRANGER & LAZARIDES 1980, WICKERT et al. 2005]. Group 3 comprises type V nuclear lamins that do not co-assemble with members of classes I to IV.

1.2.3 In vitro assembly of IF proteins

During assembly initiation, IF proteins do not bind to GTP or ATP like tubulin or actin, respectively WATERMAN-STORER & SALMON 1997, POLLARD & BORISY 2003]. Instead, they undergo self assembly under simple conditions without depending on cofactors. Additionally, unlike MTs and MFs, IFs are apolar structures as their tetramers are formed by two anti-parallel dimers. As mentioned earlier, three different assembly groups exist for IF proteins. As the biochemical properties of cytoplasmic and nuclear IFs vary considerably, these two groups also assemble into principally distinct filamentous structures. Unlike cytoplasmic IF proteins, nuclear lamins form dimers at high pH and salt conditions (pH 8-9, 150-300 mM NaCl) and paracrystalline fibers at pH 9 in 20-25 mM CaCl₂ [HERRMANN & AEBI 2004].

This study focuses on desmin, which like vimentin belongs to the assembly group 2. IF assembly using vimentin as a paradigm is described here, as multiple assembly and kinetics data are available for it. Under buffers of low ionic strength and high pH, e.g. 5 mM Tris-HCl pH 8.4, tetramer formation occurs by lateral association of vimentin dimers. Three distinct modes of lateral dimer-dimer contacts that lead to tetramer formation within the filament - A₁₁, A₁₂, and A₂₂ - have been established by chemical cross-linking experiments for a number of IF proteins, whereby the subscripts denote coil1 or coil2 [PARRY & STEINERT 1999]. The vimentin tetramers form “unit-length” filaments (ULFs) within 10 s in buffers of physiological pH and ionic strength (e.g. pH 7.5, 25 mM Tris-HCl / 50 mM NaCl) by lateral association

[HERRMANN et al. 1996]. These are non-compact filaments ~17 nm wide and ~60 nm long (**FIGURE 2**). In a subsequent elongation phase lasting up to 10 min, longitudinal annealing of ULFs alongside probable molecular rearrangements of individual ULFs occurs. In the third and final phase of assembly, further reduction of filament diameter occurs through intrafilamentous subunit reorganization in a step known as radial compaction. At this step, loosely packed (immature) structures rearrange into compacted (mature) IF proteins that are ~10-12 nm wide without reduction in their mass-per-length (MPL). MPL is a quantitative term depicting the number of molecules per filament diameter, i.e. kDa/nm. Of note, different IF proteins assemble into mature filaments that contain distinct numbers of subunits per filament cross-section, hence they exhibit different MPLs as shown by quantifying the scanning transmission electron microscopy (STEM) images [HERRMANN et al. 1999]. For instance, under identical assembly conditions, recombinant human vimentin forms ULFs with MPL value of 33 ± 4 kDa/nm corresponding to ~30 molecules per cross-section. On the other hand, MPL measured for desmin (48 ± 8 kDa/nm) corresponds to ~37 desmin subunits per filament cross-section [WICKERT et al. 2005]. Of note, the ULFs of individual IFs contain the same number of molecules per cross-section as do mature IFs.

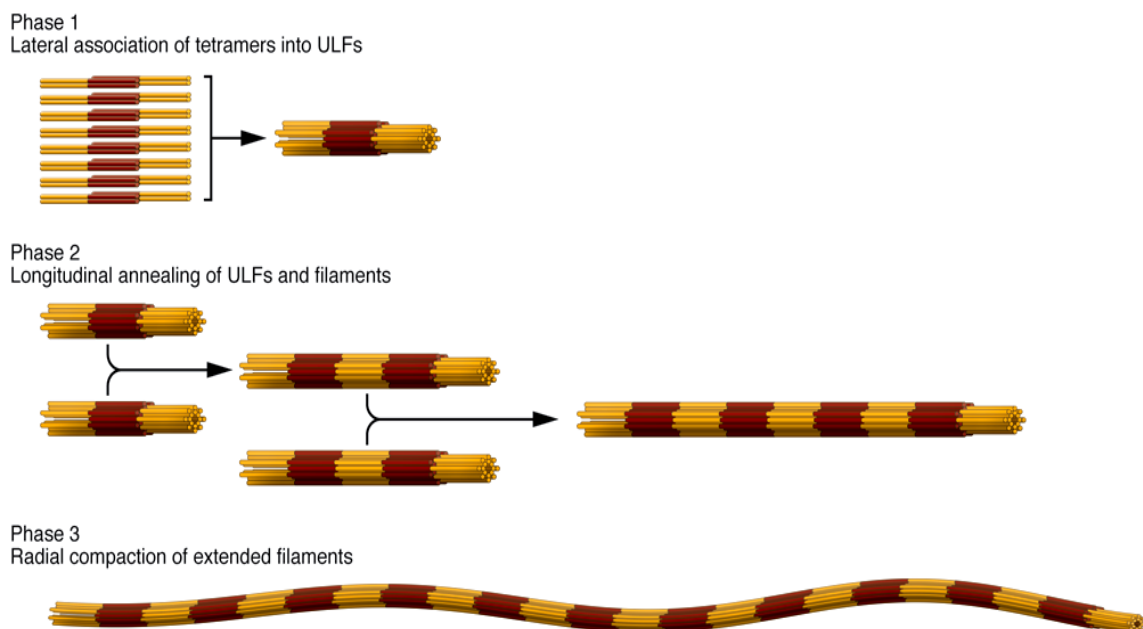


FIGURE 2 Scheme depicting three distinct assembly phases for cytoplasmic IF protein vimentin

After initiation of assembly in phase 1, eight tetrameric subunits made from two anti-parallel, half-staggered coiled-coil dimers associate laterally to form ULFs. Every single vimentin molecule is represented by one cylinder, coil 1 of each molecule is colored dark red, and coil 2 is colored yellow. In phase 2, ULFs and short filaments anneal longitudinally to other ULFs and filaments. In phase 3, filaments compact radially to a diameter of approximately 11-14 nm [Source: HERRMANN et al. 2009].

1.3 Desmin and its role in myocyte architecture

Desmin (gk *desmos*: link or bond), the IF protein expressed specifically in cardiac, skeletal as well as smooth muscle [LAZARIDES 1980], is encoded by a single copy gene (*DES*) located on chromosome band 2q35. It encompasses nine exons that code for 476 aa. Appearing during myogenesis at embryonic day 7.5 in the precardiac area of mouse embryo, desmin is one of the earliest muscle-specific markers [PAULIN & LI 2004]. In heart, desmin is abundant at intercalated discs and is the major component of Purkinje fibers (~2% of total protein, [PRICE 1984]). In mature skeletal muscle, desmin filaments (~0.4%

of total protein) as components of extrasarcomeric cytoskeleton, form a 3-D scaffold around myofibrillar Z-discs (**FIGURE 3**). Thereby, they interlink the neighbouring myofibrils and connect the myofibrillar apparatus to nuclei, subsarcolemmal cytoskeleton and cytoplasmic organelles like mitochondria via isomers of a versatile linker protein plectin [GOLDFARB et al. 2004] Mice lacking desmin (*DES*^{-/-}) produce muscle fibres with normal sarcomeric organization but weight-bearing or continually used muscles are mechanically fragile and degenerate upon repeated contractions [MILNER et al. 1996, LI et al. 1996, LI et al. 1997]. Cardiac and skeletal muscle of *DES*^{-/-} mice display aberrant mitochondrial positioning and respiratory function as well as muscle degeneration. Though *DES*^{-/-} mice develop normally and are fertile, at a later age they suffer from a cardiomyopathy, skeletal myopathy, and smooth muscle dysfunction. Thus, they exhibit reduced life span and are less tolerant to exercise –induced muscle injury [CAPETANAKI & MILNER 1998, HIJIKATA et al. 1999].

1.4 Desminopathy as a subtype of myofibrillar myopathy

Myofibrillar myopathies (MFMs) are a clinically and genetically heterogeneous group of neuromuscular disorders that are histopathologically characterized by desmin-positive protein aggregates and myofibrillar degeneration. While MFMs are partly caused by mutations in genes encoding for extramyofibrillar proteins (desmin, α B-crystallin, plectin) or myofibrillar proteins (myotilin, Z-band alternatively spliced PDZ-containing protein, filamin C, Bcl-2-associated athanogene-3, four-and-a-half LIM domain protein 1), a large number of these diseases are caused by still unresolved gene defects [SCHRÖDER & SCHOSER 2009]. Desmin is the most consistent protein found to accumulate within the muscle fibers of affected patients. It is postulated that MFM is not a general disease of the myofibril, but

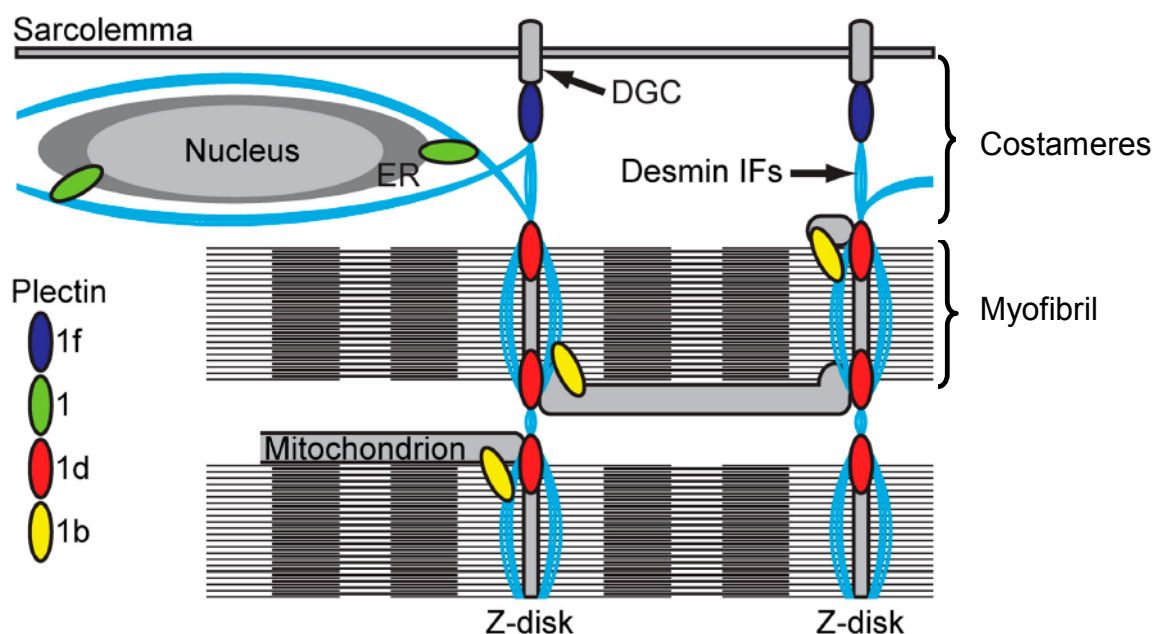


FIGURE 3 Scheme depicting architecture of a myocyte and role of desmin in myofibrillar integrity

The muscle-specific IF protein desmin interacts with associated proteins to support myofibrils at the level of the Z disc, forming a continuous cytoskeletal IF network that maintains a spatial relationship between the contractile apparatus and other structural elements of the cell. Plectin isoforms 1d, 1f, 1b, and 1 link desmin IFs with Z-discs, costameres (DGC: dystrophin glycoprotein complex), mitochondria, and the outer nuclear/ER membrane system, respectively [Adapted from: KONIECZNY et al. 2008].

it primarily affects a subgroup of stress-responsive Z-disc proteins [CLAEYS et al. 2009]. There is growing evidence that extralysosomal degradation of proteins within muscle fibers fails in MFM which might then burden the ubiquitin proteasome system (UPS), however, another school of thought points to failed UPS that induces protein aggregation. Originally described as skeletal and cardiac myopathy that is morphologically characterized by abnormal accumulation of desmin with muscle fibers, desminopathy is now better known as a subgroup of MFM arising from mutations in desmin [GOEBEL 1995, GOLDFARB et al. 1998]. The age of disease onset and rate of progression may vary depending on the type of inheritance and location of the causative mutation. The illness typically presents with lower and later upper limb muscle weakness slowly spreading to involve truncal, neck-flexor, facial, bulbar and respiratory muscles. Skeletal myopathy is often combined with cardiomyopathy, which is manifested by conduction blocks, arrhythmias and chronic heart failure resulting in premature sudden death. Sections of the affected skeletal and cardiac muscles show abnormal fibre areas containing chimeric aggregates consisting of desmin and other cytoskeletal proteins [FIGURE 4].

1.4.1 Current state of knowledge on desmin disease mutations

Mutations in the gene coding for desmin are recognized to cause up to 1-2% of dilated cardiomyopathies [TAYLOR et al. 2007]. Thus far, the number of known disease-causing DES mutations has reached 45 (*Supplementary: FIGURE S10*; [GOLDFARB & DALAKAS 2009]). Although mutations affect different domains, the disease phenotype can be identical in some cases. Frequently, variations in the age of onset of cardiomyopathy for different mutations have been observed [ARBUSTINI et al 2006]. Former studies have systematically dissected the impact of various mutations, residing in the rod and tail domain of desmin, on filament assembly as well as network formation. The important observations from these studies can be summarized as follows: (i) desmin disease mutations can be grouped into two classes: assembly-competent and assembly-incompetent ones, (ii) up to 40% of these mutations do allow *bona fide* filament formation, both *in vitro* and in transfected cell lines, that integrate into a pre-existing IF network, and are considered to be fully assembly-competent, (iii) mutations in the tail domain of desmin have no significant effect on assembly of mutant desmin protein. The various mutations interfere with filament assembly *in vitro* at four distinct stages of filament assembly process: (a) at ULF formation, (b) when ULFs anneal longitudinally to generate extended filaments, (c) in the course of radial compaction of assembled filaments, and (d) during network formation [BÄR et al. 2005]. In cells, it has been shown that assembly incompetent mutants segregate from the endogenous cytoplasmic IF system and alter its normal localization [BÄR et al. 2006a].

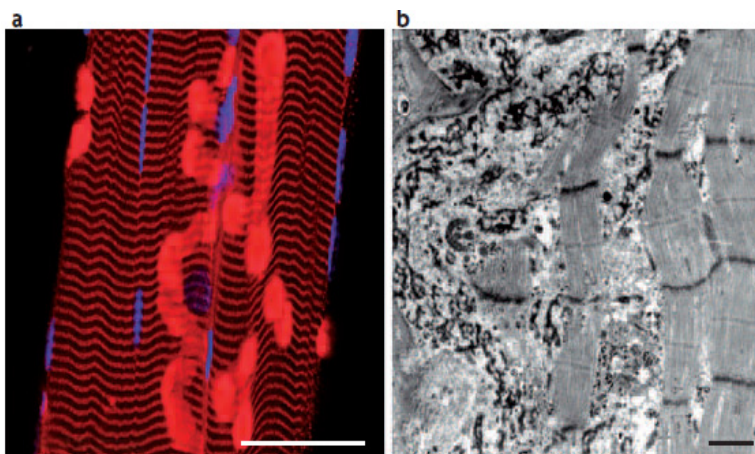


FIGURE 4 Histopathological hallmarks of desminopathy

(a) Immunofluorescence microscopy shows desmin-positive (red) aggregates deposited alongside preserved desmin IFs in the myofibre of a desminopathy patient. Red; desmin, blue: nucleus. Scale bar: 50 µm. (b) Ultrastructural analysis of skeletal muscle showing desmin-containing granulo-filamentous deposits (on left side) and disruption of Z-disc in a patient harboring R350P desmin mutation. Scale: 500 nm. [Source: HERRMANN et al. 2007]

Small Heat Shock Proteins

2.1 General features of small heat shock proteins

The highly conserved heat shock proteins (Hsps), found in both pro- and eukaryotes, are dramatically upregulated in response to heat shock stress [SCHLESINGER 1990]. As molecular chaperones, Hsps play an important role in facilitating protein synthesis, folding and assembly of nascent and stress-accumulated protein-substrate, preventing the aggregation of these proteins, as well as their transport across membranes and the degradation of other proteins. The principal Hsps belong to five conserved classes: Hsp100, Hsp90, Hsp70, Hsp60 and the small heat-shock proteins (sHsps). sHsps are widely believed to act as molecular chaperones in an ATP-independent manner in stress conditions. In addition to suppression of protein aggregation, sHsps show diverse physiological functions such as, involvement in the dynamics of cytoskeletal proteins, cellular growth, transcription and differentiation.

The human genome encodes ten sHsps: HspB1–10. These include Hsp27/Hsp25/HspB1, HspB2, HspB3, α A-crystallin/HspB4, α B-crystallin/HspB5, Hsp20/HspB6, cardiovascular Hsp/HspB7, Hsp22/Hsp11/HspB8, and HspB9 and a sperm tail protein designated as HspB10. [KAPPE' et al. 2003]. However, only few of them such as Hsp27, Hsp22 and α B-crystallin are true heat shock proteins that display an enhanced synthesis in response to stress [ARRIGO et al. 2007]. Although proteins belonging to the sHsp superfamily are diverse in sequence and size, most share few common structural and functional features, including (i) a moderately conserved C-terminal α -crystallin domain of ~80-100 residues in the central region of the protein, (ii) a small molecular mass between 12 and 43 kDa, (iii) formation of large globular oligomers or oligomeric complexes composed of α A-crystallin, α B-crystallin and Hsp27 in mammalian cells ranging from 50 to 800 kDa, (iv) a dynamic quaternary structure, and (v) stress-induced activation and chaperone activity in suppressing protein aggregation [HASLBECK et al. 2005].

2.2 Structure and assembly of sHsps

The α -crystallin core domain represents a distinguishing feature of sHsps. It is surrounded by N- and C-terminal extensions that are variable in length and sequence (**FIGURE 5a**). Though the amino acid sequence of α -crystallin domain is rather variable among different members of sHsps, the domain structure comprising a compact β -sheet sandwich similar to the immunoglobulin-like fold is conserved throughout the sHsp family [HASLBECK et al. 2005]. The β -sheet is composed of two layers of three to six antiparallel strands that are connected by a short interdomain loop. A conserved feature of sHsps is that the α -crystallin domains can dimerize through the formation of an intersubunit composite β -sheet

(**FIGURE 5b**). These dimers act as basic building blocks for sHsp assembly and oligomerization. The N-terminal domain though shows α -helical components, its partially resolved crystal structure suggests a lack of stable secondary structure. The C-terminal domain is supposedly flexible and makes essential contacts to stabilize the oligomeric structure. It has been shown that contacts between a conserved motif Ile-Xxx-Ile/Val in the C-terminal region and a hydrophobic patch in the α -crystallin domain of a neighbouring subunit are critical for oligomer formation. However, recent data from structural analyses show that certain amino acid residues in all three regions of sHsps are required for oligomerization. Whereas α -crystallin domain is pivotal for dimer formation, both flanking regions promote the formation of higher-order structures. Additionally, it has been shown for different sHsps, such as Hsp27 and α B-crystallin, that phosphorylation of serine residues reduces the size of respective oligomers [ITO et al. 2001].

Cryo-EM and x-ray crystallography have shed light on the oligomeric structures of sHsps, which are ordered spherical or ring-like structures with internal cavities composed of symmetrically packed dimeric subunits [MCHAOURAB et al. 2009]. sHsps occur as homo- or heteromeric complexes, comprising 2 to about 50 subunits per complex. Even when there is a predominance of oligomers of a specific size, dimeric subunits can escape and rejoin in a dynamic fashion. Crystallization is, therefore, generally a problem, and crystal structures are only known for two oligomeric sHsps: the 24-subunit Hsp16.5 from archaeon *Methanococcus jannaschii* (**FIGURE 5c**; [KIM et al. 1998]) and the dodecameric Hsp16.9 from wheat plant *Triticum aestivum* [VAN MONTFORT et al 2001]. Both of these are built from homogeneous dimers, unlike Hsp25, Hsp27, α A- or α B-crystallin that form heterogeneous structures.

2.3 Chaperoning function of sHsps

For chaperone activity, sHsp do not require ATP and their binding capacity can reach one substrate protein per sHsp subunit of equal molecular mass [SHASHIDHARAMURTHY et al. 2005]. Thus, sHsp can be a major contributor to the chaperone capacity of a cell. sHsps act as a reservoir for misfolded proteins for an extended period of time, allowing subsequent refolding after restoration of physiological conditions in cooperation with other chaperone systems [EHRNSPERGER et al. 1997]. Like other classes of Hsps, sHsps also bind to a wide range of cellular proteins to prevent their aggregation [BASHA et al. 2004]. Studies of the mechanism of sHsp chaperone function have been hampered by the apparent heterogeneity of the sHsp-substrate complexes. Structural data suggest that sHsps undergo subunit exchange and structural rearrangement during thermal and physico-chemical stress. Thereby hydrophobic surfaces of sHsps are exposed and these may then interact with hydrophobic patches of partially denaturing proteins. The substrate-bound sHsps assemble into large soluble complexes, thus preventing further aggregation of the denatured proteins that are subsequently released by ATP-dependent Hsps (**FIGURE 5d**). Several hydrophobic sites in the N-terminal, α -crystallin domain as well as the C-terminal have been proposed to be involved in the chaperone function of sHsps [GHOSH et al. 2007, JAYA et al. 2009]. However, with present data it is not possible to distinguish between substrate interaction sites necessary for chaperone function versus those involved in oligomer interactions or to determine if there is substantial crosstalk between these two functions. The subunit exchange of sHsps occurs on a timescale of minutes and it is inhibited by binding to large denatured or partially unfolded proteins, suggesting that subunit exchange may have an important role in the mechanism of chaperone action [WAUDBY et al. 2010].

2.4 Implications of sHsps in human diseases and therapy

The differences in expression patterns of sHsps suggest their general as well as specialized functions in cells. Significance of sHsps has been highlighted by their involvement in critical cellular processes such as aging and apoptosis. Expression and/or mutation of specific sHsps are linked to cataract, neurodegeneration, cardiomyopathy as well as cancer. For instance, α A-crystallin is abundantly expressed in the eye lens and its targeted disruption leads to cataract development in mice [BRADY et al. 1997]. Mutations in Hsp22 have been associated with neuropathies like distal hereditary motor neuropathy and Charcot-Marie-Tooth disease [SUN & MACRAE 2005]. Overexpression of Hsp27 and α B-crystallin occurs in the brain tissues of patients suffering from Alexander's disease, and their astrocytes display "Rosenthal" fibres consisting of aggregates of α B-crystallin, Hsp27 as well as GFAP [PERNG et al. 2006]. A missense mutation R120G in α B-crystallin is genetically linked to desmin related myopathy (DRM) as well as cataract, and the corresponding R116C mutation in α A-crystallin leads to hereditary cataract [VICART et al. 1998]. Upregulation of Hsp27 is associated with poor prognosis in gastric, liver, breast, lung as well as prostate cancer [CIOCCA & CALDERWOOD 2005]. Furthermore, Hsp27 has been suggested to have therapeutic potential for amyotrophic lateral sclerosis as well as multiple sclerosis [JAYA et al. 2009]. Intriguingly, in the model organism *Drosophila melanogaster* (fruitfly), ubiquitous or targeted expression of *DmHsp22* results in 30% increment of longevity [WADHWA et al. 2010].

2.5 α B-crystallin and its role in desmin related myopathy

α B-crystallin is encoded by a single copy gene (CRYAB) mapped to chromosome 11q22.3-q23.1. Along with α A-crystallin, α B-crystallin is a major protein of mammalian eye lens. The two sHsps, known collectively as α -crystallin, form heterogeneous oligomers (3:1 ratio) and thereby, maintain lens transparency by solubilizing associated proteins [HORWITZ 2003]. CRYAB is also abundantly expressed in heart, skeletal muscle, brain and kidney [KATO et al. 1992]. Here, it appears to be involved in signalling pathways activated during growth, differentiation and in response to various forms of stress [ARRIGO et al. 2007]. Like other sHsps, α B-crystallin is amphipathic and contains a hydrophobic N- and a hydrophilic C-terminal domain. Quaternary structure of this protein, as seen by cryo-EM, reveals spherical assemblies between 8 and 18 nm in diameter with a central cavity. This indicates that α B-crystallin assemblies are polydisperse in nature and, thus, difficult to crystallize (**FIGURE 5e**; [HALEY et al. 2000])

α B-crystallin knock out mice develop skeletal muscle dystrophy and show shorter life spans compared to controls [BOYLE et al. 2003]. In humans, α B-crystallin has been implicated in various protein aggregation diseases including cataract, DRM, as well as Alzheimer's, Parkinson's and Alexander's disease [GHOSH & CLARK 2005]. Of the three CRYAB mutations causing inherited MFM (R120G, Q151X, and 464delCT), CRYAB R120G is the best studied [SIMON et al. 2007]. Biochemical and structural studies have confirmed that R120G α B-crystallin is an aggregate-prone protein with compromised chaperone function due to altered secondary, tertiary, as well as quaternary structures. This DRM-linked mutant promotes desmin network aggregation both *in vitro* and in cells [PERNG et al. 2004]. Cardiac specific transgenic expression of CRYAB R120G in mice leads to a collapse of the desmin network, perturbations in mitochondrial-sarcomere architecture, deficits in mitochondrial function as well as accumulation of insoluble amyloid positive protein aggregates within cardiac muscle. Apoptotic pathways are subsequently activated, which eventually results in cardiomyocyte death, dilation, and heart failure by the age of 5–7 months [MALOYAN et al. 2005].

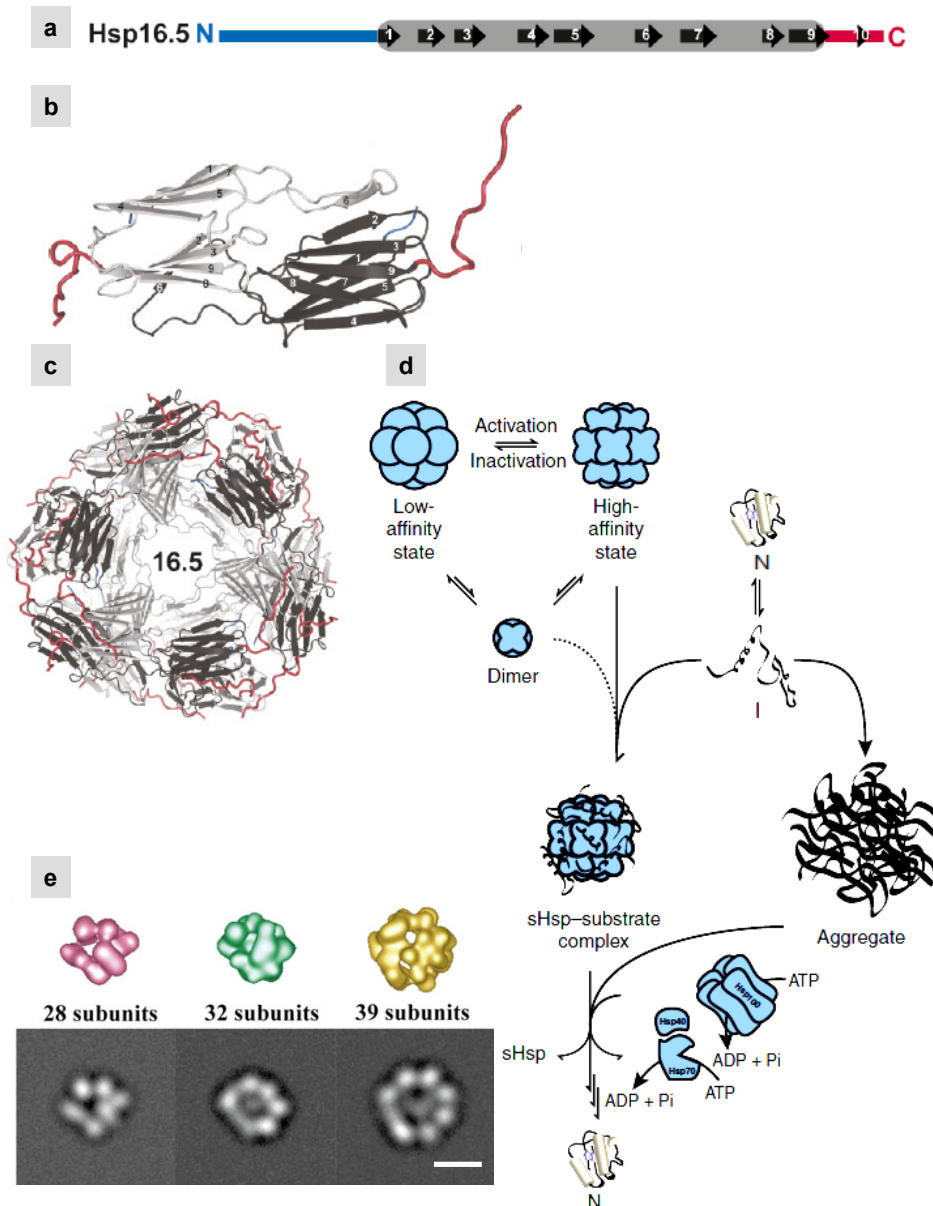


FIGURE 5 Architecture of sHsp and a model for its chaperone function

(a-c) Architecture of Hsp16.5 from *Methanococcus jannaschii*. (a) Domain organization of *Mj*Hsp16.5 drawn to scale depicting the α -crystallin domain (gray) containing β -strands (black arrows) flanked by an N-terminal (blue) and a C-terminal region (red). (b) The corresponding *Mj*Hsp16.5 dimer is shown with numbered β -strands and terminal domains colored as in panel a. (c) Quaternary structure of *Mj*Hsp16.5 depicting spherical 24-mer with N- and C-terminal extensions colored as in panel a [Source: MCHAOURAB et al. 2009]. (d) A model for the chaperone function of sHsps. sHsps (blue) are dynamic oligomeric structures, exchanging their subunits constantly. The equilibrium between an inactive, low-affinity state and an active, high-affinity state is controlled in a temperature-dependent manner. Upon heat shock, the equilibrium shifts towards the high-affinity state of sHsp and the substrate protein changes from a native (N) to an unstable yet reversible intermediate state (I) before aggregating irreversibly. The high-affinity state active oligomer becomes competent to associate with intermediate substrate protein to form a stable sHsp-substrate complex. This allows efficient prevention of irreversible substrate aggregation. Release of active substrate proteins from these complexes requires cooperation with proteins of ATP-dependent chaperone families such as Hsp40-Hsp70. Although Hsp40-Hsp70 can act directly on protein aggregates, the presence of sHsps increases the efficiency of the process [Source: HASLBECK et al. 2005]. (e) Three-dimensional quaternary models of α B-crystallin assembly generated to match the corresponding two-dimensional experimental cryo-EM class-sum images. The models are generated from 28, 32, and 39 monomers. Scale bar: 10 nm [Source: HALEY et al. 2000]

Motivation, objectives & chronology of result presentation

3.1 Motivation

Protein aggregation resulting from mutation poses a major threat to all cells. This is due to toxic accumulation of damaged or incorrectly assembled proteins that interferes with dynamic protein turnover as well as cellular homeostasis. Desminopathy is characterized by abnormal accumulation of desmin and associated proteins, like α B-crystallin, within muscle fibres. Currently, it is not possible to predict the outcome of a certain desmin disease mutation on filament morphology *in vitro* and in transfected cells or to establish if the filament properties are disturbed at all, such that desmin aggregation ensues eventually in desminopathy patients. Cells have developed mechanisms for protein “quality control” involving molecular chaperones like the small heat shock protein α B-crystallin to resolve protein misfolding. CRYAB R120G mutation that causes desmin-related myopathy, thereby rendering desmin protein aggregation-prone, has been well analyzed. On the other hand, interaction of desmin disease mutants with α B-crystallin, which also colocalizes in intracytoplasmic deposits in desminopathy, has not been investigated in detail.

3.2 Objectives

During this Ph.D. thesis, we aim at understanding desminopathy by investigating structural and functional aspects that may lead to the disease. First, we want to understand how point mutation or deletion in desmin causes “intrinsic” filament modification and gives rise to a distinct mutant phenotype as seen for *in vitro* assembly studies and in transfected cells. Second, we aim at analyzing how α B-crystallin recognizes and selectively binds unfolded mutant desmin disease variants under so called “extrinsic” mechanism of desminopathy. This is a key to determining how sHsps function *in vivo*, and understanding how protein aggregation processes leads to desminopathy. Hence, with this study we expect to identify the causal relationship between structurally modified desmin filaments, arising due to desmin disease mutations, and altered interaction of these mutants with the chaperone α B-crystallin.

To achieve our first objective, we aim at characterizing several desmin mutants in the head, rod or tail domain in terms of filament architecture *in vitro* using recombinant proteins as well as in cultured cells by transfection. For all mutants, the assembly competence is analyzed by biophysical methods and time-lapse EM. We investigate the ability of desmin mutants to form *de novo* filaments or integrate into pre-existing cytoskeleton by using cell lines exhibiting diverse cytoskeletal background. These data should

give us a more comprehensive understanding of the expression of a certain phenotype in the context of cellular background.

As a second objective, we aim at analyzing how α B-crystallin recognizes and binds unfolded mutant desmin variants. Thereby, our ultimate goal is to characterize desmin disease mutations based on their interaction with α B-crystallin. This is a major challenge because it is not known how filament-forming desmin mutants cause abnormal aggregates in patient cells. The systematic characterization of desmin disease mutants with respect to their interaction with α B-crystallin should lead to a comprehensive understanding of the mechanisms of desminopathy. Since α B-crystallin has been shown to play a role in various diseases, defining the mechanism of its chaperone action with desmin disease mutants will have a strong impact on understanding other stress-related disease processes as well.

3.3 Chronology of result presentation

For the head desmin disease mutations, we want to determine how a certain mutation and its location might influence the morphology of individual filaments. To this end, we want to meticulously analyze the effect of 5 mutants (DesS2I, DesS13F, DesR16C, DesS46F, DesS46Y) with respect to their filament formation properties by subjecting the mutant proteins to three rigorous methods of dialysis (**Section 4.1**). The behaviour of a novel desmin homozygous mutant DesL377 Δ 22fs is investigated by biochemical assay (oxidative crosslinking). Furthermore, the myotubes from heterozygous unaffected patient are subjected to proteasome inhibition to detect the variant protein (**Section 4.2**). Next, a desmin deletion variant *Des*(ESA) Δ C244 resembling “first half” of desmin molecule is characterized in terms of its assembly and interaction with wild-type desmin (**Section 4.3**). Finally, six mutants in the tail domain of desmin (DesT442I, DesK449T, DesI451M, DesR454W, DesS460I, DesV469M) are analyzed by assembling them at a high protein concentration (**Section 4.4**).

To analyze the interaction of α B-crystallin with desmin disease mutants, we first aim at addressing few basic questions in a consecutive manner: (i) does desmin interact with α B-crystallin in yeast two-hybrid screening? (**Section 5.1**), (ii) what is the solubility behaviour of α B-crystallin in various buffer systems? (**Section 5.2**), (iii) can we detect an interaction between desmin and α B-crystallin under various buffer conditions? (**Section 5.3**), (iv) can the chosen buffer system be further optimized to maximize the interaction of the two proteins without affecting their physiological properties? (**Section 5.4**), (v) is it possible to pinpoint the desmin domain/s that is/are involved in interaction with α B-crystallin? (**Section 5.5**), and (vi) does binding of α B-crystallin to desmin occur at all stages of desmin assembly? (**Section 5.6**). Based on these analyses, we will study the influence of disease-causing desmin mutants on association with α B-crystallin both *in vitro* and in a cell line (**Section 5.7**).

Part II Results

Characterization of mutations in the head, rod and tail domain of desmin

- 4.1 Assembly and network-forming properties of desmin head mutants are modified to various extents**
- 4.2 A novel homozygous mutation L377 Δ 22fs leads to the total absence of desmin in humans**
- 4.3 The truncated desmin variant Des(ESA) Δ C244 has deleterious effects on filament assembly**
- 4.4 The majority of desmin tail mutants exhibit undisturbed filament morphology both *in vitro* and in cell lines**

4.1 Assembly and network-forming properties of desmin head mutants are modified to various extents

The five desminopathy-causing mutants - DesS2I, DesS13F, DesR16C, DesS46F and DesS46Y – located in the head domain of desmin, have not been analyzed systematically with respect to their filament formation properties. In the following sections, the data obtained from *in vitro* analyses and cellular transfection are presented for these five mutants.

4.1.1 *In vitro* analyses of head domain desmin disease mutants

4.1.1.1 Head mutants form soluble assembly precursors similar to wild-type desmin

IF proteins are insoluble in buffers of physiological ionic strength and pH, thus a strong denaturant like 8 M urea is employed to dissociate filaments and to obtain monomeric subunits. After serial dialysis from 8 M urea into low ionic strength and high pH buffer (5 mM Tris-HCl pH8.4) anti-parallel half staggered tetramers, acting as precursors for filament formation are obtained. Sedimentation behaviour of authentic and recombinant IF proteins is similar and, whereas a *s*-value of 5.2 S has been measured for desmin isolated from chicken gizzard in 10 mM Tris-acetate pH 8.5, recombinant wild-type desmin precursors sediment with a *s*-value of ~5.2 S when analyzed by analytical ultracentrifugation (AUC) in 5 mM Tris-HCl pH 8.4 [HERRMANN & AEBI 2004, BÄR et al. 2006b]. Soluble assembly intermediates of recombinant desmin harboring disease-causing mutations show altered sedimentation behavior when assessed by AUC. Thus, the five desmin head variants were compared against wild-type desmin by AUC.

Previous studies employed desmin and vimentin that contain an alanine instead of serine at aa position 2, i.e. Des2A and Vim2A, respectively. This is because *Ser* residue at position 2 is rapidly degraded in bacteria and has a short intracellular half-life [ROGERS et al. 1986]. Since the disease-causing mutant DesS2I [SELCEN et al. 2004] located at NH₂-terminus of desmin has an isoleucine residue at 2nd position, wild-type desmin harbouring *Ser* residue in position 2 (Des2S) was generated to make a comparison. Notably, wild-type vimentin protein with *Ser* residue in second position was employed as additional control because both desmin and vimentin show similar sedimentation behaviour [WICKERT et al. 2005]. The soluble assembly entities of Des2S, Des2A, Vim2S as well as Vim2A were compared by AUC on a single day. Both Des2S and Des2A or Vim2S as well as Vim2A proteins exhibited similar sedimentation curves with *s*-values of 5.8 S for desmin 2S and 2A, and 5.1 S for vimentin 2S and 2A, respectively (**TABLE 2, Supplementary FIGURE S1**). Similarly, *in vitro* assembly assays and transfection studies did not show any detectable difference between Des2S and Des2A at various stages of filament assembly. These data suggest that the alteration of *Ser* to *Ala* at position 2 does not affect the desmin filament properties. Next, the soluble precursors of head desmin disease variants - DesS2I, DesS13F, DesR16C, DesS46F & DesS46Y – were investigated relative to wild-type desmin (Des2S) by AUC in sedimentation velocity mode. Four of the head mutants harbour a *Ser* residue at 2nd position, except for DesS2I. For desmin wild-type (DesWT) and the mutant DesS13F, peak *s*-values ranged between 4.9 to 5.5 S which suggests the presence of soluble tetramers. In contrast, for desmin head mutants - DesS2I, DesR16C, DesS46F and DesS46Y - *s*-values are higher than 6.0. This suggests potential interaction of tetramers to yield additional higher order oligomeric complexes. Taken together, these four head mutants did not differ significantly from wild-type desmin at the level of soluble assembly precursors (**TABLE 2, FIGURE 6**).

TABLE 2 Sedimentation coefficient of wild-type desmin, vimentin and desmin head mutants

	Peak value $s^*(20,w)$ [S]
Vim2S	5.1
Vim2A [#]	5.1
Des2S	5.8
Des2A [#]	5.8
<i>Des2S</i>	5.5, 5.3
<i>DesS2I</i>	6.1, 5.7
<i>DesS13F</i>	5.4, 4.9
<i>DesR16C</i>	7.0, 6.3
<i>DesS46F</i>	6.5, 5.6
<i>DesS46Y</i>	6.7, 6.2

Peak value $s^(20,w)$ indicates sedimentation coefficient that has been corrected for the viscosity and density of solvent, relative to that of water at 20°C.

[#]Vim2A and Des2A indicate vimentin and desmin, respectively that have been used conventionally as wild-type. However, for characterization of desmin head mutants, Des2S is used as wild-type for all assays.

All runs in AUC were performed after step-wise renaturation of samples from 8 M urea into “Tris-buffer” (5 mM Tris-HCl, 1 mM EDTA, 0.1 mM EGTA, 1 mM DTT, pH 8.4). For desmin head mutants, s -values were measured in two independent experiments.

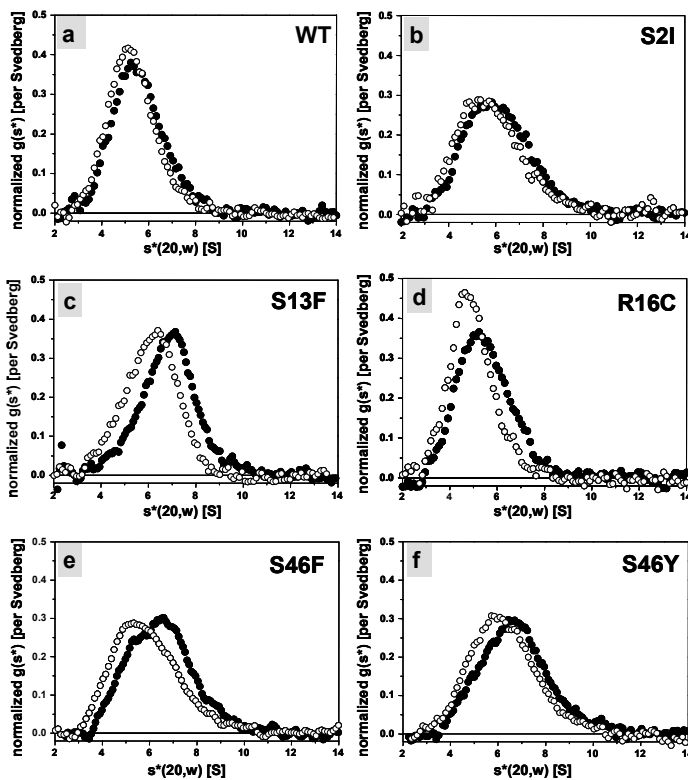


FIGURE 6 Sedimentation behaviour for wild-type and desmin head mutants

The head mutant proteins do not diverge significantly from the wild-type desmin at the level of soluble assembly precursors. All runs in AUC were performed by step-wise renaturation of recombinant protein samples from 8 M urea into “Tris-buffer” overnight at a concentration of 0.5–1.0 mg/ml. Results of two independent experiments are depicted for each sample as empty and filled circles. $s^*(20,w)$ indicates sedimentation coefficient that has been corrected for the viscosity and density of solvent, relative to that of water at 20°C. To make direct comparisons, area normalization was done for different concentrations. Data analysis was performed using the software DCDT+.

4.1.1.2 Assembled head mutant proteins reveal two distinct categories of filament-forming behaviour

In vitro assembly of desmin is an instant process occurring by lateral association of tetramers into ULFs within first few seconds after raising the ionic strength, e.g., by addition of an equal volume of 100 mM NaCl [HERRMANN & AEBI 2004]. Time-lapse EM allows visualization of different assembly stages, i.e., ULF formation, longitudinal annealing, radial compaction, and finally formation of mature extended filament networks [KREPLAK et al. 2008]. The two main purposes of protein assembly studies are: (i) to observe if the *in vitro* assembly path followed by a given mutant resembles or diverges from that of wild-type desmin for various time points, and (ii) to characterize morphological features of filaments formed by different desmin variants at given time points.

Under standard assembly conditions, when equal volume of “assembly buffer”, i.e., 100 mM NaCl, 40 mM Tris-HCl, pH 7.0 is added at 37°C (**Section 8.4**: method 1), DesWT forms ULFs at 10 s. These ULFs are rod-like structures 60-65 nm in length. The same was observed for the head mutant proteins DesS2I, DesS46F, and DesS46Y. In contrast, DesS13F and DesR16C assembled into clusters of ULF-like structures, i.e, for these two mutant proteins not individual but multiple ULFs that cohere together were observed. At 5 min, DesWT had assembled into smooth, extended filaments, while both DesS13F and DesR16C differed drastically in their morphology from DesWT. These mutants showed aggregated structures consisting of multiple filaments bundled tightly together. In contrast, DesS2I, DesS46F, and DesS46Y were able to assemble into extended filamentous networks which appeared slightly irregular compared to DesWT (**FIGURE 7**, *Supplementary FIGURE S2*). In an effort to minimize the bundling and aggregation of filaments observed for DesS13F and DesR16C, a lower protein concentration of 0.1 mg/ml was employed. However, even after reducing the protein concentration by 75% for assembly, there was no reduction in filament bundling for these two mutant proteins (data not shown).

In order to analyze whether the mutants DesS2I, DesS46F, and DesS46Y could be induced to assemble into filaments of more regular width, and to determine whether the observed severe phenotype of the mutants DesS13F and DesR16C could be rescued, a 2nd method of filament assembly was employed. Here, the head mutant proteins were dialyzed as above in “Tris buffer” but assembly was initiated by further dialysis of samples into “filament buffer” containing 50 mM NaCl, 20 mM Tris-HCl, pH 7.5 at 37°C for 1h (**Section 8.4**: method 2). In contrast to rapid addition of assembly buffer, this method enables a slower change to higher salt and lower pH conditions. This, in turn, should allow the formation of more uniform and homogeneous filaments. This is also the method of choice for assembly in order to measure the width of mature filaments. Using this 2nd method, wild-type desmin formed more regular filaments, yet same assembly defects of the desmin head mutants were observed. Specifically, irregular protein filaments were observed for DesS2I, DesS46F, and DesS46Y. For DesS13F and DesR16C bundles of filamentous aggregates were seen (**FIGURE 8**, *Supplementary FIGURE S3*).

In a 3rd method to rescue phenotype of desmin head mutants, samples were dialyzed out of 8 M urea directly into “filament buffer” at 37°C for 5, 60 and 120 min (**Section 8.4**: method 3). The morphology of wild-type desmin filaments appeared regular, whereas entangled filaments were seen for DesS2I, DesS46F, and DesS46Y after 60 min and 120 min of dialysis. Moderately bundled, yet individually distinguishable filaments were observed for DesS13F and DesR16C at 5 min. These formed aggregates at longer assembly time points of 60 min and 120 min (**FIGURE 9**, *Supplementary FIGURE S4*).

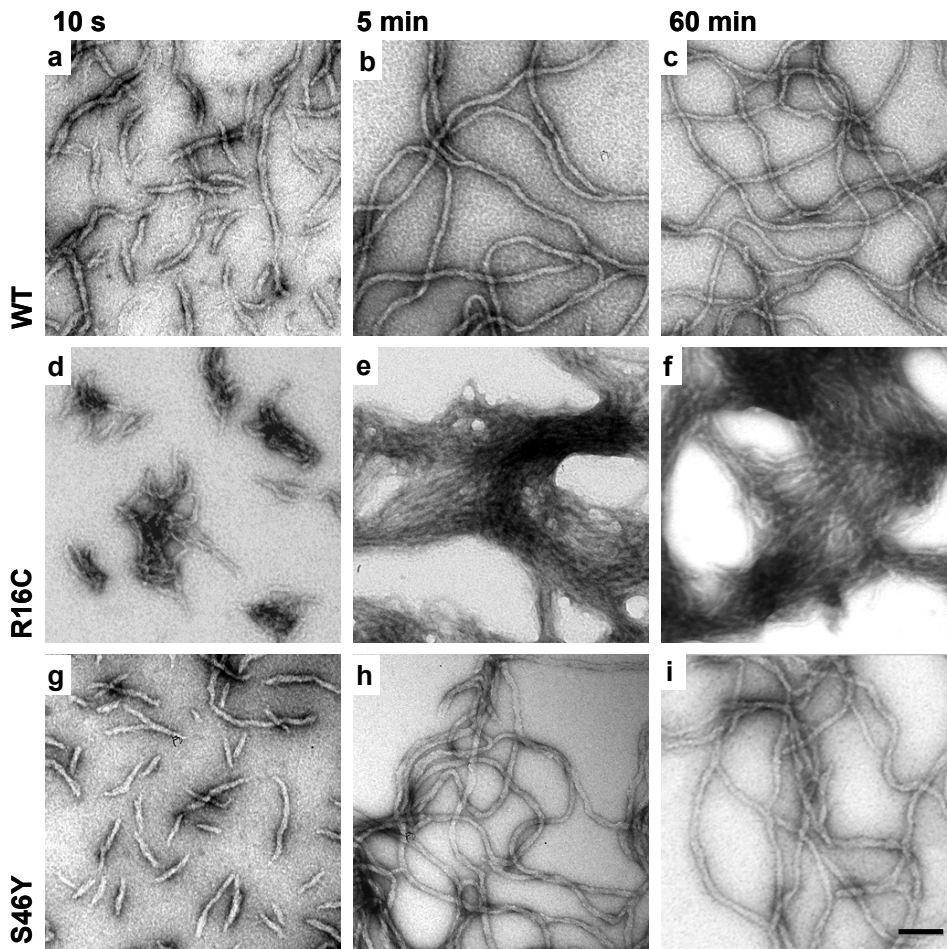


FIGURE 7 Assembly of desmin head mutant proteins in “assembly buffer” leads to aggregates for DesR16C and irregular filaments for DesS46Y

Electron micrographs of negatively stained samples of desmin wild-type (WT) and head mutant proteins (DesR16C, DesS46Y) are shown at three assembly time points. Assembly was performed at 37°C by addition of equal volume of “assembly buffer” (100 mM NaCl, 40 mM Tris-HCl, pH 7.0 at 37°C) and stopped by adding 0.1% glutaraldehyde at 10 s, 5 min and 60 min, respectively. (a, g) At 10 s, uniformly distributed ULFs are seen for wild-type and mutant desmin DesS46Y. (d) In contrast, for mutant protein DesR16C separate clusters of ULF-like structures are seen. (b, e, h) At 5 min, the differences in the structure of DesWT and DesR16C are particularly noticeable. Wild-type desmin shows regular filaments whereas mutant variant DesR16C forms highly cohesive filamentous aggregates. Mutant protein DesS46Y forms slightly irregular filaments at this time point. (c, f, i) The phenotypes seen at 5 min remain similar for each of the three proteins at 60 min. Scale bar: 100 nm.

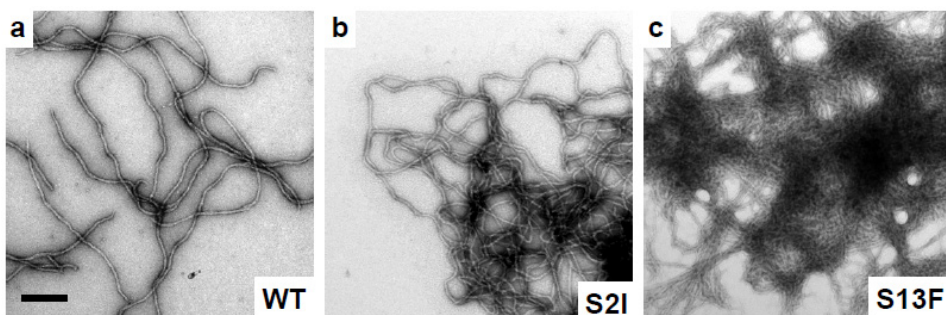


FIGURE 8 Assembly of desmin head mutant proteins in “filament buffer”

(please refer to figure legend on next page)

FIGURE 8 Assembly of desmin head mutant proteins in “filament buffer”

Electron micrographs of negatively stained samples of desmin wild-type (WT) and head mutant proteins DesS2I and DesS13F are shown. Proteins were dialyzed in “Tris buffer” and assembly was initiated by further dialysis of samples into “filament buffer” containing 50 mM NaCl, 20 mM Tris-HCl, pH 7.5 at 37°C for 1h. Assembly was stopped by adding 0.1% glutaraldehyde. (a) Wild-type desmin forms regular filaments, whereas (b) irregular protein filaments are observed for DesS2I. (c) Bundles of filamentous aggregates are seen for DesS13F. Scale bar: 100 nm.

4.1.1.3 Co-polymers of head mutants and desmin wild-type form regular filamentous network

To investigate the influence of desmin head mutant proteins on wild-type desmin assembly, we

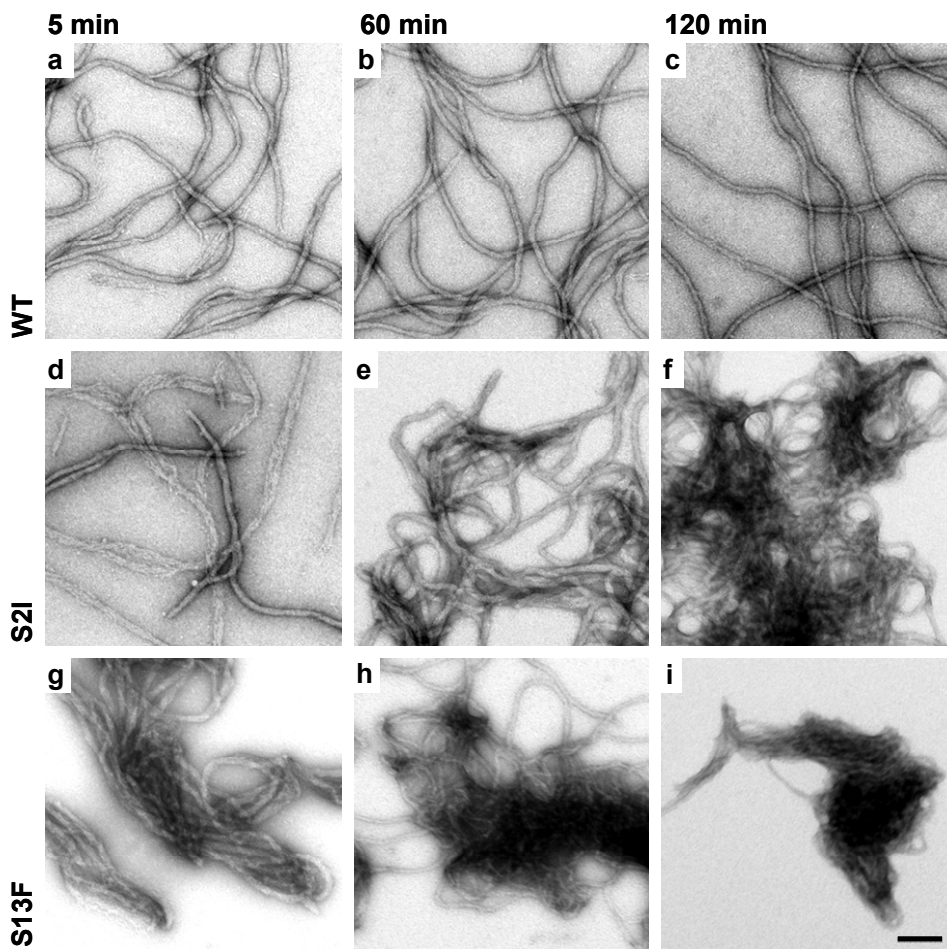


FIGURE 9 Assembly from 8 M urea into “filament buffer” reveals compromised phenotype for all desmin head mutant proteins at advanced time points

Electron micrographs of negatively stained samples of desmin wild-type (WT) and head mutant proteins DesS2I and DesS13F are shown for three assembly time points. Samples were dialyzed directly out of 8 M urea into “filament buffer” containing 50 mM NaCl, 20 mM Tris-HCl, pH 7.5 at 37°C for three different time points: 5 min, 60 min and 120 min. (a-c) The morphology of wild-type desmin filaments appeared regular at all time points. (d-f) For DesS2I, regular filaments are observed at 5 min, whereas entangled filaments are seen at 60 min and 120 min. (g-i) Bundled, yet individually distinguishable filaments are seen for DesS13F at 5 min, whereas aggregate formation occurs at assembly time points of 60 and 120 min. Of note, as compared to the 60 min time point, both head mutant proteins assemble more irregularly at 120 min. Scale bar: 100 nm.

combined equimolar amounts of each mutant with DesWT in 8 M urea prior to overnight dialysis into “Tris Buffer” (5 mM Tris-HCl, 1 mM EDTA, 0.1 mM EGTA, 1 mM DTT, pH 8.4) and assembly was initiated by addition of equal volume of “assembly buffer”. This is expected to allow heteropolymerization of the respective mutant proteins with wild-type desmin from dimer-stage onwards. Copolymers of desmin head mutant and wild-type protein showed extended filamentous networks (**FIGURE 10**, *Supplementary FIGURE S5*). However, filament width measurement for mixture of desmin wild-type and mutant DesS13F or DesR16C showed distinctly thinner filaments, indicating subtle alteration of filament morphology (**TABLE 3**). This was also seen in EM at 60 min, as exemplified for DesR16C (**FIGURE 11 b, e**).

Additionally, the mixtures were dialyzed directly out of 8 M urea into “filament-buffer” and assembled for 5 min and 120 min. In contrast to the altered filament morphology observed for all desmin head mutants dialyzed alone in the same manner (**FIGURE 9**), no bundling of filaments was observed for any of the mixtures, as exemplified for DesS2I, DesS13F, and Des46F (*Supplementary FIGURE S6*).

In summary, two different assembly behaviours are observed for desmin head variants by EM: (a) DesS2I, DesS46F, and DesS46Y form irregular filaments and this mutant phenotype can be completely rescued by DesWT, whereas (b) DesS13F and DesR16C form aggregating, cohesive filaments and this phenotype is not rescued completely by addition of equimolar DesWT. Although the “co-polymers” of DesS13F and DesR16C form filamentous networks, their filament diameter is reduced significantly.

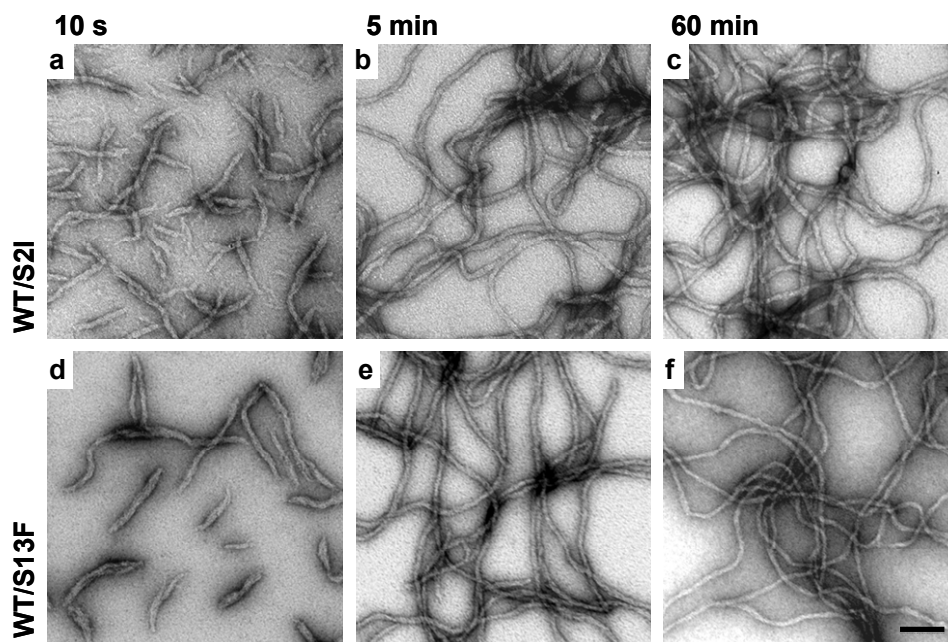


FIGURE 10 Coassembly of desmin head mutant proteins with the wild-type desmin

Electron micrographs of negatively stained samples of equimolar mixture of desmin wild-type (WT) with the head mutant proteins DesS2I and DesS13F are shown for three assembly time points. Assembly was performed at 37°C by addition of equal volume of “assembly buffer” (100 mM NaCl, 40 mM Tris-HCl, pH 7.0 at 37°C) and stopped by adding 0.1% glutaraldehyde at 10 s, 5 min and 60 min, respectively. (a-c) Mixture of desmin head mutant S2I and wild-type protein are able to form extended filamentous networks (d-f) Equimolar mixture of desmin head mutant S13F and wild-type protein also form extended filamentous networks, yet these co-polymers appear visibly thinner. However, co-polymer of DesS46F with DesWT exhibits a normal filament morphology. Bar 100 nm

4.1.1.4 The irregular width of filaments formed by head mutants is corrected by the presence of equal amounts of desmin wild-type

Filament diameter of an IF protein is proportional to the number of molecules per cross-section of the filament. Previous studies with desmin have shown that irrespective of assembly mode and origin, i.e. recombinant or authentic, comparatively heterogeneous IFs are formed. These findings emphasize that the polymorphism exhibited by desmin upon *in vitro* assembly is an intrinsic filament property [HERRMANN et al. 1999, BÄR et al. 2004]. Filament width measurements were carried out for desmin head mutant proteins, both alone and for their equimolar mixture with DesWT, to investigate the impact of a given mutation on filament morphology. Samples were dialyzed from “Tris-buffer” into “filament buffer” for 1h at 37°C. For mixtures, equimolar amount of wild-type and mutant protein was combined in 8 M urea prior to reconstitution in “Tris-buffer”. For diameter measurement, the EM images were processed using ImageJ 1.32j (<http://rsb.info.nih.gov/ij>). At least 100 measurements were carried out per sample. In order to determine if the difference in filament diameter of mutants or their mixtures with respect to DesWT is statistically significant, Student’s *t*-test (Excel 2003) was used. All reported *p* values were two-sided and considered to be statistically significant at *p*<0.05. Graphs were generated using the software Origin 8.1 (FIGURE 11d, e, f).

TABLE 3 Filament width of head mutant proteins and mixtures with wild-type desmin

Sample	Sample size “n”	Range	Mean ± SD
DesWT	116	8.1 - 12.7	10.7 ± 0.8
DesS2I	116	8.2 - 15.6	12.0 ± 1.5***
DesS46F	116	9.5 - 14.8	13.0 ± 1.1***
DesS46Y	116	9.6 - 15.1	13.8 ± 0.9***
Mixtures			
WT+S2I	103	8.4 - 13.4	10.5 ± 1.0
WT+S13F [#]	103	6.5 - 11.7	9.4 ± 1.3***
WT+R16C [#]	103	6.1 - 11.8	8.8 ± 1.0***
WT+S46F	103	8.1 - 12.9	10.4 ± 1.1
WT+S46Y	103	8.2 - 13.5	10.7 ± 1.2

Filament width measurements were carried out after dialysis of samples from “Tris-buffer” into “filament buffer” for 1h. For mixtures, equimolar amount of wild-type and mutant protein was combined in 8 M urea prior to reconstitution in “Tris-buffer”. All EM images were processed in ImageJ 1.32j for measurement of filament width.

[#]For DesS13F and DesR16C alone, no separate filaments were obtained, thus, no width measurements could be performed.

****p*<0.001, diameter is significantly different from wild-type desmin for this sample.

DesWT assembled into filaments with an average diameter of 10.7 ± 0.8 nm within a range of 8.1 – 12.7 nm (Table 3, FIGURE 11a, d), while the average filament diameter of the assembled head mutant proteins DesS2I, DesS46F and DesS46Y was between 12 - 13.8 nm, within a range of 8.2 – 15.6 nm. For the two mutant variants - DesS13F and DesR16C - no separate filaments were obtained, thus, no width measurements could be performed. Although DesS2I, DesS46F and DesS46Y assembled into extended filamentous networks, their mean filament diameter was significantly higher than that of DesWT after 1 h of assembly. These desmin mutants exhibited a more irregular filament diameter than DesWT as indicated by their broader range of filament width distribution (FIGURE 11c, f).

Upon co-polymerization with DesWT, most head mutants showed a wild-type-like filament morphology. However, for the equimolar mixtures of either DesS13F or DesR16C with DesWT, a significantly reduced filament diameter than that of DesWT alone was obtained (**FIGURE 11b, e**). This indicates that though DesWT/DesS13F and DesWT/DesR16C form *bona fide* IFs, a severe alteration of intra-filamentous architecture takes place in the heteropolymeric situation. In contrast, there was no significant difference between the mean filament diameters of DesWT and DesWT/DesS2I, DesWT/DesS46F or DesWT/DesS46Y.

In summary, filament width measurements indicate that point mutations in the head domain of desmin considerably alter the intrafilamentous architecture, probably by altering the arrangement of molecules within the mature filament. Thus, except for the mixtures of DesS2I, DesS46F and DesS46Y, all other mixtures or mutants exhibit altered filament width as compared to the wild-type desmin.

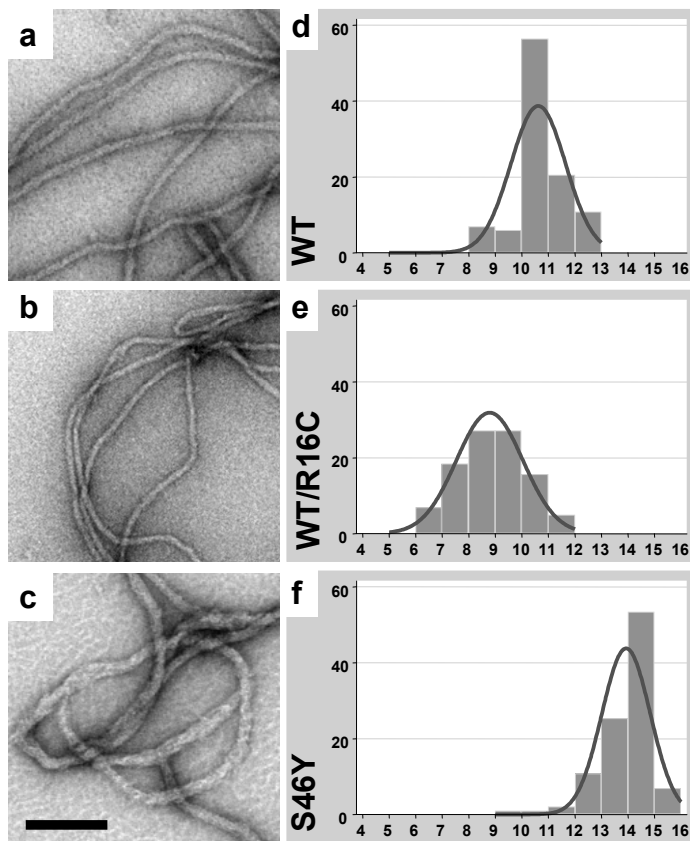


FIGURE 11 Head mutants or their mixtures exhibit polymorphism with respect to filament width

(a, d) Desmin WT assembled into filaments with an average diameter of 10.7 nm within a range of 8.1 – 12.7 nm. (b, e) For the equimolar mixture DesWT/DesR16C, visibly thinner filaments than that of DesWT alone were observed and this mixture assembled into filaments with an average diameter of 8.8 nm within a range of 6.1–11.8 nm. (c, f) For DesS46Y visibly thicker filaments than for DesWT alone were observed, and it assembled into filaments with a mean diameter of 13.8 nm within a range of 9.6 – 15.1 nm. Samples were dialyzed overnight in “Tris-buffer” and further dialyzed the following day in “filament buffer” for 1 h at 37°C for protein assembly before being fixed in 0.1% glutaraldehyde and mounted on carbon-coated grids. The EM images were processed in ImageJ 1.32j for measurement of filament width. At least 100 measurements were carried out per sample and the graphs were generated in Origin 8.1. Abscissa: filament width (nm), ordinate: frequency of measurement. Scale bar: 100 nm.

4.1.1.5 Viscometric analyses depict two different behaviours of desmin head variants either alone or in combination with wild-type desmin

To characterize the property of mutants and their equimolar mixtures with DesWT quantitatively in bulk solution, viscometric measurements were carried out. Viscometry is considered to be a robust tool for quantitative analysis of filament assembly and networking behaviour. Wild-type desmin and DesS2I exhibited a similar increase of relative viscosity after the initiation of assembly, reflecting the formation of extended filamentous networks (**FIGURE 12a**). After ~30 min of assembly, a plateau viscosity was

reached for mutant DesS2I and wild-type desmin alone. Head mutants - DesS13F, DesR16C, DesS46F and DesS46Y - exhibited a drop of relative viscosity after 25 to 35 min of assembly, even though their initial increase in relative viscosity was comparable to that of wild-type desmin (**FIGURE 12b-e**). This effect was most pronounced for DesS13F and DesR16C as both mutants showed a significant drop in relative viscosity (**FIGURE 12b, c**). This can be explained by the formation of bundled filament aggregates as observed by EM for either of the mutants. Similar viscometry profiles have also been obtained for other desmin rod and tail mutant proteins [BÄR et al. 2005, 2007].

Except for the mixture of DesWT with DesS46F (**FIGURE 12d**), which exhibited a viscometric profile comparable to that of DesWT alone, the other 4 head desmin mutants exhibited a dominant-negative effect on wild-type filament assembly. In case of these mutants, a drop in relative viscosity was observed for their equimolar mixtures with DesWT (**FIGURE 12a-c, e**). This indicates that in the presence of DesWT, though these mutants form apparently normal filaments as observed by EM, the mechanical properties of their co-polymeric networks are distinctly modified when compared to those of wild-type desmin alone. Of note, the mutant DesS2I alone showed a normal viscometric profile, whereas, in presence of desmin wild-type it showed a significant drop in relative viscosity.

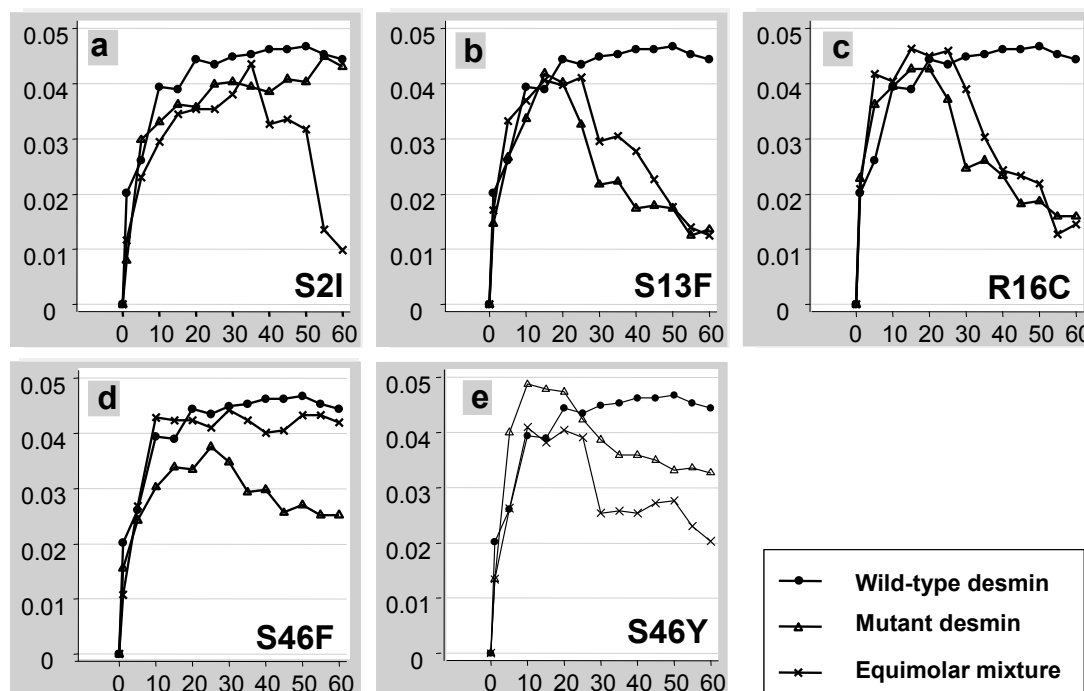


FIGURE 12 Viscometric analyses show that DesS46F is rescued by wild-type desmin

Two different behaviours of desmin head variants, either alone or in combination with wild-type, are depicted. (a) DesS2I shows normal rise of relative viscosity that corresponds to increment in filament length and network formation. However, in the copolymeric situation with wild-type desmin its relative viscosity drops significantly. (b, c, e) The deleterious effects of DesS13F, DesR16C or DesS46Y on filament assembly is not inhibited by addition of equimolar amount of DesWT, (d) whereas mixture of DesWT with DesS46F exhibits a viscometric profile comparable to that of DesWT alone. The rapid drop of relative viscosity after ~25-30 min indicates protein aggregation. All measurements were performed at a protein concentration of 0.1 mg/ml. The graphs were generated in Origin 8.1. Abscissa: time (min), ordinate: relative viscosity.

4.1.2 Filament formation behaviour of desmin head mutants in cells

4.1.2.1 Aberrantly formed filaments are observed for a subset of desmin head mutants in SW13 and MEF Vim^{-/-} cells

In contrast to the well-defined stages of assembly *in vitro* starting with ULF formation, as seen by EM, it is not so straightforward to follow the distinct assembly stages of IFs proteins in cells by fluorescence microscopy using fluorescently tagged protein. To analyze the ability of mutant desmin variants to form *de novo* filaments in cells, transient transfection studies were carried out in cells completely devoid of endogenous cytoplasmic IFs, i.e. human adrenocortical carcinoma cell line (SW13) and primary fibroblasts obtained from vimentin knockout mice (MEF Vim^{-/-}). It has been shown that transfection with cDNA coding for wild-type desmin in SW13 results in failure to form extended filament networks [BÄR et al. 2006]. Most likely, these cells lack certain IF-associated proteins required for proper network formation. Upon transfection of human desmin cDNA, the MEF Vim^{-/-} cells exhibit a more elaborate desmin cytoskeleton than SW13 cells, thus emphasizing the suitability of these cells to assess IF network formation properties of various desmin mutants.

Our results show that in SW13 cells, DesS2I and DesR16C form filamentous networks comparable to those of DesWT (**FIGURE 13a, b, d**). In case of DesS13F, DesS46F and DesS46Y, however, only short filamentous aggregates distributed all over the cytoplasm were observed (**FIGURE 13c, e, f**).

In contrast to the SW13 cells, in MEF Vim^{-/-} cells DesS46F and DesS46Y were able to form extended filamentous networks similar to that of wild-type desmin and DesS2I (**FIGURE 14a, b, e, f**). For DesS13F and DesR16C (**FIGURE 14c, d**), cytoplasmic aggregates of the mutant protein were observed in approximately 12–15% of all transfected cells, whereas an extended filament network was seen for the rest of the transfected population

To express mutant and wild-type desmin genes simultaneously, and thereby mimic the situation in the patient muscle, we co-transfected equal amount of wild-type and mutant cDNA into MEF Vim^{-/-} cells. We observed a well developed network for all combinations of mutants with DesWT, including DesR16C (**FIGURE 15**). As mentioned before, when transfected alone in these cells this mutant formed aggregates in 12-15% of cells. The mutant DesR16C displayed network morphology indistinguishable from that of the wild-type desmin in MEF Vim^{-/-} upon co-transfection with DesWT, indicating that the phenotype of this mutant can be rescued by wild-type desmin in cells. However, in case of DesWT/DesS13F, approximately 15% of transfected cells continued to form desmin-positive aggregates in the vicinity of cells showing normal filament network. Such an effect reiterates the dominant-negative effect of this mutant on desmin wild-type filaments (**FIGURE 15a, b**). Remarkably, this heterogeneity of phenotypes for a given mutant is also observed in muscle of patients suffering from desminopathy, whereby myocytes with desmin-positive cytoplasmic aggregates are seen next to apparently normal cells.

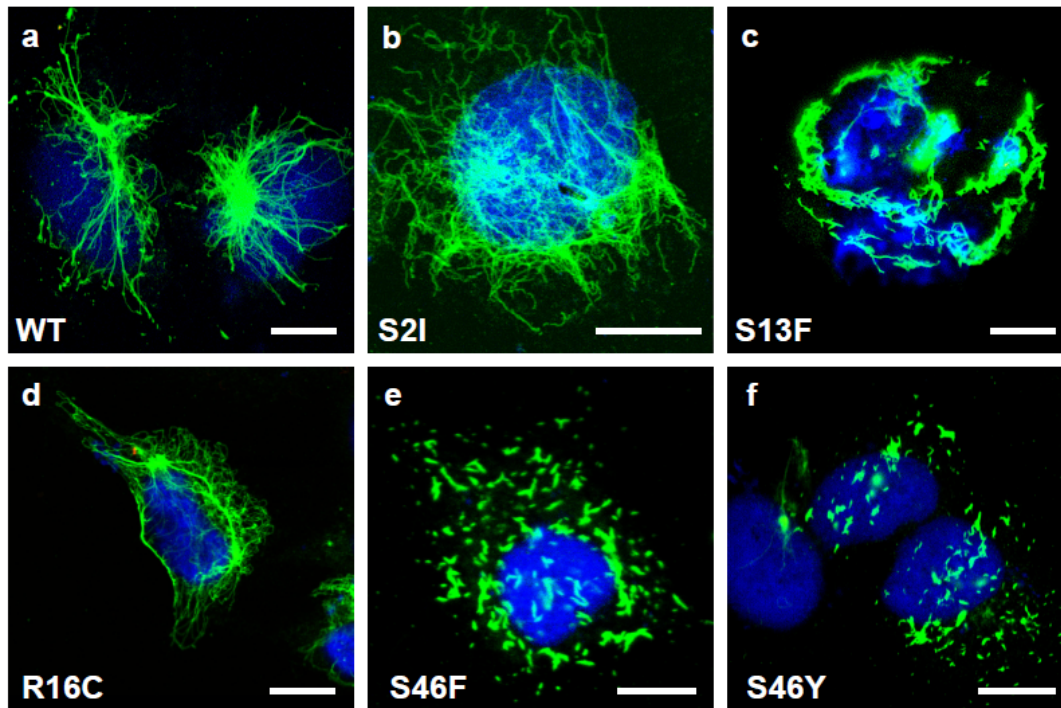


FIGURE 13 DesS2I and DesR16C form filamentous network comparable to wild-type desmin in SW13 cells

Immunofluorescence images are shown for filaments formed by desmin head mutants in SW13 cells upon transfection. (a, b, d) DesS2I and DesR16C form a cytoskeleton similar to that of DesWT, (c, e, f) whereas cytoplasmic aggregates are seen for DesS13F, DesS46F and DesS46Y. Green: transfected desmin variant, blue: nuclear DAPI stain. Scale bar: 10 μm .

4.1.2.2 Desmin head mutants display perinuclear, cytoplasmic aggregates as well as normal filaments in 3T3, HL-1 cells

It has been shown in the past that mutant desmin variants which are not able to self-assemble into *bona fide* IFs *in vitro* also segregate from the endogenous vimentin cytoskeleton in 3T3 cells instead of forming heteropolymeric filaments and integrating into the pre-existing cellular IF network [BÄR et al. 2006]. To assess the ability of the desmin head mutants to integrate into preexisting IF networks, we employed murine 3T3 fibroblasts expressing endogenous vimentin and murine atrial cardiomyocyte cell line HL-1 expressing endogenous desmin.

In 3T3 cells, mutants DesS2I, DesS46Y and DesS46F formed extended cytoplasmic networks that integrate into the endogenous vimentin cytoskeleton, similar to those seen for wild-type desmin (FIGURE 16a-c, Supplementary FIGURE S7). Both DesS13F and DesR16C, however, segregated from the endogenous vimentin protein and, furthermore, caused the vimentin network to collapse and aggregate in the perinuclear region (FIGURE 16d-i).

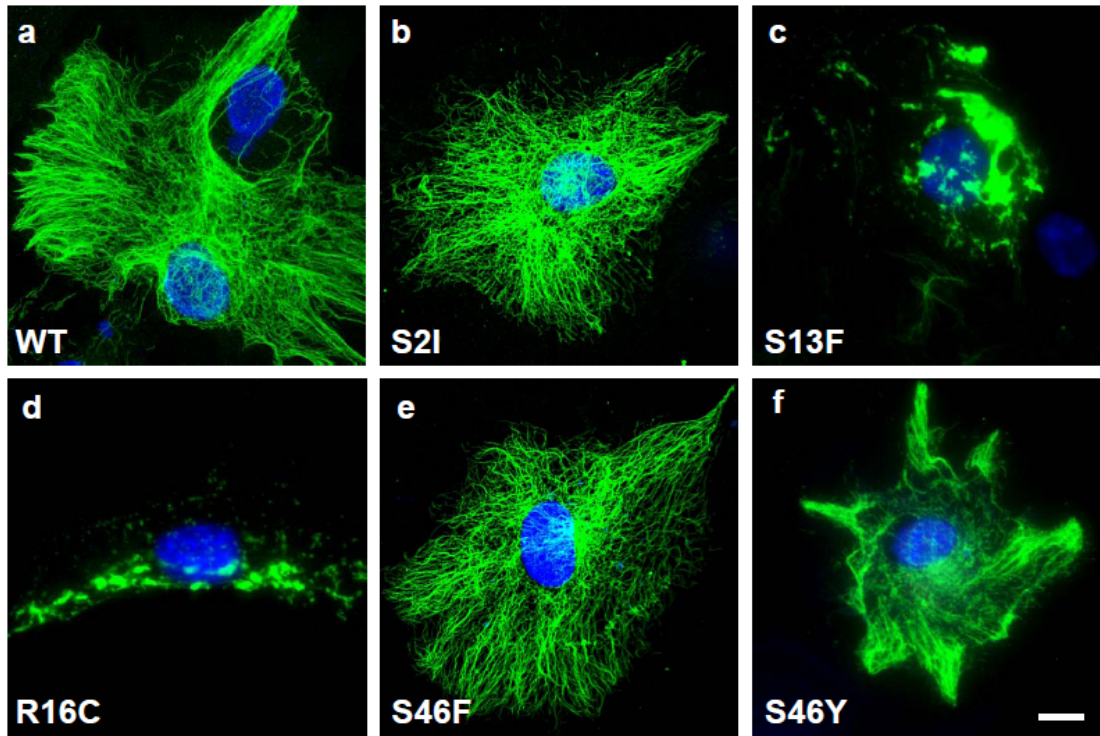


FIGURE 14 **Vim^{-/-} cells expressing DesS13F or DesR16C show aggregates in up to 15% of transfected cells**

Immunofluorescence images are shown for filaments formed by desmin head mutants in MEF Vim^{-/-} cells upon transfection. (a, b, e, f) All mutants form an extended desmin cytoskeleton as shown for DesWT, DesS2I, DesS46F and DesS46Y. (c, d) However, DesS13F and DesR16C also show aggregating behaviour in up to 12–15% of transfected cells. Green: transfected desmin variant, blue: nuclear DAPI stain. Scale bar: 10 μm.

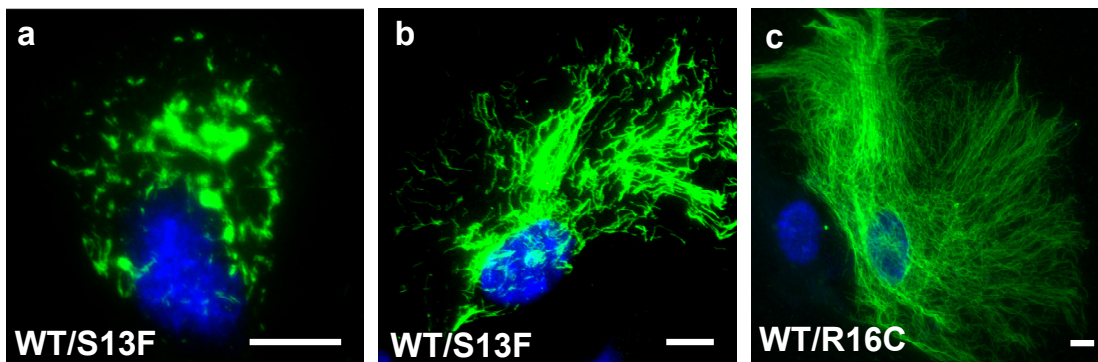


FIGURE 15 **Co-transfection in Vim^{-/-} cells**

Immunofluorescence images are shown for co-transfection of equal amount of wild-type and head mutation cDNA into MEF Vim^{-/-} cells. (a) For DesWT/DesS13F, approximately 15% of transfected cells show aggregate formation (b) alongside normal desmin filaments, whereas (c) DesR16C exhibits seemingly normal filaments in presence of wild-type desmin. Green: transfected desmin variant, blue: nuclear staining with DAPI. Scale bar: 10 μm.

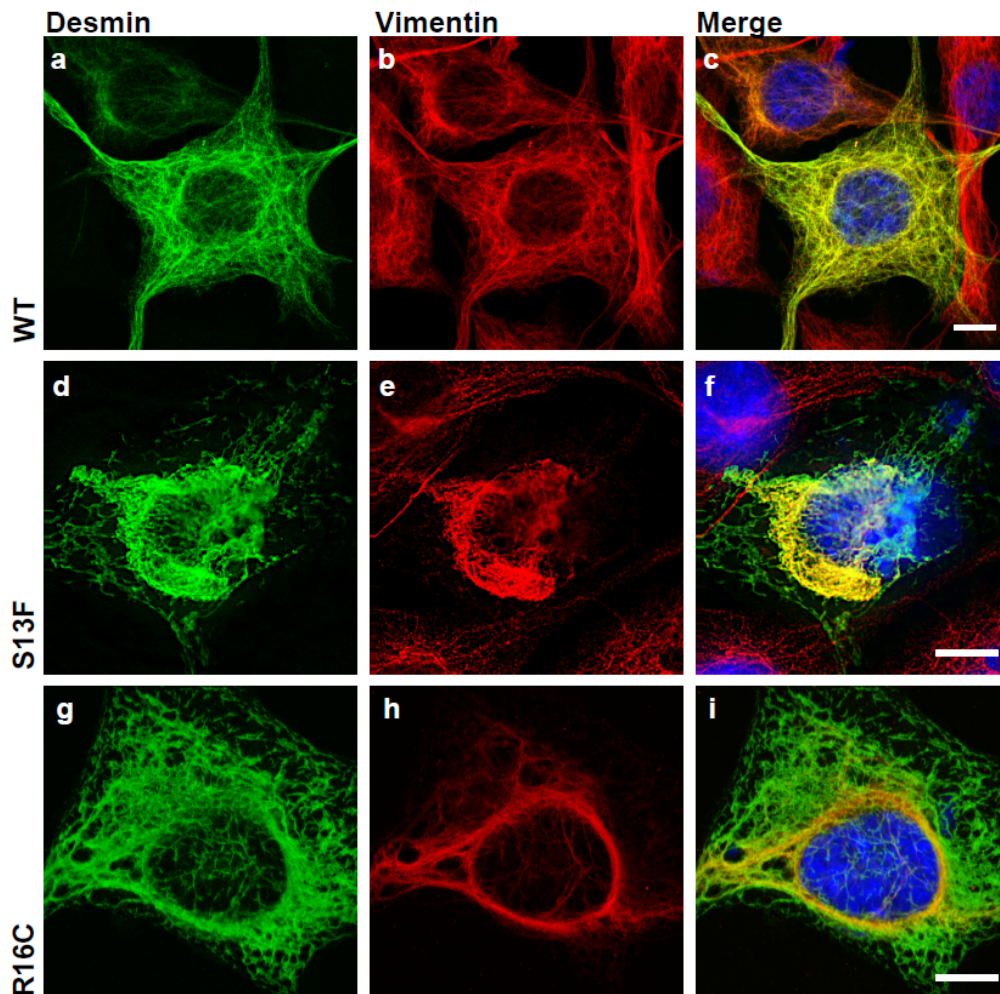


FIGURE 16 Perinuclear aggregates are observed for DesS13F and DesR16C in 3T3 cells

3T3 cells express endogenous vimentin but no desmin. (a-c) In cells transfected with wild-type desmin cDNA, extended cytoskeleton is observed, whereas (d-f) for S13F or (g-i) R16C desmin-positive aggregates are obtained. Note that for wild-type desmin (green), thorough co-localization with endogenous vimentin (red) is observed. Co-localization of desmin and vimentin is depicted in yellow for the merged image. For DesS13F and DesR16C, we observe segregation of desmin from vimentin cytoskeleton at the periphery and perinuclear aggregation of the endogenous vimentin along with desmin in all transfected cells. Green: desmin, red: vimentin, blue: nuclear DAPI stain. Scale bar: 10 μ m.

In HL-1 cells [CLAYCOMB et al. 1998], the co-polymeric situation can be investigated due to endogenously expressed wild-type desmin. The transfected cells can be identified by LMNB1-EYFP fluorescence due to co-transfection of both desmin and lamin B1. Upon transfection, a seemingly normal filamentous network was observed for all five desmin head mutants (*Supplementary FIGURE S8*). However, for cells expressing DesS13F, DesR16C, and DesS46F, we also observed that roughly 12–15% of transfected cells contained cytoplasmic aggregates of desmin (**FIGURE 17**).

Taken together, cell expression studies show that except for DesS2I, the remaining four mutants located in the head domain of desmin show altered filament-forming behaviour in one or more of the cell lines studied. Irrespective of the cellular background, this altered behaviour leads to the formation of proteinaceous aggregates of desmin, segregation from endogenous IFs and eventually to the collapse of endogenous IF networks in vimentin or desmin expressing cells.

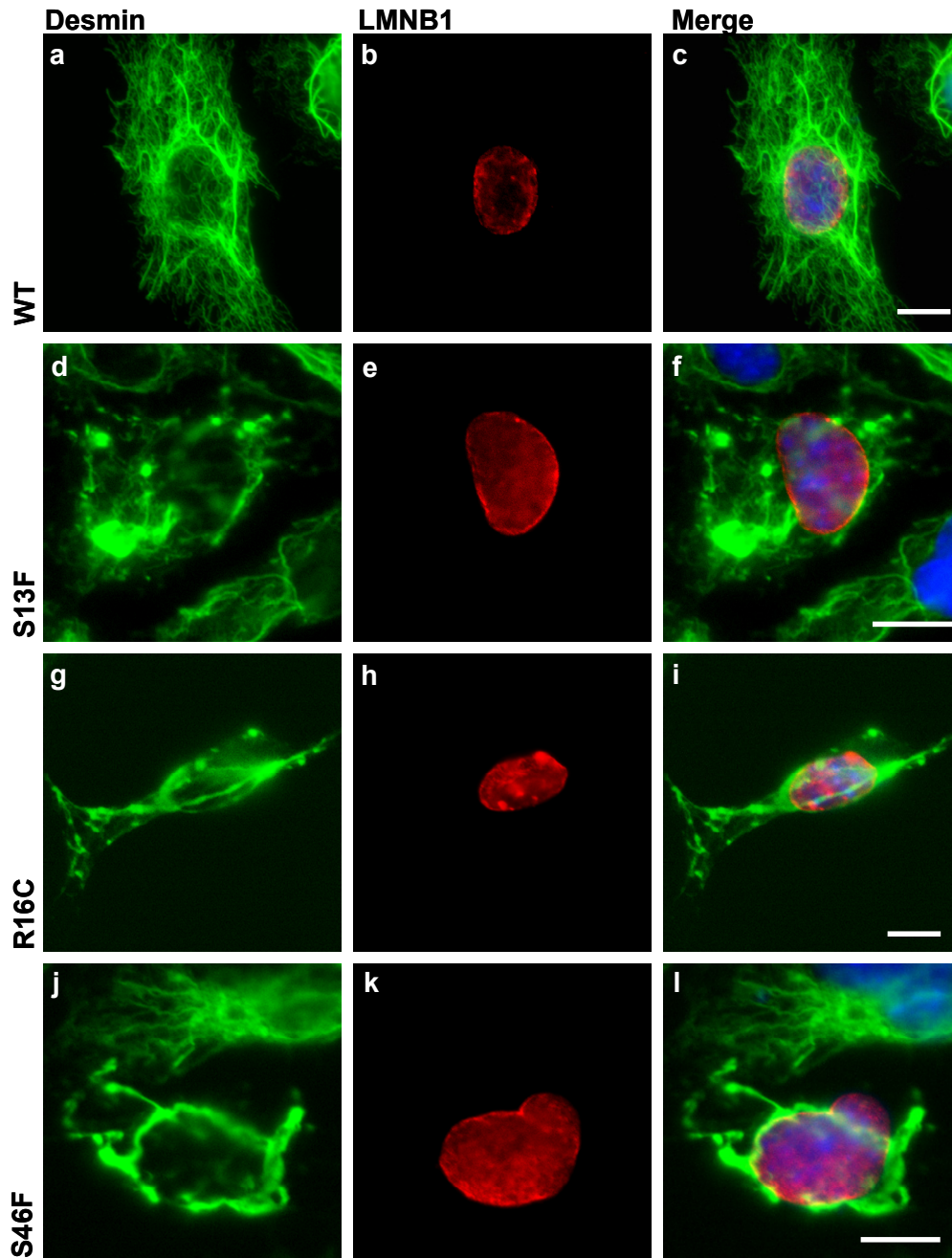


FIGURE 17 HL-1 cells transfected with S13F, R16C and S46F show cytoplasmic or perinuclear desmin aggregates in up to 15% of transfected cells

In HL-1 cells, transfected cells can be identified by LMNB1-EYFP fluorescence (red) due to co-transfection of both desmin and lamin B1. (e). (a-c) Cells transfected with wild-type desmin cDNA show an extended desmin cytoskeleton, whereas transfection of (d-f) S13F, (g-i) R16C or (j-l) S46F leads to formation of desmin-positive aggregates in up to 15% of transfected cells. For the mutant DesS46F, a collapsed perinuclear desmin cytoskeleton is reminiscent of the behaviour of DesS13F or DesR16C in 3T3 cells. Green: desmin, red: LMNB1-EYFP, blue: nuclear DAPI stain. Scale bar: 10 μ m

4.2 A novel homozygous mutation L377 Δ 22fs leads to the total absence of desmin in humans

The novel mutation L377 Δ 22fs was identified in two children of French consanguineous parents. Characterization of this desmin mutation was performed in collaboration with Dr. Ana Ferreiro (Inserm, Institute of Myology, Paris). The L377 Δ 22fs frame-shift mutation results in truncation of the last 83 amino acids of desmin, including the C-terminal end of coil 2B in rod domain and the entire tail domain, addition of nine new residues, and a premature stop codon insertion at aa position 386 (**FIGURE 18a**). Both parents and one son are heterozygous carriers with no clinical abnormalities. A homozygous out-of-frame desmin deletion in exon 6 was identified in 2 siblings. Interestingly, this mutation causes total desmin depletion in the muscle of the affected homozygous siblings, and it is not associated with desmin-positive aggregates commonly seen in desminopathy patients.

Our *in vitro* assembly studies indicate that the mutant DesL377 Δ 22fs likely interacts with wild-type desmin at the dimer level and tetramer level, as shown by oxidative cross-linking and AUC data, respectively (**Section 4.2.1.1 - 4.2.1.2**). It forms mature filaments at all stages of assembly in presence of wild-type desmin, whereas, it fails to form *bona fide* filaments on its own (**Section 4.2.2**). It fails to form an extended cytoskeleton in all four cell lines that were investigated, though to varying extents (**Section 4.2.3**). Furthermore, the truncated desmin variant is absent in the muscle of the heterozygous carrier mother and cannot be detected even when the proteasome degradation machinery is inhibited in the primary myotubes of the mother (**Section 4.2.4**). Based on our results, we propose that the mutant transcript is most likely downregulated by nonsense-mediated mRNA decay (NMD), hence no desmin-positive protein aggregate is seen in the muscle of homozygous siblings or the heterozygous mother.

4.2.1 DesL377 Δ 22fs apparently interacts with wild-type desmin at dimeric and tetrameric stages in vitro

4.2.1.1 Oxidative cross-linking shows that DesL377 Δ 22fs and wild-type desmin form heterodimers

To assess if DesL377 Δ 22fs interacts with wild-type desmin at the dimer level, oxidative cross-linking of the two proteins was performed. The mutant, wild-type and their equimolar mixtures were dialyzed step-wise from 8 M urea into “Tris buffer” ON and in freshly prepared “Tris buffer” without DTT the following day in order to remove the reductant. Cross-linking was done at a protein concentration of 0.4 mg/ml with 50 μ M H₂O₂/5 μ M CuCl₂ for 1 h at RT as described [ROGERS et al. 1996]. The cross-linked products were analyzed by SDS-PAGE, whereby the reductant DTT was omitted from the protein sample buffer. Desmin, like all other members of the type III IF proteins, contains a single cysteine residue at position 333 which is highly conserved across the animal species [SCHAFFELD et al 2001]. It can form disulfide cross-linked dimers within filaments [QUINLAN & FRANKE 1982]. If the mutant DesL377 Δ 22fs and the wild-type proteins are capable of interacting at dimer level *in vitro*, then we propose that they might also form an integrated desmin filament network in the myocyte of patient. Upon oxidative cross-linking of mutant and wild-type desmin at equimolar ratio, an additional band appeared at ~97 kDa (**FIGURE 18b**). This band summed up to the MW of wild-type desmin (~54 kDa) and mutant protein (~44 kDa) and was absent for either the wild-type or the mutant protein cross-linked alone. This suggests that

the mutant DesL377 Δ 22fs and wild-type desmin proteins are capable of interacting at the level of single molecule and, thus, form heterodimers when cross-linked through their cysteine residues.

4.2.1.2 AUC shows apparent interaction between dimers of DesL377 Δ 22fs and the wild-type desmin

Sedimentation behaviour of soluble assembly entities of mutant desmin or its equimolar mixture was compared to wild-type desmin alone by AUC. Our analysis shows that full length wild-type desmin sediments at a peak *s*-value of 5.3 S, indicating soluble tetrameric species [BÄR et al. 2006]. On the other hand, the mutant protein DesL377 Δ 22fs and its equimolar mixture sediment at 6.2 and 6.7 S, respectively, indicating formation of higher order complexes. As the AUC analysis was only performed once, we must interpret the close proximity of the sedimentation peak of the mixture to the mutant as well as the wild-type desmin cautiously. It indicates that the soluble species of DesL377 Δ 22fs and wild-type desmin might interact potentially to form heterotetramers (FIGURE 18c).

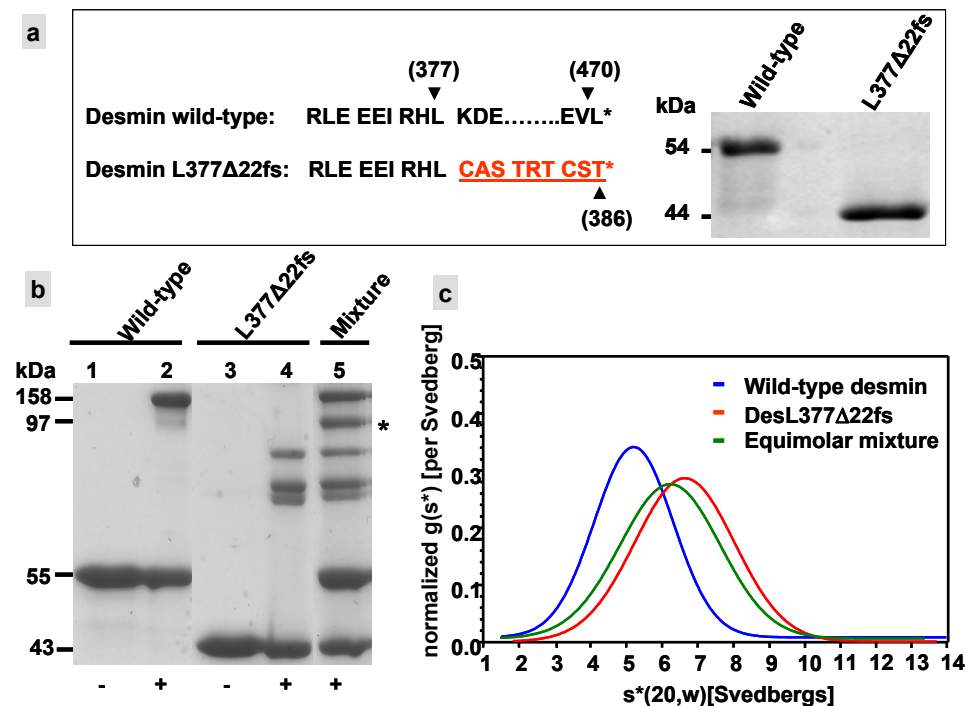


FIGURE 18 The novel desmin mutant DesL377 Δ 22fs and analysis of its interaction with wild-type desmin at dimer as well as tetramer level

(a) Position of the mutation for L377 Δ 22fs is depicted. The nine novel residues inserted in the mutant desmin are shown in red. As seen in the Coomassie-stained gel, the MW of recombinantly synthesized wild-type desmin corresponds to ~54 and of DesL377 Δ 22fs to ~44 kDa. (b) Oxidative cross-linking of the monomers of wild-type and DesL377 Δ 22fs was performed using the cross-linker 50 μ M H₂O₂ / 5 μ M CuCl₂ at RT for 1 h and the products were analyzed by SDS-PAGE. The Coomassie-stained gel shows an additional band in the mixture at ~97 kDa (marked, lane 5) which is absent for either the wild-type (lane 2) or the mutant protein (lane 4) cross-linked alone. This suggests interaction between wild-type and truncated mutant protein at the dimer level. Lane 1 and lane 3 depict non-cross-linked wild-type and mutant proteins, respectively. (c) AUC data suggest a possible interaction between DesL377 Δ 22fs and wild-type desmin protein at the tetramer level. This is because the sedimentation profile of the equimolar mixture (green) lies between that of the wild-type (blue) and truncated mutant protein (red). To make direct comparisons, area normalization was performed for different concentrations.

4.2.2 Analysis of DesL377 Δ 22fs alone and in equimolar mixture with wild-type desmin during in vitro assembly

Starting with tetrameric assembly precursors in “Tris-buffer” at 0 s, DesL377 Δ 22fs formed adhering filamentous structures at 2 s as observed by EM (FIGURE 19a, b). Moreover, this mutant showed assembly incompetence at advanced stages by forming aggregates as seen at 5 min (FIGURE 19c). Remarkably, for the assembled equimolar mixture of wild-type desmin and mutant protein, an extended filament network was observed at all time points (data not shown). This indicates that the mutant DesL377 Δ 22fs does not exert a dominant-negative effect on wild-type protein in terms of filament formation. Nevertheless, we measured significant differences in filament diameter for equimolar mixture (15.2 ± 1.1 nm) and wild-type desmin (10.9 ± 0.7 nm) after 1 h of assembly (FIGURE 19d). For width measurement, the EM images were processed in ImageJ 1.32j and at least 100 measurements were carried out per sample. Viscometry analyses of assembled proteins show that the relative viscosity of mutant and equimolar mixture is severely reduced as compared to desmin wild-type alone, suggesting lack of proper network due to aggregate formation and enhanced filament adhesiveness (FIGURE 19e). Accordingly, a 3:1 ratio of wild-type and mutant protein is required to normalize the viscosity profile. Thus, our data suggest that even though the filaments of equimolar mixture of mutant DesL377 Δ 22fs and desmin wild-type appear normal in EM, they exhibit altered filament width and viscosity profile corresponding to modified intrafilamentous architecture and bulk solution properties, respectively.

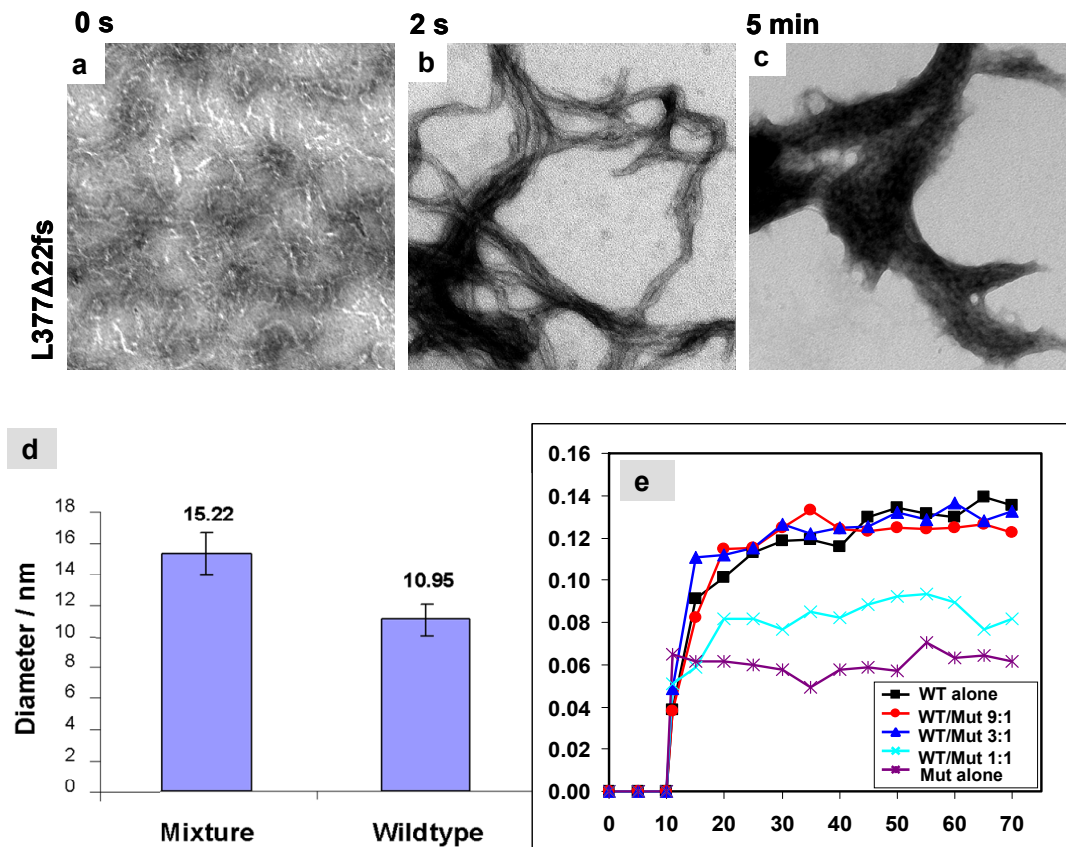


FIGURE 19 Assembly of DesL377 Δ 22fs alone and as equimolar mixture with wild-type desmin (Please refer to figure legend on next page)

FIGURE 19 Assembly of DesL377 Δ 22fs alone and as equimolar mixture with wild-type desmin

(a-c) Electron micrographs for negatively stained samples of DesL377 Δ 22fs is shown for three time points: 0 s, 2 s and 5 min. (a) For the time point 0 s, samples dialyzed in “Tris-buffer” are mounted directly on carbon-coated grids. (b) For time points 2 s and (c) 5 min, assembly was performed at 37°C by addition of an equal volume of “assembly buffer” (100 mM NaCl, 40 mM Tris-HCl, pH 7.0 at 37°C) and stopped by adding 0.1% glutaraldehyde at 2 s and 5 min, respectively. The mutant protein alone forms aggregates at 5 min. Scale bar: 100 nm. (d) The filament diameter of 15.22 nm for the equimolar mixture is higher than that of wild-type desmin filament at 10.95 nm. The EM images were processed in ImageJ 1.32j for diameter measurement. At least 100 measurements were carried out per sample and the graphs were generated in Excel 2003. (e) Relative viscosity of assembled DesL377 Δ 22fs protein drops below 50% to that of wild-type desmin. A 3:1 ratio of wild-type desmin:mutant protein restores the viscosity to normalcy. Abscissa: time (min), ordinate: relative viscosity, WT: wild-type desmin, Mut: L377 Δ 22fs desmin.

4.2.3 Disrupted IF cytoskeleton is observed in cells expressing DesL377 Δ 22fs

Further, the filament-forming behaviour of DesL377 Δ 22fs was analyzed in cells either devoid of type III cytoplasmic IF proteins (SW13 and MEF Vim^{-/-}) or those expressing the same (3T3 and HL-1 cells; **FIGURE 20**). In SW13 and MEF Vim^{-/-} cells, the transfection of L377 Δ 22fs resulted in formation of aggregates and short fibers, respectively. In 3T3 cells, our transfection data show that the mutant protein failed to form heteropolymers with endogenous vimentin and segregated to form desmin aggregates without severely disrupting the vimentin cytoskeleton. In HL-1 cells, mostly perinuclear aggregates of mutant and endogenous desmin protein were observed. This indicates the dominant-negative effect of the mutant desmin on endogenous desmin cytoskeleton of HL-1 cells.

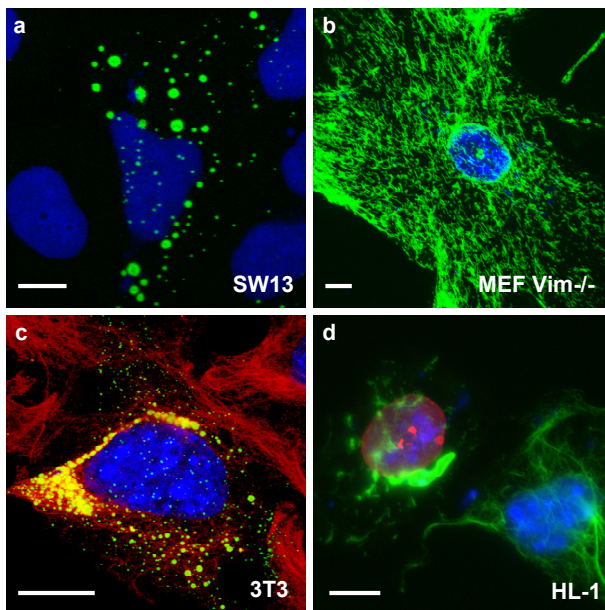


FIGURE 20 Impact of expressing DesL377 Δ 22fs in different cell lines

Mutant DesL377 Δ 22fs forms aggregates both in cells devoid of and cells expressing endogenous type III IF protein, as shown for (a) SW13, (b) MEF Vim^{-/-}, (c) 3T3 and (d) HL-1 cells. In HL-1 cells, transfected cells can be differentiated from non-transfected cells due to co-transfection of L377 Δ 22fs with LMNB1-EYFP. Note, in MEF Vim^{-/-} cells, no aggregates are formed. Instead, short filamentous structures spanning the entire cytoplasm were observed. Green: desmin, red: vimentin / LMNB1-EYFP, blue: nuclear DAPI stain. Scale bar: 10 μ m.

4.2.4 Mutant protein DesL377 Δ 22fs is not detectable in myotubes of heterozygous mother even after inhibiting the proteasome

The ubiquitin proteasome machinery is critical to cellular function for removal of misfolded or aggregated proteins [CIECHANOVER et al. 2000]. Absence of expression of the mutant desmin in the homozygous children or their heterozygous mother could be attributed to a rapid degradation by the

proteasome system. To elucidate this hypothesis, we performed Western-blots on primary myotubes from a skeletal muscle biopsy of heterozygous mother, the myoblasts from homozygous patients being unavailable. The myoblasts were induced to differentiate into myotubes for 2 weeks in culture and incubated in the absence or presence of two proteasome inhibitors - 60 μ M lactacystin for 7 h or 10 μ M epoxomicin for 22 h - at 37°C. The cells were harvested and the whole cell lysate was probed against suitable antibodies to detect the truncated protein DesL377 Δ 22fs. We used a desmin monoclonal antibody that specifically binds to its N-terminus (DK26), thus detecting the truncated DesL377 Δ 22fs recombinant protein, and another that specifically binds to C-terminus of desmin (Epitomics), thus failing to detect DesL377 Δ 22fs. We found that the inhibition of proteasome by lactacystin or epoxomicin did not lead to the detection of truncated desmin protein in our assays (**FIGURE 21**). This indicates that rapid proteasomal degradation is unlikely to be the underlying cause for absence of mutant desmin in the myotubes of the heterozygous mother. Instead, mechanisms that control protein expression already at RNA level, for instance NMD, most likely inhibit the expression of the mutant DesL377 Δ 22fs. Further investigations need to be done in order to resolve this issue.

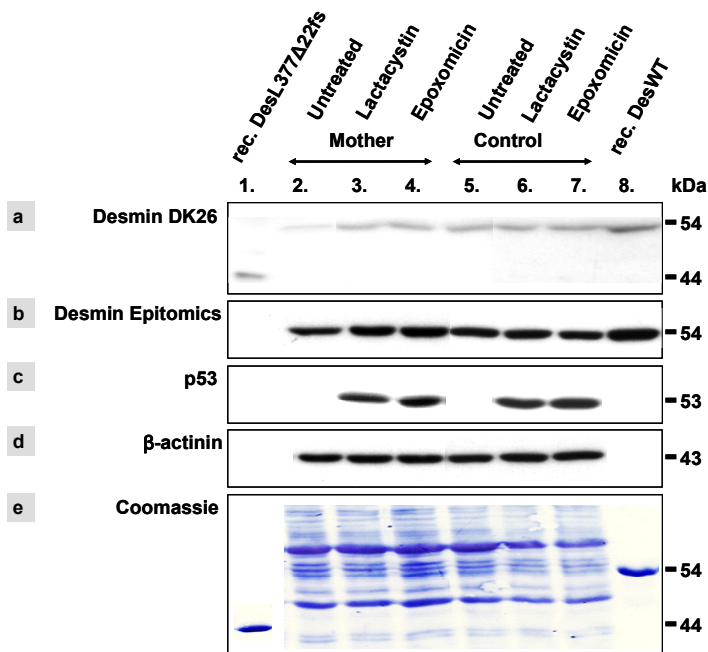


FIGURE 21 Inhibition of proteasomal degradation machinery does not lead to detection of DesL377 Δ 22fs in myotubes of heterozygous mother

To elucidate if the absence of expression of the mutant desmin DesL377 Δ 22fs in the heterozygous mother occurs due to rapid degradation by the proteasome system, we performed Western-blot on primary myotubes of heterozygous mother. The myoblasts were induced to differentiate into myotubes for 2 weeks in culture and incubated in the absence or presence of two proteasome inhibitors - 60 μ M lactacystin for 7 h or 10 μ M epoxomicin for 22 h - at 37°C. As a control, myotubes of heterozygous mother and a healthy individual were treated with same volume of solvent (water/DMSO) in which the proteasome-inhibitor had been dissolved. The cells were harvested and the whole cell lysate was probed against suitable antibodies to detect the truncated protein DesL377 Δ 22fs. (a) DK26 is a monoclonal desmin antibody that specifically binds to its N-terminus, thus detecting the truncated DesL377 Δ 22fs recombinant protein in lane 1. However, no truncated protein is observed in the heterozygous mother (lanes 2-4) or healthy control (lanes 5-7). Note the desmin expression is visibly reduced in untreated mother (lane 2) compared to untreated control (lane5). (b) Epitomics antibody specifically binds to C-terminus of desmin, hence the recombinant DesL377 Δ 22fs is not detectable in lane 1. (c) Enhanced p53 expression in patient and healthy myotubes corresponds to inhibition of proteasome degradation machinery. (d, e) β -actinin level and Coomassie staining demonstrate that equal amount of protein was loaded for each sample. rec: recombinant.

4.3 The truncated desmin variant Des(ESA) Δ C244 has deleterious effects on filament assembly

A report studied a mutant desmin Des(ESA) Δ C244 that caused desminopathy in humans. Here, desmin-positive aggregates were observed in isolated muscle fibres of affected patient as well as upon transfection in SW13 cells or BHK21 cells that express desmin, vimentin and keratin IFs [SCHRÖDER et al. 2003]. Four years later, a correction in the sequencing for this human mutation was published that showed a loss of a single lysine residue at aa 240 instead of a premature stop codon [SCHRÖDER et al. 2007]. In spite of Des(ESA) Δ C244 not being a true desmin mutant, we analyzed this originally published truncated desmin variant for filament assembly *in vitro* because it virtually corresponds to the “first half” of the 476 aa long desmin molecule [BÄR et al. 2009]. Based on molecular size alone, a 240 amino acids long fragment is slightly larger than the numerical “first half” of desmin, which would contain 235 amino acids. However, it does not enclose the entire coil 1B and breaks up one heptad before the supposed end of coil 1B [HERRMANN & AEBI 2004]. The novel last three amino acids in Des(ESA) Δ C244, Glu-Ser-Ala, fit well into a coiled-coil topology. They replace Lys-Leu-His, which are in f, g and a position of the heptad. We analyzed the assembly behaviour of this desmin variant both alone and in equimolar mixture with desmin wild-type. Also, we examined its ability to form *de novo* filaments in SW13 cells or to integrate into preformed type III IF cytoskeleton of 3T3 and HL-1 cells using a mouse monoclonal antibody (DK8, DK26) that specifically recognizes the truncated protein. In addition to the five residues from wild-type desmin sequence, the epitope of this antibody (IAFLKESA) consists of three aa residues “ESA” found exclusively in this truncated variant.

Consistently, we observed that in contrast to WT desmin, Des(ESA) Δ C244 protein precipitates in higher amounts as soon as urea concentration is lowered to 2 M during step-wise dialysis from 8 M urea into “Tris-buffer” (5 mM Tris-HCl, 1 mM EDTA, 0.1 mM EGTA, 1 mM DTT, pH 8.4). Thus, we analyzed this variant in “Tris-buffer” without salt addition by EM. Wild-type desmin forms tetrameric precursors under these conditions. For Des(ESA) Δ C244, “peanut”-shaped aggregates ~120–150 nm long and ~20–30 nm wide as well as roundish aggregates with a diameter of ~30 nm were the two representative structures observed in “Tris-buffer” (**FIGURE 22a**). Upon addition of equal volume of “assembly buffer”, Des(ESA) Δ C244 exhibited thick extended fibrous structure of irregular diameter at 60 min (**FIGURE 22b**). This was most likely formed by annealing of both the round and the “peanut”-shaped precursors seen in “Tris-buffer”. For equimolar mixture of Des(ESA) Δ C244 with WT desmin, “peanut”-shaped aggregates, of similar dimensions as mentioned above, merging with WT desmin filaments were distinctly visible at 60 min (**FIGURE 22c**). Hence, under assembly conditions, Des(ESA) Δ C244 resembling “first half” of desmin molecule is capable of interacting with wild-type desmin in a conservative manner, as seen by intact “peanut”-shaped structures that fuse to WT desmin filaments.

The impact of expressing Des(ESA) Δ C244 in SW13, 3T3 and HL-1 cells was evaluated by transfection (**FIGURE 22d-f**). Transient transfection in SW13 cells showed formation of Des(ESA) Δ C244-positive aggregates that were confined to the nucleus without alteration of nuclear size or shape. Few granules were occasionally located in the cytoplasm, and a small population of short filamentous fragments was also observed. In 3T3 fibroblasts, Des(ESA) Δ C244 formed both nucleoplasmic and cytoplasmic desmin-positive aggregates. Most notably, Des(ESA) Δ C244 network caused a severe reorganization of the endogenous vimentin IF network in 3T3 cell by displacing it. Des(ESA) Δ C244-positive deposits did not induce the collapse but largely segregated from the vimentin network. The integrity of nuclear envelope

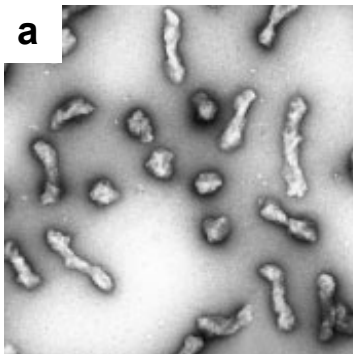
was not affected in these transfected cells. This was confirmed by normal staining of nuclear envelope-specific proteins, such as lamin B receptor and lamin A (data not shown). A phenotype similar to 3T3 cells was observed in HL-1 cells, where the endogenous desmin cytoskeleton exhibited a severe reorganization and the Des(ESA) Δ C244-positive aggregates apparently segregated from the endogenous desmin network. However, in HL-1 cells, Des(ESA) Δ C244 protein did not appear in the nucleoplasm but was concentrated as small aggregates in the perinuclear region. Using a monoclonal antibody (DK8, DK26) that specifically recognizes the truncated protein Des(ESA) Δ C244, we could distinguish its localization in transfected HL-1 cells from that of endogenous WT desmin which was detected by a rabbit monoclonal antibody (Epitomics #1466-1).

Because of the drastic behaviour of Des(ESA) Δ C244, both *in vitro* and in transfected cells, as an extension of this study, assembly behaviour of various amino-terminal fragments was also investigated [BÄR et al. 2009]. Here, the molecular properties of desmin amino-terminal fragments that span the end of coil 1B, the linker L12, or even reach into coil 2 were followed up. The desmin amino terminal fragment Des Δ C265 and the carboxy-terminal fragment Des Δ N264, which are generated by caspase cleavage in linker L12, were also analyzed. These data indicate that such large IF protein fragments have a strong potential to interfere with filament formation and network integrity both *in vitro* and in cells

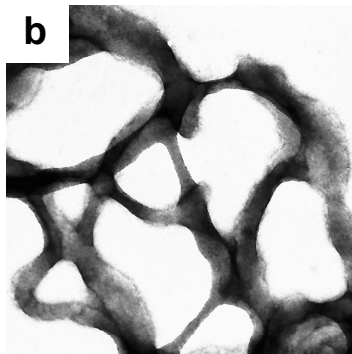
In summary, despite the fact that Des(ESA) Δ C244 interacts with WT desmin to a limited extent during assembly *in vitro*, expression of Des(ESA) Δ C244 appears to be “noxious” to cytoplasmic IF system of 3T3 and HL-1 cells. Here, it interferes with the organization of endogenous cytoskeleton by forming aggregates. Furthermore, Des(ESA) Δ C244 enters the nucleus of SW13 and 3T3 cells and forms nucleoplasmic aggregates, but it does not alter the integrity of nuclear envelope in these cells.

In vitro assembly:

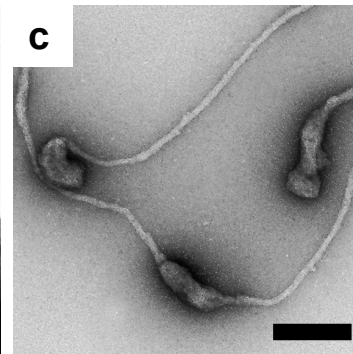
Des(ESA) Δ C244 in
"Tris-buffer"



Des(ESA) Δ C244
assembled for 60 min



Mixture assembled
for 60 min



Transfection in cells:

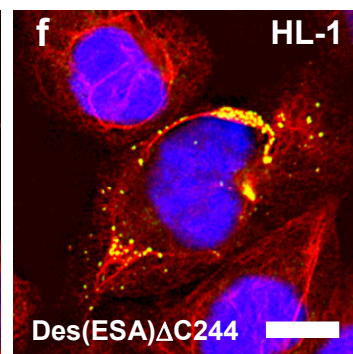
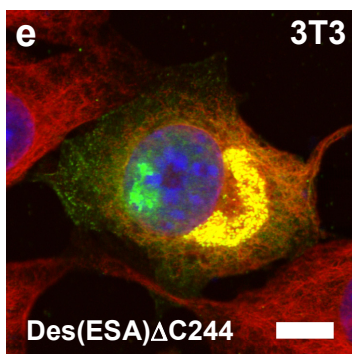
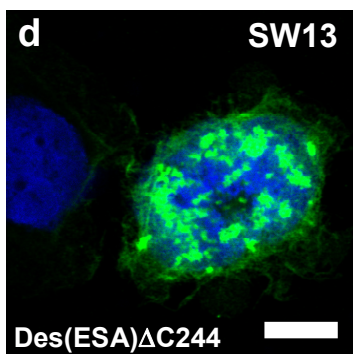


FIGURE 22 Interference of amino-terminal desmin fragment Des(ESA) Δ C244 with desmin filament formation

(a-c) Electron micrographs of negatively stained structures of Des(ESA) Δ C244 alone and in equimolar mixture with desmin wild-type. (a) "Pea"- and "peanut"-shaped aggregates of Des(ESA) Δ C244 are obtained after reconstitution into "Tris-buffer" (5 mM Tris-HCl, 1 mM EDTA, 0.1 mM EGTA, 1 mM DTT, pH 8.4). These structures are ~120–150 nm long ("peanuts") and have a diameter of ~20–30 nm. (b, c) Upon assembling, Des(ESA) Δ C244 forms extended thick filaments alone and for equimolar mixture "peanut"-shaped aggregates merging with WT desmin filaments are visible. Assembly was performed at 37°C by addition of equal volume of "assembly buffer" (100 mM NaCl, 40 mM Tris-HCl, pH 7.0 at 37°C) and stopped by adding 0.1% glutaraldehyde at 60 min. Scale bar: 100 nm. (d) Expression of Des(ESA) Δ C244 in SW13 cells leads to formation of mostly nucleoplasmic aggregates as shown in green. (e) In 3T3 cells, nucleoplasmic and cytoplasmic aggregates are formed (green: Des(ESA) Δ C244, red: endogenous vimentin). (f) In HL-1 cells, only cytoplasmic aggregates are seen for Des(ESA) Δ C244 (green: Des(ESA) Δ C244, red: endogenous desmin). Des(ESA) Δ C244 interferes with the organization of endogenous cytoskeleton in 3T3 and HL-1 cells. Using a monoclonal antibody (DK8, DK26) that specifically recognizes the truncated protein Des(ESA) Δ C244, we could distinguish its localization in transfected HL-1 cells from that of endogenous WT desmin which was detected by a rabbit monoclonal antibody (Epitomics #1466-1). Blue: nuclear DAPI stain. Scale bar: 10 μ m.

4.4 The majority of desmin tail mutants exhibit undisturbed filament morphology both *in vitro* and in cell lines

Previous investigations have revealed the impact of six desmin tail mutants – DesT442I, DesK449T, DesI451M, DesR454W, Des460I and DesV469M - on filament properties ([BÄR et al. 2007]; *Supplementary FIGURE S10*). Other than DesR454W, all mutants assembled into *bona fide* filaments *in vitro*. When co-assembled with wild-type desmin, these mutants revealed filament-formation competence. Remarkably, DesK449T, which formed extended filaments alone, exhibited a dominant-negative effect on wild-type desmin assembly by simultaneously forming ULF-like structures and highly irregular filaments. In SW13 cells, except for DesR454W and DesS460I that failed to form filaments, all other desmin tail mutants were capable of forming *de novo* filaments. All these mutants also showed incorporation into the IF skeleton of C2C12 cells. The filament forming ability of most desmin tail mutants is surprisingly preserved both *in vitro* and in cells, yet desmin-positive aggregates are observed in desminopathy patients harbouring these mutations.

To gain novel insight into network forming property of desmin tail mutants *in vitro*, we slightly modified the assembly protocol. Here, instead of the standard protein concentration of 0.4 µg/µl, we assembled the recombinantly synthesized desmin tail mutant proteins at 1 µg/µl. After ON dialysis in “Tris-buffer” (5 mM Tris–HCl pH 8.4, 1 mM EGTA, 0.1mM EGTA and 1 mM DTT), all samples were assembled by adding equal volume of “assembly buffer” (40 mM Tris–HCl, 100 mM NaCl, pH 7.0) at 37 °C for 1 h. After fixation and dilution of the samples to 0.1 g/l, filaments were negatively stained and analyzed by EM. Furthermore, to gain novel insight into network forming property of desmin tail mutants in cellular systems, we used two cell lines – MEF Vim^{-/-} and HL-1 - to express the six desmin tail mutants by transfection. In MEF Vim^{-/-} cells, derived from mouse embryonic fibroblasts of vimentin knockout mice, no type III IF protein is expressed, similar to SW13 cells. However, for SW13 cells it has been previously shown that transfection with cDNA coding for wild-type desmin does not always lead to extended desmin network formation [BÄR et al. 2006]. Most likely, these cells lack certain, as yet unknown, IF-associated proteins and factors required for proper network formation. On the other hand, MEF Vim^{-/-} cells exhibit an elaborate cytoskeleton for wild-type desmin, emphasizing the suitability of these cells for assessment of *de novo* IF network formation. HL-1 cells are derived from mouse atrial cardiomyocyte tumor lineage and express endogenous desmin. They can be repeatedly passaged and yet maintain the ability to contract and retain differentiated morphological features of a cardiomyocyte [CLAYCOMB et al. 1998]. Hence, they are superior to C2C12 mouse myoblasts for evaluating the ability of desmin mutants to integrate into preformed desmin network. C2C12 cells, though express muscle-specific desmin, unlike HL-1 cells they do not show typical functional and morphological features of a cardiomyocyte.

When assembled at a starting protein concentration of 1 µg/µl, all desmin tail mutants, except DesR454W, were able to form extended filamentous networks (**FIGURE 23a, b**). DesR454W exhibits defective longitudinal annealing as only short filamentous structures are observed for this desmin mutant. Upon co-polymerization with an equimolar ratio of wild-type desmin, most mutants are capable of filament formation. However, for the equimolar mixture of DesK449T and wild-type protein short and irregular filaments of varying lengths were observed (**FIGURE 23c**). Thus, as compared to previous data, no difference in the assembly property of desmin tail mutants was observed even when the proteins were assembled at a higher concentration of 1 µg/µl.

With respect to the behaviour of desmin tail mutants in MEF Vim^{-/-} cells, all mutants, except DesR454W, were able to form filamentous network comparable to those of wild-type desmin (**FIGURE 23d, g**). DesR454W formed only short filamentous structures distributed all over the cytoplasm. These short filamentous structures failed to fuse to form a full network. Upon co-transfection with wild-type desmin in these cells, all mutants, including DesR454W but excluding DesK449T formed filamentous networks (**FIGURE 23e, h**). In combination with wild-type desmin, DesK449T formed short filamentous particles and aggregates that were dispersed all over the cytoplasm, comparable to those seen for DesR454W alone. These transfection data corroborate the *in vitro* assembly data, where we observed assembly incompetence for DesR454W alone or for the mixture of desmin wild-type and DesK449T proteins.

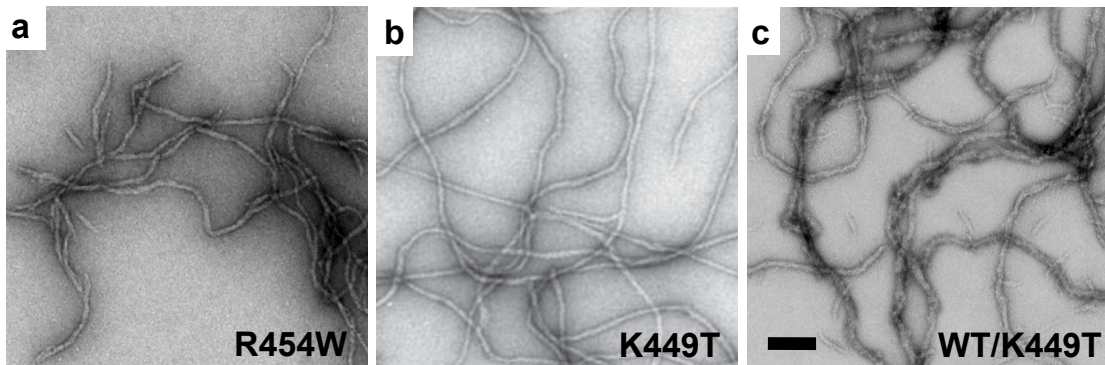
As for the impact of desmin tail mutants on the authentic desmin network of HL-1 cells, all mutants including DesR454W and DesK449T, were able to integrate into the endogenous desmin network (**FIGURE 23f, i**). This might be explained by a low expression level of mutant desmin in HL-1 cells or by the protective effect of chaperones expressed in these cells. These data comply with the transfection data obtained for desmin tail mutants in C2C12 cells, where all investigated desmin tail mutants formed filaments. Hence, cultured myoblasts expressing a robust desmin cytoskeleton are probably able to neutralize the “deleterious” effect of mutated proteins. Of note, aggregates were seen for S460I in SW13 cells [BÄR et al. 2007], but no such aggregates are observed in Vim^{-/-} cells. This indicates that the factors required for formation of filaments are more preserved in Vim^{-/-} cells as compared to SW13 cells.

In summary, our investigations reveal that only two out of the six desmin tail mutants – DesR454W and DesK449T - form abnormal filaments upon *in vitro* assembly and correspondingly generate abnormal filaments in MEF Vim^{-/-} cells. Thus, we propose that abnormal desmin-positive aggregates seen in the myocyte of desminopathy patients harbouring these mutations are likely caused by aberrant interaction of desmin tail variants to their binding partners that might modulate its cellular function.

FIGURE 23 Desmin tail mutants DesR454W and DesK449T showed disturbed filament formation *in vitro* and in Vim^{-/-} cells (Please refer to figure on next page)

(a-c) Electron micrographs of negatively stained samples of desmin tail mutants assembled for 60 min are shown. Assembly was performed at a concentration of 1.0 µg/µl. DesR454W only assembles into short filamentous structures, whereas DesK449T is able to form an extended filament network. In the heteropolymeric situation, DesK449T no longer assembles into extended filamentous networks. Instead, it forms ULF-like short structures indicating a disturbed longitudinal annealing. It also forms extended but highly irregular filaments that indicate disturbed radial compaction. Hence, DesK449T mutant protein exerts a dominant-negative effect on wild-type desmin assembly. Scale bar: 100 nm. (d, g) Transfection studies in MEF Vim^{-/-} cells show short filamentous structures distributed across entire cytoplasm for DesR454W, whereas an extended network is seen for DesK449T. (e, h) Upon co-transfection with wild-type desmin, DesR454W assembles into normal filamentous networks, whereas DesK449T forms intracellular aggregates. (f, i) In HL-1 cells, DesR454W and DesK449T can integrate into the endogenous desmin filament network. In HL-1 cells, transfected cells can be differentiated from non-transfected endogenous desmin-expressing cells due to co-transfection of mutant and LMNB1-EYFP. Green: desmin, blue: nuclear DAPI stain, red: LMNB1-EYFP. Scale bar: 10 µm.

***In vitro* assembly:**



Transfection in cells:

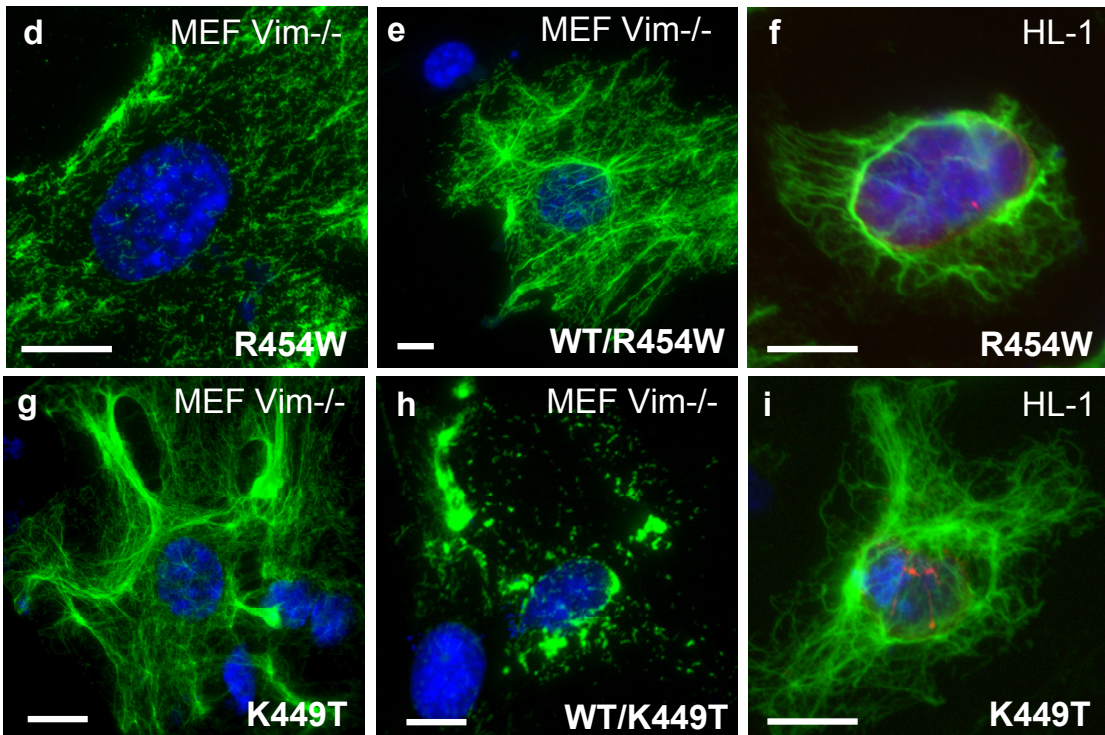


FIGURE 23 Tail mutants - DesR454W and DesK449T - show disturbed filament formation *in vitro* and in Vim^{-/-} cells

Interaction of desmin with α B-crystallin

- 5.1 α B-crystallin is the major binding partner of desmin by yeast two-hybrid analysis**
- 5.2 Oligomers of α B-crystallin sediment at 17 S as a complex comprising ~22 subunits**
- 5.3 Binding properties of α B-crystallin to desmin under different buffer conditions**
- 5.4 Binding of α B-crystallin to desmin is enhanced by lowering the pH and ionic strength of “Tris-NaCl” buffer system and on increasing the assembly temperature**
- 5.5 The C-terminal domain of desmin modulates the binding of α B-crystallin to desmin filaments**
- 5.6 Binding of α B-crystallin to desmin is influenced by the desmin filament architecture**
- 5.7 Desminopathy mutations influence the interaction of desmin with α B-crystallin**

5.1 α B-crystallin is the major binding partner of desmin by yeast two-hybrid analysis

In humans, specific association of α B-crystallin with glial fibrillary acidic protein, a type III IF protein, was identified more than two decades ago in Alexander's disease. Here, aggregates of α B-crystallin and GFAP are present in astrocytes within the so-called "Rosenthal fibres" [IWAKI et al. 1989]. In NIH 3T3 cells, recruitment of α B-crystallin to vimentin, another type III IF protein, was detected upon incubation at elevated temperature of 44°C or after addition of sodium arsenite to these cells [KLEMENZ et al. 1991]. A specific interaction of purified desmin with α B-crystallin was shown in the early 1990s by means of slow speed centrifugation procedure [BENNARDINI et al. 1992]. These data show that in the absence of desmin, α B-crystallin could not be sedimented even by high-speed centrifugation (150,000g for 30 min) at any condition of pH, temperature, or ionic strength. However, after incubation with desmin at pH 7.5 and 37°C for 30 min, approximately half of the total α B-crystallin was recovered in the pellet at low-speed centrifugation (3,000g for 10 min), together with desmin filaments. Association of desmin with α B-crystallin was shown in case of the CRYAB R120G mutation that cosegregates with desmin-related myopathy [VICART et al. 1998]. Muscle fibres of affected patients show proteinaceous aggregates that stain positive for both desmin and α B-crystallin. Muscle cell lines, like C2.7 (myoblasts) and BHK21 (kidney smooth muscle cells), upon transfection with the CRYAB R120G cDNA also show intracellular aggregates consisting of both desmin and α B-crystallin as observed in muscle fibres from DRM patients. Over the years, it has been shown that in normal tissues, α B-crystallin interacts directly with a number of filament proteins, such as phakinin, filensin, desmin, GFAP, vimentin, and actin. It is proposed that α B-crystallin functions in the organization and stabilization of diverse filament networks formed by these proteins [GHOSH et al. 2007].

To determine the subcellular localization of desmin and α B-crystallin in primary cultures of rat cardiomyocytes as well as in cultured cells, such as 3T3 and C2C12 used in this thesis, we stained them with monoclonal antibodies specific for desmin and α B-crystallin (**TABLE 5**). Consistent with previous findings, we saw that desmin and α B-crystallin co-localize along Z-bands in cardiomyocytes (**FIGURE 24a-d**). We also found that α B-crystallin co-localizes with endogenous vimentin and with transiently expressed desmin in 3T3 cells, even though the endogenous expression level of α B-crystallin in these cells is fairly low as compared to cardiomyocytes (**FIGURE 24e-h**). In C2C12 cells expressing endogenous desmin, we also saw a co-localization of α B-crystallin with desmin (data not shown).

For yeast two-hybrid (Y2H) screening, nucleotides coding for the last 67 amino acids of desmin (Des Δ N403) were used as bait. As discussed before, the head and rod domains of desmin molecule are essential to the formation of dimers and higher order structures, respectively. On the other hand, the tail domain does not seem to play a critical role in the formation of filaments, because tailless desmin is capable of forming filaments [HERRMANN et al. 1996]. Thus, we speculated that the tail domain of desmin might have a role in binding to its interaction partners at subcellular level. Based on this assumption, a construct coding for the last 67 aa residues of desmin from the C-terminus and starting at the motif TYRKLLEGEE were used as bait for Y2H screening. The screening was performed against libraries of the human heart, skeletal muscle and smooth muscle from aorta by Dr. Manfred Kögl (Core Facilities, DKFZ).

The Y2H screening shows that the C-terminus of desmin interacts with α B-crystallin. These two partners have been identified in as many as five different screenings performed at the DKFZ core facility, and in

the current screening CRYAB was identified as many as 60 times (**TABLE 4**). Smoothelin - a cytoskeletal protein for smooth muscles - and H1FO - a member of the histone family of nuclear proteins - were also identified as potential interactors of desmin, though with a low score than CRYAB. In addition, FHOD1 - formin homology 1,2 domain-containing protein 1 - and MYBPC1- myosin-binding protein C, slow-type - two proteins that are binding to numerous other baits, also showed up in the screening but these appear to bind rather non-specifically to various other cellular partners as shown by their high “prey promiscuity” score.

Taken together, desmin and α B-crystallin co-localize in cells and the Y2H data support a strong interaction between the C-terminal of desmin and N-terminal of α B-crystallin.

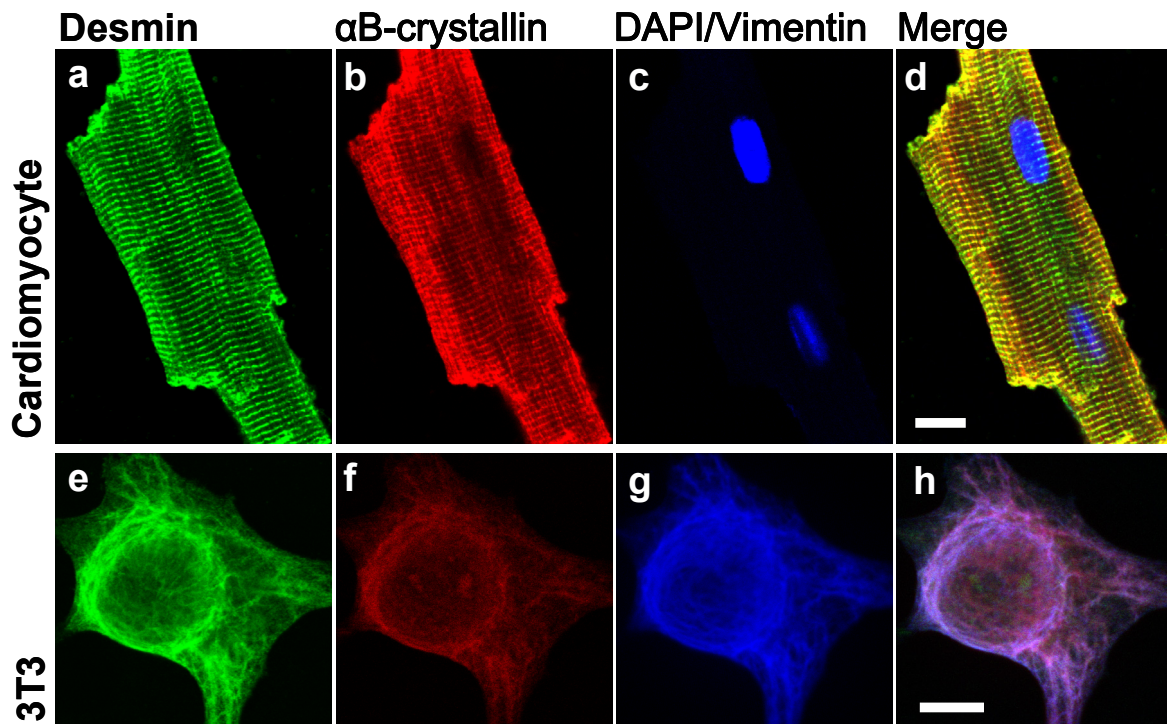


FIGURE 24 α B-crystallin co-localizes with desmin in cells

(a-d) As shown for the primary culture of rat cardiomyocytes, α B-crystallin is distributed along Z-bands together with desmin filaments. Cells were plated on fibronectin coated chamber slides for 2 h prior to fixation with 4% paraformaldehyde. Isolated rat cardiomyocytes were kindly provided by Dr. Sven Pleger (Dept. of Cardiology, University Hospital Heidelberg). (e-h) Triple immuno-staining shows distribution of desmin, α B-crystallin and vimentin in 3T3 cells. Of note, the endogenous expression level of α B-crystallin in these cells is fairly low as compared to those of cardiomyocytes. 3T3 cells were transfected with wild-type desmin and after two days fixed in methanol-acetone prior to staining. Scale bar: 10 μ m.

TABLE 4 Yeast two-hybrid screening shows interaction of desmin tail domain with α B-crystallin

Bait	Prey gene symbol	Number of times this prey has been isolated	Number of times the fragment starts in the coding sequence	Prey promiscuity	Number of different screens identifying this pair	Number of different cDNA libraries identifying this pair
Des(Δ N403)	CRYAB	60	18	2	5	3
Des(Δ N403)	SMTN	7	7	1	2	1
Des(Δ N403)	H1F0	2	0	3	1	1
Likely false positives: promiscuous preys						
Des(Δ N403)	FHOD1	14	14	10	3	2
Des(Δ N403)	MYBPC1	2	2	13	2	1

Y2H data show that the C-terminus of desmin likely interacts with α B-crystallin as the fragment is identified 18 times in the coding sequence.

In terms of prey promiscuity, α B-crystallin scores lower than FHOD1 or MYBPC1. FHOD1 and MYBPC1, two proteins that are binding to numerous other baits, also showed up as hits in the screening but they appear to bind rather non-specifically.

Abbreviations:-

Des(Δ N403): desmin with 67 amino acids from C-terminus; CRYAB: α B-crystallin, SMTN: smoothelin - a cytoskeletal protein for smooth muscles; H1F0: H1 histone family, member 0: a member of the histone family of nuclear proteins; FHOD1: formin homology 1,2 domain-containing protein 1; MYBPC1: Myosin-binding protein C, slow-type.

5.2 Oligomers of α B-crystallin sediment at 17 S as a complex comprising ~22 subunits

The absence of x-ray or NMR structure for full length α B-crystallin has impeded the progress in understanding the interdependence between primary, secondary and tertiary structure and the interactions necessary for subunit assembly of α B-crystallin [HALEY et al. 1998]. The quaternary structure of the protein, as investigated by cryo-EM, shows an asymmetric structure of spherical assemblies that are 8 - 18 nm in diameter with a central cavity. A major limitation to the structural characterization of α B-crystallin by crystallization is the self-association of monomers into large, polydispersed assemblies with molecular masses varying from 300 kDa to more than 1 MDa with an average mass of around 800 kDa [HORWITZ 2003]. This implies that α B-crystallin, with a monomeric molecular weight of 20 kDa, is present as a heterogeneous multimeric assembly complex under native conditions and its oligomeric state comprises as less as 15 and as many as over 50 subunits.

The MW of α B-crystallin complex is known to vary according to concentration, temperature, pH and ionic strength of the buffer used. Hence, before optimizing the buffer for interaction of desmin with α B-crystallin, we evaluated the oligomeric state of recombinant α B-crystallin by AUC in three different buffer systems – “Tris-NaCl” (22.5 mM Tris-HCl / 50 mM NaCl, pH 7.5), “PO₄-KCl” (2 mM PO₄-HCl / 100 mM KCl, pH 7.5) as well as “Tris-imidazole” (5 mM Tris-HCl / 100 mM imidazole, pH 7.5) – which were chosen as a starting point for these investigations. AUC is believed to be reliable tool to estimate the MW of sedimenting complexes. For AUC analysis, we used the sedimentation equilibrium mode to estimate the size of complexes of α B-crystallin in each buffer system (**FIGURE 25a**). From the size of the α B-crystallin complex, we can deduce the oligomeric state of this sHsp. Thus, we can estimate the number of subunits of α B-crystallin that are directly binding to desmin during assembly as seen in EM.

Also, by performing AUC in sedimentation velocity mode using three different concentrations of α B-crystallin (0.5 μ g/ μ l, 1.0 μ g/ μ l and 1.5 μ g/ μ l) in “Tris-NaCl” buffer system, we analyzed if the oligomeric state of α B-crystallin can be influenced by altering the protein concentration (**FIGURE 25b**).

AUC analyses show that at a fixed pH value of 7.5, the sedimentation behaviour of α B-crystallin complex is not influenced by the ionic strength of buffer in which the protein has been dissolved. The oligomeric complexes show a similar apparent MW between 400 – 500 kDa in all three buffer systems used (**FIGURE 25a**).

A range of protein concentrations of α B-crystallin between 0.5 - 1.5 μ g/ μ l did not lead to any significant variation in the sedimentation behaviour of the complex. This suggests that the oligomeric state of α B-crystallin is not influenced by its protein concentration within the range that we used for our investigations (**FIGURE 25b**).

All in all, the oligomeric complexes of α B-crystallin sediment relatively homogeneously at pH 7.5 with a MW corresponding to ~450 kDa in all three buffer systems. They sediment at a *s*-value of ~17 S for three concentrations. This *s*-value corresponds to ~22 subunits of α B-crystallin per complex.

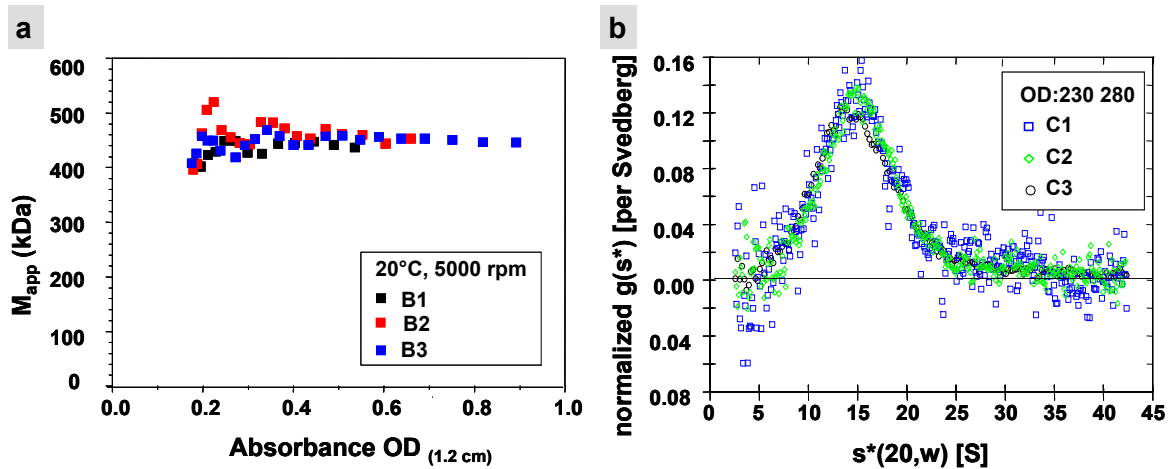


FIGURE 25 The oligomeric state of α B-crystallin is not influenced by the ionic strength of the buffer or its protein concentration

(a) Sedimentation equilibrium run in order to determine the self-association / oligomeric state of α B-crystallin in three different buffer systems: B1, B2 and B3. B1: "Tris-NaCl" (22.5 mM Tris-HCl / 50 mM NaCl, pH 7.5), B2: "PO₄-KCl" (2 mM PO₄ / 100 mM KCl, pH 7.5), B3: "Tris-imidazole" (5 mM Tris / 100 mM imidazole, pH 7.5). The oligomeric complexes show a similar apparent molecular weight between 400 – 500 kDa in all three buffer systems. AUC analyses show that at a fixed pH of 7.5, the sedimentation behaviour of α B-crystallin complex is not influenced by the ionic strength of buffer in which the protein has been dissolved. The MW of the complex for each buffer system corresponds to approximately 450 kDa. Abscissa: absorbance, ordinate: apparent molecular weight M_{app} of the sedimenting complex in kDa.

(b) Sedimentation velocity run of α B-crystallin in "Tris-NaCl" buffer system to determine if oligomeric state of α B-crystallin is influenced by altering the protein concentration. A range of protein concentrations of α B-crystallin (0.5 to 1.5 μ g/ μ l) did not lead to any variation in the sedimentation behavior of the complex, suggesting that the oligomeric state of α B-crystallin is not influenced by its protein concentration. The oligomeric complexes sedimented relatively homogeneously at an average of \sim 17 S for all three concentrations. $s^*(20,w)$ indicates sedimentation coefficient that has been corrected for the viscosity and density of solvent, relative to that of water at 20°C. To make direct comparisons, area normalization was done for different concentrations: C1 = 0.5 μ g/ μ l, C2 = μ g/ μ l C3 = μ g/ μ l. All runs were performed at 20°C and at 5000 rpm. Data analysis is performed using the software DCDT+.

5.3 Binding properties of α B-crystallin to desmin under different buffer conditions

α B-crystallin is a *bona fide* sHsp, and its chaperone activity was shown by its ability to suppress thermally induced protein aggregation [HORWITZ 1992]. One important functional characteristic that distinguishes sHsps from other molecular chaperones is a higher capacity of sHsps to bind non-native proteins. For instance, α A-crystallin binds to an unstable T4 lysozyme mutant F153A with a stoichiometry of one substrate of equal MW per subunit of α B-crystallin [MCHAOURAB et al. 2002].

As a next step, our aim was to select a physiological buffer system that enables binding of α B-crystallin and desmin. In the past, interaction studies have been carried out for desmin with wild-type or R120G α B-crystallin in “Tris-imidazole” (5 mM Tris-HCl / 100 mM imidazole, pH 7.5) buffer system. These studies revealed that the CRYAB R120G mutation leads to an increased binding of α B-crystallin to desmin filaments [PERNG et al. 2004]. However, an essential prerequisite to study this interaction is to use a buffer system in which the physiological morphology of the desmin filaments is maintained. When we visualized the electron micrographs of assembled desmin filaments in this buffer system, the filaments appeared particularly thick, non-continuous and tapered. Measurement of diameter of desmin filament in this buffer gave an average filament width of \sim 25 nm (FIGURE 26c, d). This value is far above the average filament diameter of \sim 10-12 nm measured for desmin in physiological buffer systems. Hence this buffer is not suitable for characterizing the interaction of desmin and α B-crystallin.

We employed two other buffer systems to first characterize desmin filaments in terms of morphology and width, namely “Tris-NaCl” (22.5 mM Tris-HCl / 50 mM NaCl, pH 7.5) and “PO₄-KCl” (2 mM PO₄ / 100 mM KCl, pH 7.5). In the past, desmin assembly has been well characterized for these buffers [WICKERT et al. 2005]. For both “Tris-NaCl” and “PO₄-KCl” buffer system, we observed an extended, continuous network of desmin filaments. The width of individual desmin filaments was measured to be \sim 12 nm and was comparable to physiological value (FIGURE 26a, b, d).

For EM, we co-assembled desmin and α B-crystallin at an equimolar ratio for 1 h at 37°C in all three buffer systems. The EM images showed different results for each buffer system with respect to binding. For “PO₄-KCl” buffer system, we observed no specific binding of α B-crystallin to desmin along the filament length in electron micrographs (FIGURE 27a). In case of “Tris-NaCl” buffer system, binding of α B-crystallin was observed at the ends of assembled short desmin fragments (FIGURE 27b). For “Tris-imidazole” buffer, binding occurred all through the filament length, though no regular binding pattern, as seen in “Tris-NaCl”, was observed (FIGURE 27c). The difference in binding pattern of α B-crystallin for the

FIGURE 26 Desmin filaments appear physiological in both “Tris-NaCl” and “PO₄-KCl” buffer systems (Please refer to figure on next page)

(a-c) Electron micrographs of negatively stained samples of desmin wild-type are shown after assembly in three different buffer systems at 37°C for 60 min (a) For “Tris-NaCl” buffer system, desmin was dialyzed ON in 5 mM Tris-HCl, 1 mM EDTA, 0.1 mM EGTA, 1 mM DTT, pH 8.4 and assembled by addition of an equal volume of “assembly buffer” containing 100 mM NaCl/40 mM Tris-HCl, pH 7.0. (b) For “PO₄-KCl” buffer system, sample was dialyzed ON in 2 mM Na₂PO₄, 1 mM DTT pH 7.5, and for assembly an equal volume of “assembly buffer” containing 2 mM Na₂PO₄/100 mM KCl pH 7.5 was used. (c) In case of “Tris-imidazole” buffer, dialysis was performed in 10 mM Tris-HCl, pH 8.0, 1 mM DTT, 0.2 mM PMSF, and assembly was initiated by adding an equal volume of “assembly buffer” containing 200 mM imidazole-HCl/2 mM DTT/0.4 mM PMSF pH 6.8. Assembly was stopped at 60 min by addition of 0.1% glutaraldehyde. Scale bar 100 nm. (d) The EM images were processed in ImageJ 1.32j and 200 measurements were carried out for each sample. The desmin diameter measured for “Tris-NaCl” is 12.3 ± 1.6 nm, for “PO₄-KCl” 11.5 ± 1.6 nm, and for “Tris-imidazole” 25.8 ± 4.3 nm.

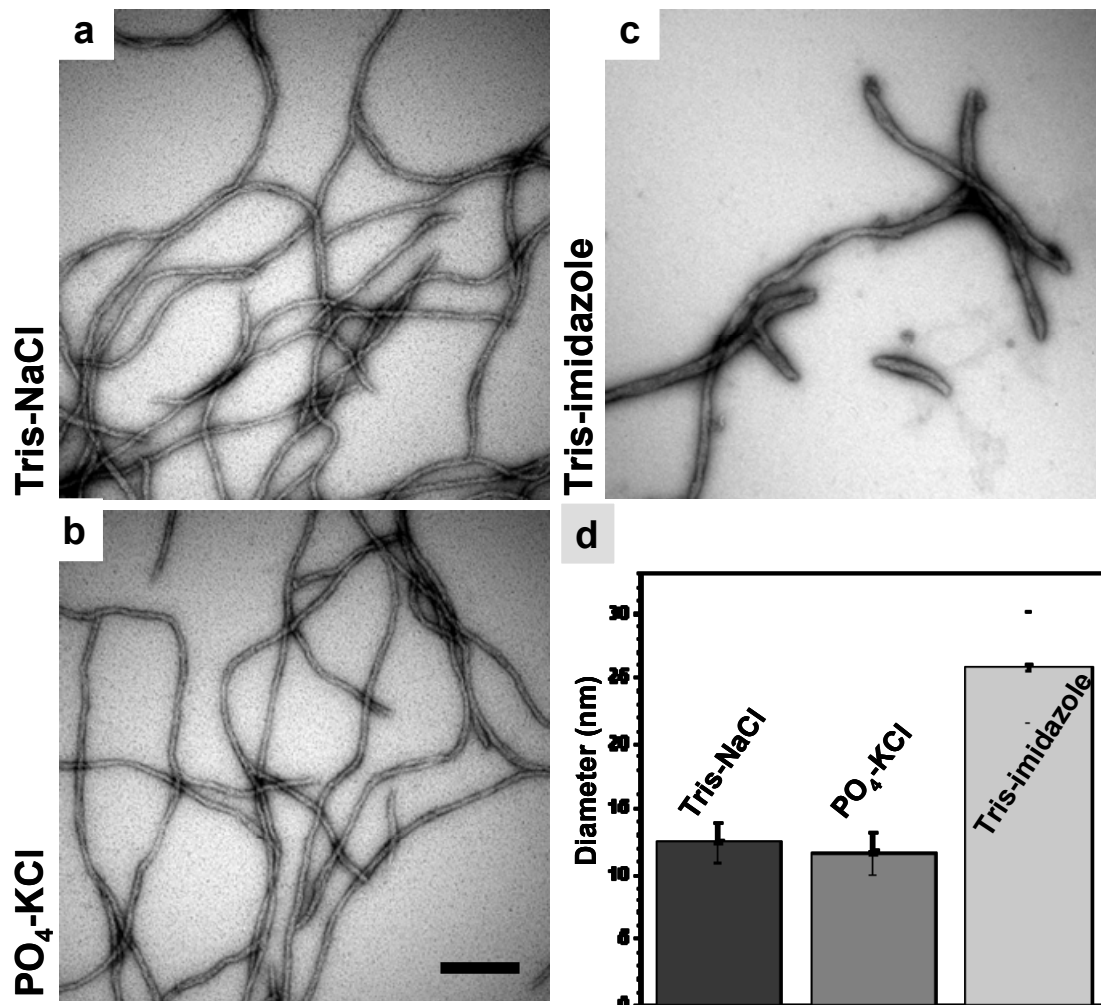


FIGURE 26 Desmin filaments appear physiological in “Tris-NaCl” and “PO₄-KCl” buffer system

three buffer systems could be attributed to altered surface properties for both desmin and α B-crystallin under varying ionic strengths of these buffer.

Next, we performed cosedimentation assays using all three buffer systems in order to establish the best system to study the binding of desmin to α B-crystallin. For all buffer systems, desmin on its own is present exclusively in the pellet, whereas >90% α B-crystallin is present in the supernatant fraction, and a minor amount in sucrose sub-fractions - 1, 2 and 6. We observed a comparable binding of α B-crystallin to desmin in the sucrose fractions of “Tris-NaCl” and “PO₄-KCl” buffer system, as well as an overall increase in the soluble desmin pool in sucrose fraction (FIGURE 27d, e). Of note, for “PO₄-KCl” buffer system the soluble desmin pool in sucrose fraction was distinctly higher than that seen for “Tris-NaCl”, which might indicate that α B-crystallin fragments the desmin more efficiently in this buffer system. However, we observed that both desmin and α B-crystallin appeared uniformly in all sucrose sub-fractions for “Tris-NaCl” buffer system, but not for “PO₄-KCl”. This suggests that desmin fragments formed through co-assembly with α B-crystallin differ in length for the two buffer systems, hence these fragments sediment differently in the sucrose fraction. We detected the strongest binding of α B-crystallin to desmin in “Tris-imidazole” buffer system (FIGURE 27f). Here, no desmin or α B-crystallin was observed in the sucrose fraction because all of α B-crystallin sedimented with desmin in the pellet

fraction. Interestingly, previous studies have also reported an increase in the level of soluble pools of vimentin, GFAP and other type III IF proteins in presence of sHsps [NICHOLL & QUINLAN 1994].

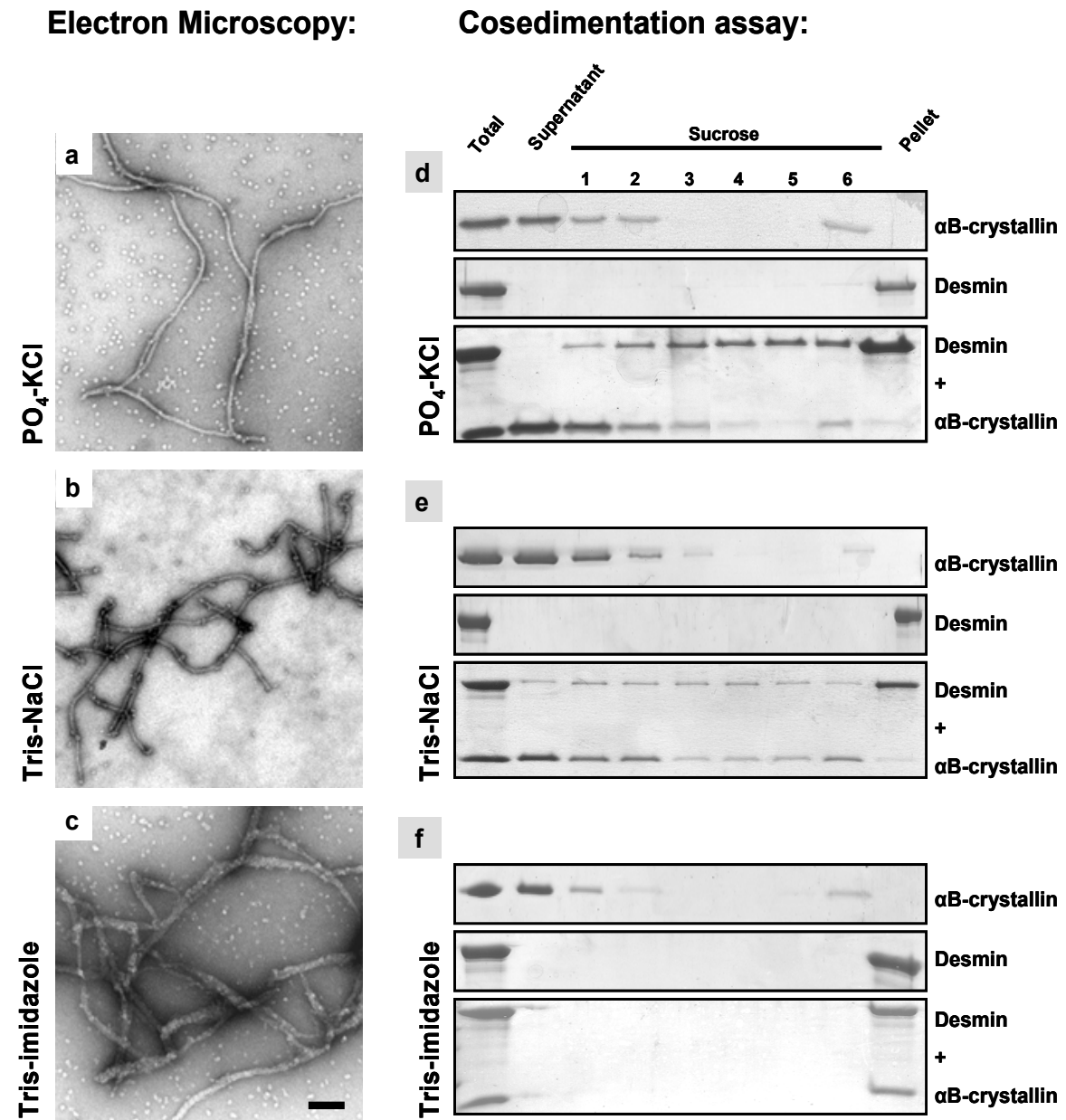


FIGURE 27 α B-crystallin shows altered binding patterns to desmin in different buffer systems

(Please refer to figure legend on next page)

FIGURE 27 α B-crystallin shows altered binding to desmin in different buffer systems

(a-c) Electron micrographs of negatively stained samples of desmin and α B-crystallin are shown in three different buffer systems after co-assembly at 37°C for 60 min. For all EM procedures, assembly was stopped at 60 min by the addition of 0.1% glutaraldehyde to samples. (d-f) Coomassie-stained gels for cosedimentation assay of desmin and α B-crystallin are shown for respective buffer systems. Protein samples were assembled in Eppendorf tubes and then layered onto 300 μ l of 0.85 M sucrose cushion. (a, d) For “PO₄-KCl” buffer system, samples were dialyzed in 2 mM Na₂PO₄, 1 mM DTT pH 7.5, and for assembly an equal volume of “assembly buffer” containing 2 mM Na₂PO₄/100 mM KCl pH 7.5 was used. A significant amount of desmin appeared in the sucrose fraction upon cosedimentation in the “PO₄-KCl” buffer system, whereas no desmin was seen in this fraction when sedimented on its own. This indicates presence of shorter desmin filaments when assembled with α B-crystallin as also seen in corresponding EM image. However, no specific binding of α B-crystallin to desmin filament is observed in “PO₄-KCl” buffer system. (b, e) For “Tris-NaCl” buffer system, desmin was dialyzed ON in 5 mM Tris-HCl, 1 mM EDTA, 0.1 mM EGTA, 1 mM DTT, pH 8.4 and assembled by addition of an equal volume of “assembly buffer” containing 100 mM NaCl/40 mM Tris-HCl, pH 7.0. Distinct gel bands are seen in sucrose fraction for both desmin and α B-crystallin upon cosedimentation. The corresponding gel bands are absent in cases when either desmin or α B-crystallin sedimented on their own. In electron micrographs, α B-crystallin binds along short desmin fragments in a regular manner, and probably inhibits filament elongation. (c, f) In case of “Tris-imidazole” buffer, dialysis was performed in 10 mM Tris-HCl/1 mM DTT/0.2 mM PMSF pH 8.0, and assembly was initiated by adding an equal volume of “assembly buffer” containing 200 mM imidazole-HCl/2 mM DTT/0.4 mM PMSF pH 6.8. Electron micrographs show no specific binding pattern between desmin and α B-crystallin in “Tris-imidazole” buffer, and cosedimentation assay shows that all of α B-crystallin is bound to desmin in the pellet fraction. After assembly, the samples were sedimented at 30,000 rpm, 20°C for 30 min. The 300 μ l sucrose fraction is subdivided into 6 sub-fractions, each representing 50 μ l volume. Scale bar: 100 nm

Because of normal morphology of desmin filaments and moderate binding of α B-crystallin to desmin in “Tris-NaCl” buffer system, we analyzed the interaction of the two molecules in more detail using this buffer system. EM images show that the oligomers of α B-crystallin bound to short desmin filaments stably and in a repetitive manner. We measured the average spacing between two successive α B-crystallin oligomers bound to the ends or along the length of same desmin fragment in “Tris-NaCl” buffer system to be ~50, 100 and 200 nm (**FIGURE 28a**). We observed a similar spacing for oligomers of α B-crystallin bound to desmin fragments in the sucrose fraction upon cosedimentation, supporting our observation that in “Tris-NaCl” buffer system, α B-crystallin indeed shows a repetitive pattern of binding to desmin (**FIGURE 28b**). Although increasing the molar amount of α B-crystallin from 1 to 10-fold led to higher amounts of desmin in the sucrose fraction for “Tris-NaCl” buffer system upon cosedimentation (**FIGURE 28c**), no difference in the binding of α B-crystallin to desmin was observed by EM (data not shown). In the past it has been reported that desmin-bound α B-crystallin reaches saturation at a level corresponding to approximately five to seven α B-crystallin monomers per desmin monomer [BENNARDINI et al 1992]. Thus, we found an equimolar ratio of the two proteins to be an optimal ratio for binding studies and used it uniformly for all further experiments.

Together, these data suggest that the binding of α B-crystallin to desmin is influenced by the surface morphology of the two proteins under particular conditions of pH and ionic strength. Different buffers probably lead to altered exposure of residues for desmin as well as α B-crystallin. The near physiological appearance of desmin filament in “Tris-NaCl” buffer system, and a regular binding of α B-crystallin to desmin occurring under this buffer, as observed by EM, prompted us to optimize this buffer system in order to obtain a stronger binding of these two proteins as discussed in section 5.4.

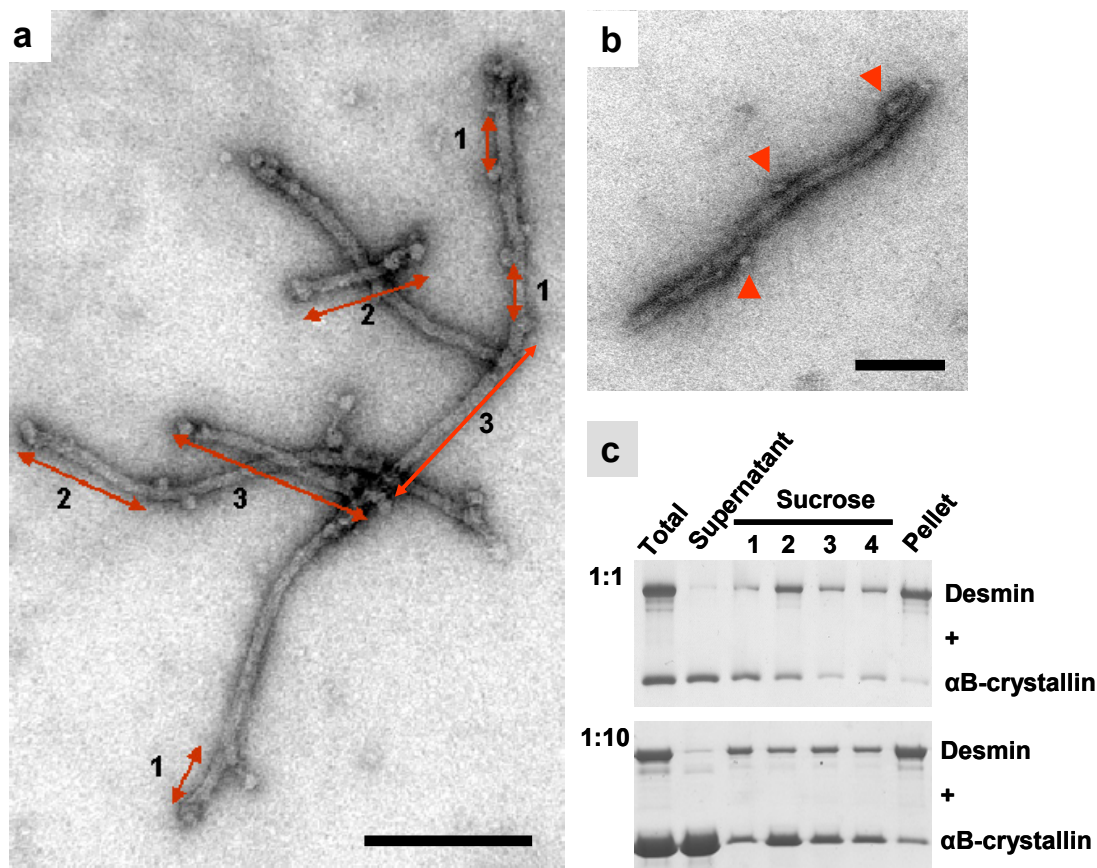


FIGURE 28 Binding α B-crystallin to desmin in “Tris-NaCl” buffer system

(a) Electron micrographs of negatively stained samples of desmin and α B-crystallin after co-assembly in “Tris-NaCl” buffer system are shown. EM data illustrate distinct binding of α B-crystallin to desmin upon co-assembly. Assembly was stopped at 60 min by addition of 0.1% glutaraldehyde. Double arrows in red depict the distance between two α B-crystallin oligomers aligned along the desmin filaments, 1: 50 nm, 2: 100 nm, 3: 200 nm. α B-crystallin binds along the tips of short desmin fragments and thereby, probably, prevents the elongation of desmin filaments. (b) Electron micrograph depicts binding of α B-crystallin oligomers to desmin even within sucrose fraction upon cosedimentation, suggesting stable interaction of the two proteins. Red arrowheads indicate the position of α B-crystallin on desmin fragment. Scale bar 100 nm. (c) Coomassie-stained gel for cosedimentation assay shows no drastic effect on the amount of desmin in sucrose fraction upon increasing the molar ratio of α B-crystallin:desmin from 1:1 versus 10:1. The amount of desmin in sucrose fraction increases only slightly by adding 10x α B-crystallin. Thus an equimolar ratio of the two proteins is considered optimal for all binding assays. For “Tris-NaCl” buffer system, all samples are dialyzed ON in 5 mM Tris-HCl, 1 mM EDTA, 0.1 mM EGTA, 1 mM DTT, pH 8.4 and assembled by addition of an equal volume of “assembly buffer” containing 100 mM NaCl/40 mM Tris-HCl, pH 7.0. For cosedimentation assay, co-assembly was performed for 1 h at 37°C on 200 μ l of sucrose cushion and the samples were sedimented at 30,000 rpm, 20°C for 30 min. The total 200 μ l sucrose fraction is subdivided into 4 sub-fractions, each representing 50 μ l volume.

5.4 Binding of α B-crystallin to desmin is enhanced by lowering the pH and ionic strength of “Tris-NaCl” buffer system and on increasing the assembly temperature”

In section 5.3 a distinct effect of α B-crystallin on desmin assembly in the “Tris-NaCl” buffer system was shown. Cosedimentation assay showed the presence of a soluble pool of desmin in the sucrose fraction. However, we have observed that in this buffer system, <10% of total α B-crystallin sediments with desmin, in contrast to 100% α B-crystallin recovered in the pellet when “Tris-imidazole” was used. With the aim to recover α B-crystallin-bound desmin in the pellet upon cosedimentation for further quantification, while simultaneously maintaining the physiological morphology of desmin filaments, the pH and ionic strength of “Tris-NaCl” buffer system was altered in a step-wise manner.

It has been reported previously for “HEPES-KCl” (50 mM HEPES, 1 mM ATP, 2 mM $MgCl_2$, and 200 mM KCl) buffer system that a sharp increase in the affinity of α B-crystallin to desmin occurs once the pH is lowered from 8.0 to 6.0. Here it was reported that as much as ~90% of total α B-crystallin cosediments with desmin at pH 6.0 as compared to ~40% at pH 8.0 [BENNARDINI et al. 1992]. However, the effect on desmin filament morphology at such lower pH condition has not been taken into account by these studies. To optimize the pH, we chose two lower pH values for assembly, i.e. 7.3 and 7.1, to see if the binding of α B-crystallin to desmin increases as the pH is lowered, while at the same time the desmin filaments appear normal in EM. We dialyzed both desmin and α B-crystallin ON in 5 mM Tris-HCl at three different pH values of 7.4, 8.0 and 8.4. We initiated assembly by adding equal volume of 100 mM NaCl / 40 mM Tris-HCl, pH 7.0 to each sample at 37°C for 1 h. Addition of assembly buffer leads to a final assembly pH of 7.1, 7.3 and 7.5 for samples dialyzed at pH 7.4, 8.0 and 8.4, respectively. Remarkably, the desmin filament morphology and width remained unaltered for all three assembly conditions as seen in EM (data not shown). Our analyses show that lowering the final assembly pH to 7.1, from the initial pH of 7.5, enhances the recovery of α B-crystallin in the pellet significantly. This was determined by evaluating the gel band density for each fraction (i.e. supernatant, sucrose and pellet) after cosedimentation. Mean gel band density was calculated from experiments performed in triplicate. In contrast to 7% α B-crystallin cosedimenting at pH 7.5, approximately 16% was recovered at the final assembly pH of 7.1, whereas the amount in sucrose fraction remained constant at all pHs tested (**FIGURE 29a, b**). Thus, lowering the pH increases the binding of α B-crystallin to desmin by a factor of two. This could be attributed to altered surface properties of both desmin and α B-crystallin, probably due to enhanced exposure of hydrophobic patches of two proteins under lower pH conditions. Decreasing the pH value even further affected the physiological morphology of desmin filament, as at pH 6.9 we observed short desmin fragments when assembled alone (data not shown). Hence, we took the assembly pH of 7.1 as the lower limit, and in the next step we optimized the binding by altering the ionic strength of the buffer.

To compare the effect of lowering the ionic strength of buffer on interaction of desmin with α B-crystallin, we performed dialysis in “Tris-buffer” at three different salt concentrations (*Buffer1*: 5.0 mM Tris-HCl, 1 mM EDTA, 0.1 mM EGTA, 1 mM DTT; *Buffer2*: 2.5 mM Tris-HCl, 0.5 mM EDTA, 0.05 mM EGTA, 1 mM DTT and *Buffer3*: 1.0 mM Tris-HCl, 0.2 mM EDTA, 0.02 mM EGTA, 1 mM DTT) at pH of 7.4 and 8.4, respectively. Assembly was initiated by adding equal volume of 100 mM NaCl, 40 mM Tris-HCl, pH 7.0 at 37°C for 1 h. Thus, the final Tris-HCl concentration upon assembly was 22.50 mM, 21.25 mM and 20.50 mM when *Buffer1*, *Buffer2* and *Buffer3* were used for dialysis, respectively. From EM images, we measured the diameter of desmin filament assembled in 50 mM NaCl / 22.50 mM Tris-HCl at 11.3 nm, in

50 mM NaCl / 21.25 mM Tris-HCl at 11.7 nm and in 50 mM NaCl / 20.50 mM Tris-HCl at 12.4 nm when samples were dialyzed in *Buffer1*, *Buffer2* and *Buffer3*, respectively, at pH 7.4. Thus, the diameter of desmin IFs was within physiological range for all three ionic strengths. Intriguingly, we observed a continuous increase in the binding of α B-crystallin to desmin in cosedimentation assay as the ionic strength of dialysis buffer was reduced from 5.0 to 2.5 and finally to 1.0 mM “Tris-HCl” for both pH conditions (exemplified for dialysis at pH 7.4 in **FIGURE 29c**). We observed maximum binding of α B-crystallin to desmin, both in EM and cosedimentation assay, when samples were dialyzed ON into 1.0 mM “Tris-HCl” pH 7.4 and assembled at a final ionic strength of 20.5 mM Tris-HCl / 50 mM NaCl pH 7.1 (**FIGURE 29c**). Here, approximately 47% α B-crystallin was recovered in the pellet as compared to 8% and 31% α B-crystallin in the pellet of samples dialyzed at the same pH in 2.5 mM and 5.0 mM “Tris-HCl” dialysis buffer, respectively. For the sake of brevity, we have named the dialysis buffer consisting of 1.0 mM Tris-HCl, 0.2 mM EDTA, 0.02 mM EGTA and 1 mM DTT, pH 7.4 as “modified Tris-buffer”.

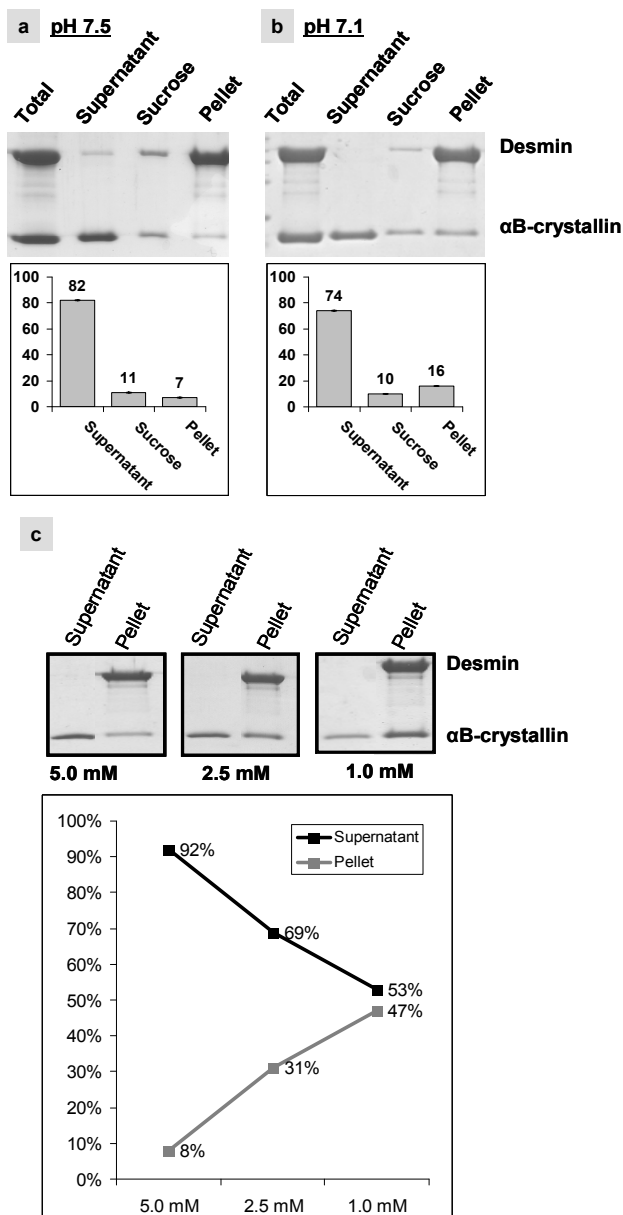


FIGURE 29 Binding of α B-crystallin to desmin is enhanced by lowering the pH and ionic strength of “Tris-buffer”

For band density evaluation, all cosedimentation assays were performed in triplicates at 30,000 rpm at 20°C. Gel band density of Coomassie-stained gels was evaluated using ImageJ 1.32j, plots were generated in Excel 2003. Value above the bar depicts mean value of three independent experiments. In Excel plot, ordinate depicts percentage of α B-crystallin distributed between different fractions (supernatant, sucrose, pellet). (a, b) To optimize the pH of the buffer, dialysis of both desmin and α B-crystallin was performed ON in 5 mM Tris-HCl pH 7.4 and 5 mM Tris-HCl pH 8.4. Assembly was initiated by addition of equal volume of 100 mM NaCl, 40 mM Tris-HCl pH 7.0 at 37°C for 1 h. Lowering the final assembly pH to 7.1, from the initial pH of 7.5, enhances the recovery of α B-crystallin in the pellet significantly. In contrast to 7% α B-crystallin cosedimenting at pH 7.5, around 16% was recovered at final assembly pH of 7.1, whereas the amount in sucrose fraction remained constant at the two tested pH values. (c) To optimize the ionic strength of the buffer, dialysis of both desmin and α B-crystallin was performed ON in 5.0 mM “Tris-HCl” (5.0 mM Tris-HCl, 1 mM EDTA, 0.1 mM EGTA, 1 mM DTT), 2.5 mM “Tris-HCl” (2.5 mM Tris-HCl, 0.5 mM EDTA, 0.05 mM EGTA, 1 mM DTT) and 1.0 mM “Tris-HCl” (1.0 mM Tris-HCl, 0.2 mM EDTA, 0.02 mM EGTA, 1 mM DTT) at pH of 7.4. Assembly was performed at 37°C for 1 h by adding equal volume of 100 mM NaCl / 40 mM Tris-HCl pH 7.5, leading to a final pH of 7.1 and final Tris-HCl concentration of 22.50 mM, 21.25 mM and 20.50 mM, respectively. In contrast to 8% α B-crystallin cosedimenting with desmin upon sample dialysis in 5 mM “Tris-HCl”, 31% is recovered at 2.5 mM and 47% at 1.0 mM. Note, the amount of α B-crystallin decreases gradually in the supernatant fraction corresponding to the gradual increase in the pellet fraction for a given buffer.

Thus, we chose “modified Tris-buffer” as the standard dialysis buffer for all the future interaction studies of desmin and α B-crystallin. Of note, we have randomly chosen as first to decrease the ionic strength of buffer in a gradual manner for enhancing the binding of the two proteins. As we observed stronger binding by decreasing the ionic strength of dialysis buffer, we did not perform the same set of experiments by increasing the ionic strength of “Tris-HCl” dialysis buffer.

5.4.1 Effect of temperature on binding of α B-crystallin to desmin

The *in vitro* binding of α B-crystallin to IF proteins like peripherin, vimentin and desmin was shown to be temperature dependent [DJABALI et al. 1997, MING et al 2004]. Past data indicate that α B-crystallin displays significant chaperone-like activity at temperatures both lower and higher than physiological temperatures [DATTA & RAO 1999]. In our chosen “Tris-NaCl”buffer system, we investigated the effects of increasing the assembly temperature on morphology of desmin filament and α B-crystallin. To this end, we have analyzed both α B-crystallin and desmin on their own after assembly at 37°C and 44°C for 1 h by EM to observe if any morphological change occurs for these proteins as the temperature increases. We have also analyzed if increasing or decreasing the assembly temperature modifies the binding of α B-crystallin to desmin. This was evaluated by cosedimentation assay after assembly at RT, 37°C and 44°C for 1 h. All samples were dialyzed in “modified Tris-buffer” and assembled by adding equal volume of “assembly buffer”.

In EM, we observed at a magnification of 240,000x that the oligomeric complexes of α B-crystallin are not altered in size at elevated temperature, suggesting that the number of subunits per complex probably remains the same at both temperatures. The oligomeric complex of α B-crystallin exhibited a similar diameter of ~13 nm at both 37°C and 44°C and no difference in morphology was observed (data not shown). However, desmin filament morphology was significantly altered at 44°C as compared to 37°C (**FIGURE 30**). We observed more “open” filament structures at 44°C. This “open” structure of desmin filaments might expose the hydrophobic residues or patches along filament length which eventually leads to a stronger binding to α B-crystallin. Similar alterations might also occur on the outer surface of α B-crystallin complex, exposing hydrophobic patches that, in turn, leads to a stronger binding to desmin. The cosedimentation assays performed at RT, 37°C and 44°C showed gradual increase of α B-crystallin in the pellet fraction from 4%, to 44% and finally to 92%, respectively (data not shown).

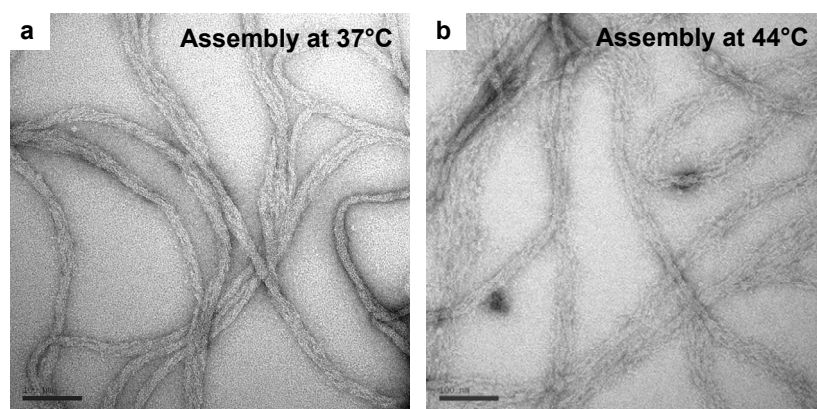


FIGURE 30 Electron microscopic observation of desmin filaments at two different temperatures

Electron micrographs of negatively stained samples of wild-type assembled desmin at (a) 37°C or (b) 44°C for 1 h are shown. Samples were dialyzed in “modified Tris-buffer” and assembled by adding equal volume of “assembly buffer” Assembly was stopped by adding 0.1% glutaraldehyde. “Open” filament structures for desmin are seen at 44°C. Scale bar: 100 nm

5.5 The C-terminal domain of desmin modulates the binding of α B-crystallin to desmin filaments

sHsps control proteins against mechanical, thermal and chemical stress. The mechanism, by which a sHsp interacts with mature IF protein filament could represent a means by which these chaperones protect cells against protein aggregation. Studies on α B-crystallin have reported that multiple interactive domains of human α B-crystallin are important for the recognition, selection, and solubility of unfolding substrate proteins [GHOSH et al. 2006]. Systematic protein pin array analysis, site-directed mutagenesis, and chaperone assays have characterized the sequences $_{41}\text{STSLSPFYLRPPSFLRAP}_{58}$ in the N-terminal domain, $_{73}\text{DRFSVNLVDVKHFS}_{85}$, $_{101}\text{HGKHEERQDE}_{110}$, $_{113}\text{FISREFHR}_{120}$, and $_{131}\text{LTITSSLSSDGV}_{142}$ in the α -crystallin core domain, and $_{156}\text{ERTIPITRE}_{164}$ in the C-terminal domain of human α B-crystallin as interactive sequences responsible for recognition, binding, and solubilization of unfolding/misfolding substrate proteins including lens crystallins, enzymes, filaments, and growth factors [GHOSH et al. 2008]. The amphipathic nature of α B-crystallin is believed to be crucial to its chaperone function, enabling it to bind to exposed hydrophobic patches of misfolded proteins. For the N-terminal region of α B-crystallin, it has been shown that hydrophobic residues 73-92 are capable of preventing aggregation of denatured substrate, similar to the action of native α B-crystallin.

To determine the corresponding regions of desmin that interact with α B-crystallin, the Y2H screening results were extended by generating five desmin C-terminal deletion variants for analysis by cosedimentation assay and EM. Desmin fragments coding for amino acids 1-403 (Δ C403, designated as Des Δ tail), 1-431 (Des Δ C431), 1-441 (Des Δ C441) and 1-451 (Des Δ C441) were generated (**FIGURE 31a**). As the tripeptide residue RDG is conserved among different species, we were also interested in analyzing how the interaction of α B-crystallin and desmin is affected if this conserved residue is deleted or scrambled. Thus, we generated two more variants – one devoid of RDG motif (Des Δ RGD), and another where the RDG sequence is scrambled to DRG (DesDRG). EM results show that all deletion variants are capable of maturing into filaments like wild-type or tailless desmin (data not shown). Of note, Des Δ head (Δ N85) and Desrod(Δ N85- Δ C409) were not used for cosedimentation assay or EM to study interaction with α B-crystallin under high salt conditions because they do not form filaments. Hence, they stay in the supernatant fraction much like α B-crystallin, whereas desmin wild-type, Des Δ tail and other tail domain deletion variants sediment completely in the pellet fraction after assembly.

We performed cosedimentation assay and EM using equimolar concentration of α B-crystallin and desmin variants after ON dialysis of samples in “modified Tris-buffer”. Assembly was performed at 37°C for 1 h by adding an equal volume of “assembly buffer” to the protein mixture. The gel band density was measured for supernatant, sucrose and pellet fractions upon cosedimentation assay and the mean was calculated for all experiments performed in triplicate. Upon cosedimentation, ~4% of total α B-crystallin is recovered in the pellet fraction for Des Δ tail, while binding is abolished for Des Δ C431 and Des Δ C441 (**FIGURE 31b**). For Des Δ C451, ~20% of total α B-crystallin is recovered in the pellet, which is almost half the amount of α B-crystallin that cosediments with wild-type desmin. Binding is comparable to DesWT for both Des Δ RGD and DesDRG, with >40% α B-crystallin recovered in each case (exemplified for Des Δ RGD in **FIGURE 31b**).

EM data show that the association of α B-crystallin with desmin filaments is comparable for DesWT, Des Δ RGD as well as DesDRG (data for DesDRG not shown), whereas only occasional associations are

observed for Des Δ C451, and no specific binding for Des Δ tail, Des Δ C431 and Des Δ C441 (**FIGURE 31c**, **FIGURE 32**). We obtained 20 EM images per variant and randomly chose 5 different areas per image to count the number of oligomers of α B-crystallin that are bound to each desmin variant within an area of 10^4 nm^2 . For the same image, we also counted the number of oligomers lying in the background and not bound to the filament for 5 different grid regions of same area (10^4 nm^2). Thus, we counted 100 different areas (each 10^4 nm^2 in size) per sample to obtain the number of bound or non-bound oligomers. We found that on average, after subtracting the unbound oligomers from the background, \sim 6-7 oligomers of α B-crystallin are bound to the filament of DesWT, Des Δ RGD or DesDRG within an area of 10^4 nm^2 (as shown for DesWT and Des Δ RGD in **FIGURE 31c**). For Des Δ C451, around 2 oligomers are bound to the filament per 10^4 nm^2 , whereas the other three desmin constructs (Des Δ tail, Des Δ C431, Des Δ C441) show unspecific binding to α B-crystallin when we subtract the oligomers bound to grid surface.

Viscometry analysis corroborated our EM and cosedimentation results that Des Δ tail does not interact with α B-crystallin. Here, no alteration in the bulk solution viscosity was observed for Des Δ tail assembled either in the presence or absence of α B-crystallin (data not shown), whereas for DesWT co-assembled with α B-crystallin, the solution viscosity dropped by 50% to that of DesWT on its own (please refer to Section 5.6, **FIGURE 34c**).

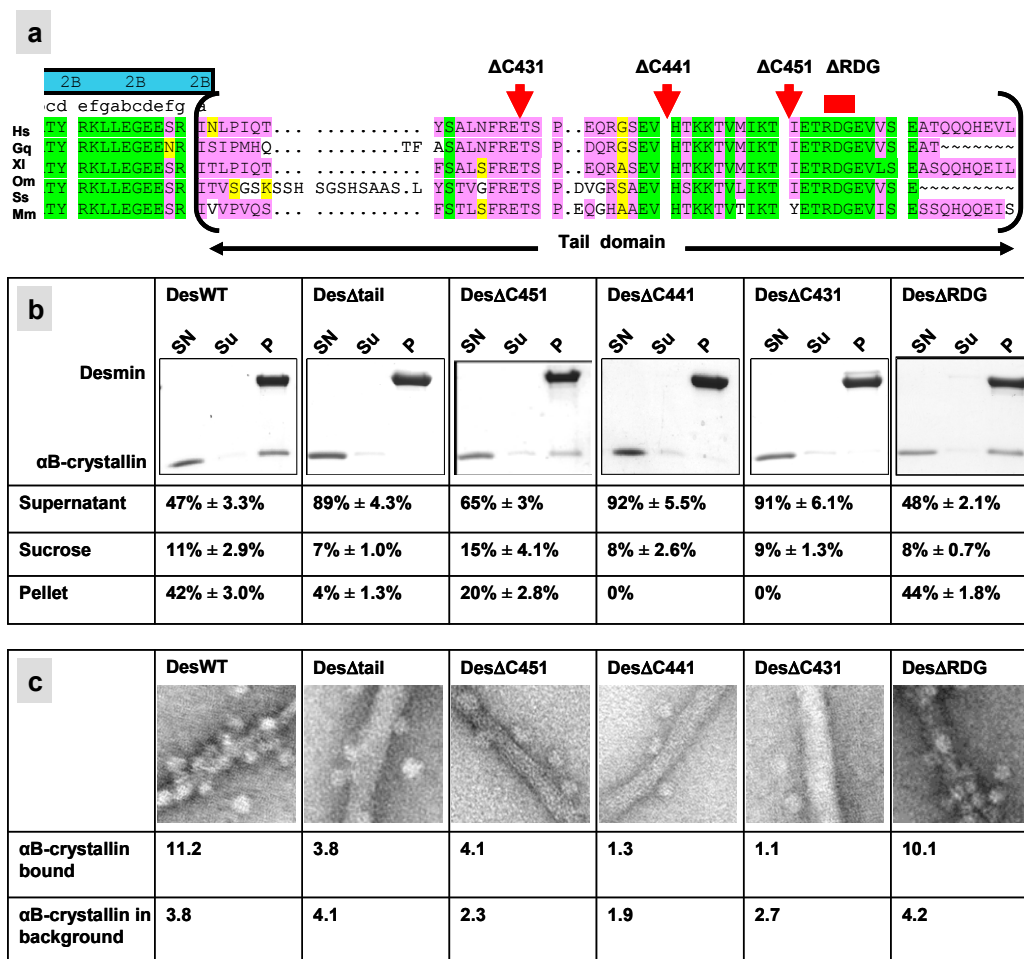


FIGURE 31 The C-terminal domain of desmin modulates the binding of α B-crystallin to desmin filaments (Please refer to figure legend on next page)

FIGURE 31 The C-terminal domain of desmin modulates the binding of α B-crystallin to desmin filaments

(a) Amino acid sequence comparison of the non- α -helical tail domain of desmin as found in different species from humans to shark is shown (Hs: *Homo sapiens*/human, Gg: *Gallus gallus*/chicken, Xl: *Xenopus laevis*/African clawed frog, Om: *Oncorhynchus mykiss*/steelhead trout, Ss: *Scyliorhinus stellaris*/shark, Ms: *Mus musculus*/mouse). Red arrowheads and bar indicate the position of aa where the deletion variant was generated. The motif RDG is well conserved among different species, thus we considered it to be a putative binding site for α B-crystallin and accordingly generated a deletion (Des Δ RDG) and scrambled variant (DesDRG). IKT is another conserved motif in the tail domain. (b, c) Cosedimentation assay and EM were performed using equimolar concentrations of desmin variants and α B-crystallin after ON dialysis of samples in “modified Tris-buffer”. Assembly was performed by adding equal volume of “assembly buffer” (40 mM Tris-HCl / 100 mM NaCl, pH7.5) at 37°C for 1 h. (b) Gel band density was evaluated for each fraction (SN: supernatant, Su: sucrose and P: pellet) after cosedimentation and the mean was calculated from experiments performed in triplicate. Upon cosedimentation, 4% of total α B-crystallin is recovered in the pellet fraction for Des Δ tail, ~20% for Des Δ C451, whereas binding is abolished for Des Δ C431 and Des Δ C441 as compared to DesWT. Binding of α B-crystallin to Des Δ RDG remains unchanged as compared to DesWT. (c) EM data show that the association of α B-crystallin to desmin filaments is comparable for DesWT and Des Δ RGD (~6-7 oligomers/ 10^4 nm²), whereas a weak association is seen for Des Δ C451 (~2 oligomers/ 10^4 nm²), and binding is non-specific for Des Δ tail, Des Δ C431 and Des Δ C441. We obtained 20 EM images per variant and randomly chose 5 different areas per image to count the number of oligomers of α B-crystallin that are bound to each desmin variant within an area of each 10^4 nm². For the same image, we also counted the number of oligomers lying in the background and not bound to the filament for 5 different grid areas (each 10^4 nm²). Thus, we counted 100 different areas (each 10^4 nm²) per sample to obtain the number of bound or non-bound oligomers. We calculated the average number of bound oligomers after subtracting the unbound oligomers from the background. After assembly, all samples were fixed in 0.1% glutaraldehyde.

Next, based on EM and cosedimentation data, we aimed at defining the region of desmin where α B-crystallin could potentially bind. In cosedimentation assay, Des Δ C451 shows weaker binding to α B-crystallin than DesWT, while binding is completely absent for Des Δ C441 or Des Δ C431. This indicates that binding between the two molecules most likely occurs between the amino acid residues 442-453 of desmin. Hence, we generated a peptide fragment SEVHTKKTVMIKTIET representing the residues 438-453 of desmin and performed a competition-based binding assay. Here desmin, α B-crystallin and the 16 aa long peptide were co-incubated in “assembly buffer” for 1 h after separate dialysis of desmin and α B-crystallin in “modified Tris-buffer” ON. The peptide was not dialyzed, but dissolved directly in “modified Tris-buffer” We expected that, due to selective binding of α B-crystallin to this peptide which represents the potential binding region of α B-crystallin to desmin, more α B-crystallin will appear in the supernatant (as it is not bound to desmin) and wither no or less α B-crystallin will be recovered in the pellet fraction upon cosedimentation assay. This is because the peptide, which is present in excess, will compete for binding to α B-crystallin, thus preventing α B-crystallin’s binding to desmin. Contrary to our expectation, at a 100-fold or 300-fold excess, all of α B-crystallin was recovered in the pellet (*Supplementary* FIGURE S9). We speculate that, this peptide probably interacts with wild-type desmin and alters its surface properties, such that, α B-crystallin can bind to DesWT more strongly than in the absence of the peptide.

To observe if desmin wild-type, Des Δ tail (Δ C409), Des Δ head (Δ N85) and Desrod (Δ N85- Δ C409) can interact with α B-crystallin in buffers of low ionic strength, after dialysis of samples in “modified Tris-buffer”, these proteins were incubated with α B-crystallin for 1 h at 37°C without addition of “assembly buffer”. Unexpectedly, all variants show binding to α B-crystallin in EM under buffers of low ionic strength (as exemplified for Des Δ tail, **FIGURE 33a**). AUC experiments also detected an interaction between all desmin variants and α B-crystallin (as exemplified for Des Δ tail, **FIGURE 33b**). Probably, the protofibrils of desmin DesWT, Des Δ tail, Des Δ head and Desrod are capable of binding to α B-crystallin due to hydrophobic interactions occurring between the two molecules under such unphysiological low salt condition.

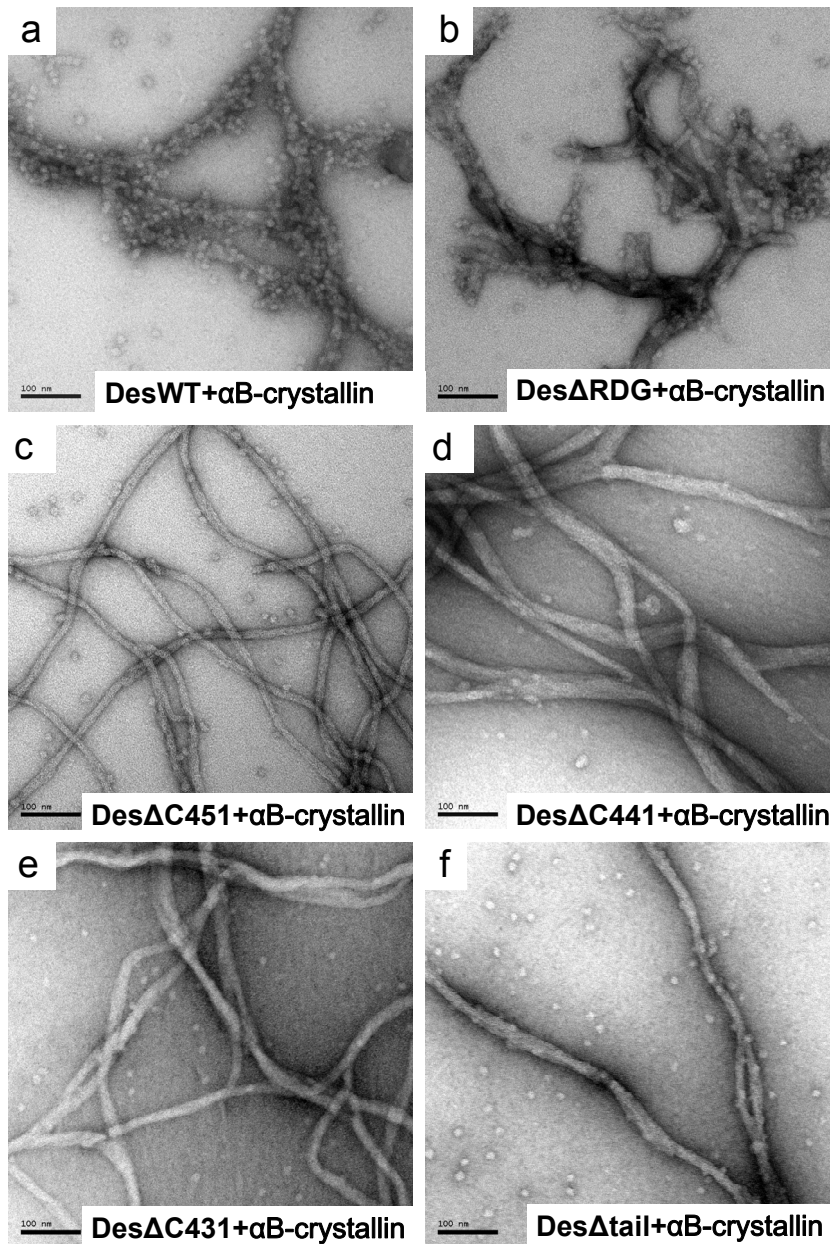


FIGURE 32 α B-crystallin binds non-specifically to filaments of Des Δ tail, Des Δ C431 and Des Δ C441

Electron micrographs of negatively stained samples of DesWT, Des Δ RDG, Des Δ C451, Des Δ C441, Des Δ C431 and Des Δ tail co-assembled with α B-crystallin are shown. Assembly was performed using equimolar concentration of desmin variants and α B-crystallin after ON dialysis of samples in “modified Tris-buffer”. Assembly was performed by adding equal volume of “assembly buffer” (40 mM Tris-HCl / 100 mM NaCl, pH7.5) at 37°C for 1 h. After assembly, all samples were fixed in 0.1% glutaraldehyde. (a, b) EM data show that the oligomers of α B-crystallin are massively recruited to DesWT or Des Δ RDG. Here, we observed depletion of α B-crystallin oligomers from grid surface and enrichment on desmin filament. Of note, when co-assembled with α B-crystallin, network formation of DesWT or Des Δ RDG is not as extensive as seen for other variants and the filament backbone of desmin is almost completely obscured due to binding of α B-crystallin. For Des Δ C451, a weak binding to α B-crystallin is observed, whereas binding is non-specific for other desmin variants because the amount of α B-crystallin oligomers bound to the filament roughly equals the amount of non-bound oligomers lying in the background. Scale bar: 100 nm

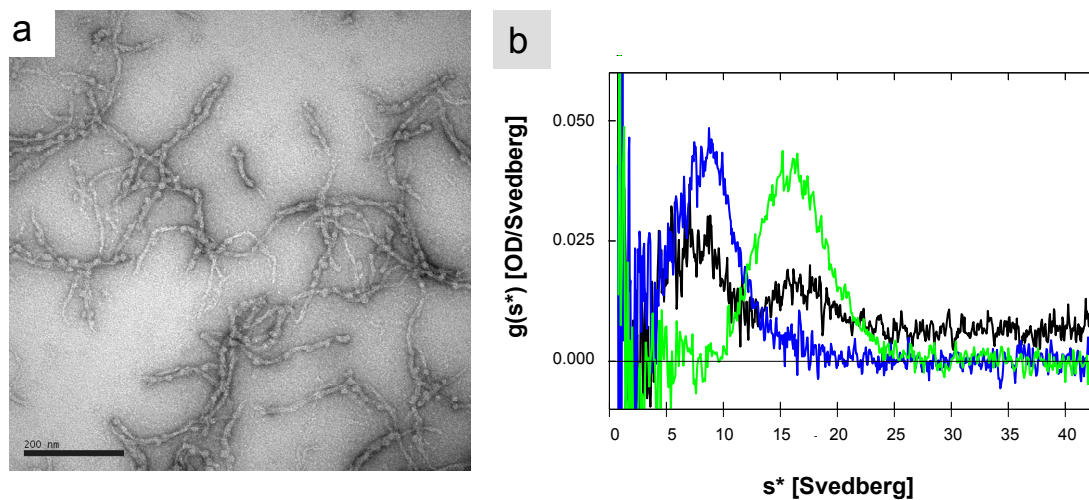


FIGURE 33 Tailless desmin interacts with α B-crystallin in buffer of low ionic strength

EM and AUC analysis was performed using equimolar concentration of the two proteins after ON dialysis of samples in “modified Tris-buffer”. (a) Electron micrograph of negatively stained sample of Des Δ tail co-incubated with α B-crystallin is shown. After ON dialysis, Des Δ tail and α B-crystallin were co-incubated for 1 h at 37°C without addition of “assembly buffer”. Sample was fixed in 0.1% glutaraldehyde after 1 h. As seen in this EM image, protofibrils of Des Δ tail bind to α B-crystallin also via non-carboxy tail domain under a buffer of low ionic strength. All α B-crystallin is bound to the protofibril and no α B-crystallin is visible in the background. Scale bar: 200 nm. (b) AUC experiment also shows an interaction between Des Δ tail and α B-crystallin under buffer of low ionic strength. Blue: desmin sedimenting alone, green: α B-crystallin sedimenting alone, black: desmin and α B-crystallin sedimenting together. Note the change in concentration for both desmin and α B-crystallin due to formation of aggregates resulting from interaction of these two molecules. These aggregates sediment faster than either desmin or α B-crystallin alone (black plot). s^* indicates sedimentation coefficient. Area was not normalized for different concentrations. Data analysis was performed using the software DCDT+.

In summary, cosedimentation, EM and viscometry data emphasize the role of C-terminal domain of desmin in modulating interaction with α B-crystallin under “high salt” assembly condition. Although the RDG motif is conserved among various species, our *in vitro* data suggest that it might not play any functional role in terms of binding to α B-crystallin. We hypothesize that the 3-dimensional structure, rather than the linear amino acid sequence involving this motif, is essential for binding. We speculate that the differential binding of α B-crystallin to DesWT or Des Δ tail most likely occurs due to differences in surface properties and exposed residues for full length and tailless desmin filaments. Binding sites for α B-crystallin might also be present in the N-terminal head and the rod domain of desmin which are probably obscured due to the peculiar rearrangement of filaments of Des Δ tail. We come to this speculation based on the fact that under unphysiological salt condition, protofibrils bind to α B-crystallin also via non-carboxy terminal domains.

5.6 Binding of α B-crystallin to desmin is influenced by the desmin filament architecture

A mathematical model was developed for the assembly kinetics of vimentin based on average length distribution of filaments measured in EM and atomic force microscopy (AFM) images [KIRMSE et al. 2007]. In this study, the vimentin assembly has been described to proceed via formation of ULFs within the first few seconds of assembly. This is followed by filament elongation occurring predominantly via

end-to-end annealing of ULFs and subsequent annealing of more extended filaments. The longitudinal annealing takes about one minute and occurs as an irreversible event *in vitro*. Desmin, like vimentin, is presumed to undergo the same process of assembly. However, we have noticed that desmin assembles more rapidly than vimentin under standard buffer conditions (22.5 mM Tris-HCl / 50 mM NaCl, pH 7.5). To analyse if the binding between desmin and α B-crystallin occurs at all stages of assembly, the kinetics of co-assembly was evaluated by time lapse EM, viscometry and cosedimentation assays.

First, we evaluated the assembly kinetics of desmin on its own for ten different points between 10 s and 60 min (10s, 1min, 2 min, 3 min, 4 min, 5 min, 10 min, 30 min, 45 min and 60 min) in EM by measuring the filament width at each time point. It is important to establish the assembly kinetics of desmin by itself, in order to choose appropriate time points for co-assembly with α B-crystallin. Desmin was dialyzed ON in “modified Tris-buffer”. Assembly was performed at 37°C by adding an equal volume of “assembly buffer” for the different time points and the samples were fixed in 0.1% glutaraldehyde to stop assembly. Our data show that as the desmin filament matures, the width of the filament is modified (**FIGURE 34a**). Whereas the filament width averages to 19 nm at 10 s due to the open ULF structures, it stabilizes to around 12.3 nm at a 60 min. At five time points - 10s, 1min, 3 min, 10 min and 60 min - we observed that desmin filament width alters significantly, indicating corresponding alteration of filament architecture. Based on the assembly kinetics of desmin alone, these five time points were chosen for co-assembly of desmin and α B-crystallin in cosedimentation assay.

We dialyzed desmin and α B-crystallin separately, co-assembled them under aforementioned buffer conditions and centrifuged the samples at 30,000 rpm, 20°C for 30 min. For band density evaluation, all cosedimentation assays were performed in triplicates. The cosedimentation data for the 5 different time points show that binding of α B-crystallin to desmin occurs predominantly within the first 10 s of desmin assembly (**FIGURE 34b**). Rapid binding at 10 s likely occurs because hydrophobic surface residues for binding of α B-crystallin are available on desmin shortly after assembly is initiated. Compared to co-assembly, the binding is reduced to ~30% if α B-crystallin is added to desmin filaments that have been pre-assembled for 1 min. Binding of α B-crystallin to desmin is reduced to ~10% at 3 min and it is abolished completely for all time points beyond 3 min. These data support our hypothesis that the filament architecture influences binding because we have observed a time dependent decrease in binding. Once the filaments have a mature surface, binding of α B-crystallin to desmin is prevented due to altered surface properties of the filament. These data also indicate that once bound to desmin, α B-crystallin is retained bound to the filament.

Viscometry and EM analyses corroborate the above results. When desmin and α B-crystallin were co-assembled, i.e. α B-crystallin was added to desmin before initiation of filament assembly, there was ~50% reduction in bulk viscosity as compared to desmin assembled on its own (**FIGURE 34c**). This is because α B-crystallin binds stably to the surface of elongating desmin filaments, thus, strongly impeding filament elongation and network formation (as seen in EM). However, this effect was not observed, once α B-crystallin was added to pre-assembled desmin filament (for 45 min). Here, the viscometry profile resembles that of wild-type desmin alone, suggesting that α B-crystallin does not bind to the mature surface of desmin IFs, and accordingly, no decrease in viscosity is observed. EM data show that the oligomers of α B-crystallin are recruited to desmin when the two are co-assembled for 120 min (**FIGURE 34d**). We observed depletion of α B-crystallin from the grid surface and enrichment on the desmin filament surface. Of note, when co-assembled with α B-crystallin, network formation of desmin is not as extensive as that of desmin alone or when α B-crystallin is added to pre-assembled desmin (**FIGURE 34e**). Of note, the filament backbone of desmin is almost completely obscured due to binding of α B-crystallin

upon co-assembly. Upon dialysis in “Tris-buffer” (5 mM, 1 mM EDTA, 0.1 mM EGTA, 1 mM DTT pH 8.4) and addition of “assembly buffer”, we had observed short desmin fragments with α B-crystallin bound to its tips in a regular manner (**Section 5.3**). On the other hand, for our “modified Tris-buffer” (1.0 mM Tris-HCl, 0.2 mM EDTA, 0.02 mM EGTA, 1 mM DTT, pH7.4) we observed a distinctly stronger binding of α B-crystallin to desmin filaments upon assembly but the periodic binding pattern was absent. The desmin filaments appeared longer after co-assembly with α B-crystallin if the samples are dialyzed in “modified Tris-buffer” as compared to “Tris-buffer”. In contrast, we did not observe any α B-crystallin bound to fully formed desmin network if it was added subsequently after 1 h of desmin assembly. Here, the amount of α B-crystallin oligomers bound to desmin filament was comparable to those lying freely on the grid surface.

In conclusion, our kinetics data suggest that binding of α B-crystallin to desmin occurs in a time-dependent manner and most of the binding occurs within the first 10 seconds of initiation of assembly, presumably due to the “open” filament structure of desmin. Once the filaments have a mature surface, binding of α B-crystallin is prevented due to altered surface properties of the desmin filament.

FIGURE 34 **Binding of α B-crystallin to desmin is influenced by the assembly status of desmin**

(Please refer to figure on next page)

(a) The Excel plot shows kinetics of desmin filament compaction. Desmin filament width is measured at five time points after initiation of assembly - 10s (19 nm), 1min (17.6 nm), 3 min (13.9 nm), 10 min (11.8 nm) and 60 min (12.3 nm). Alteration in filament width indicates corresponding alteration of filament architecture. (b) The cosedimentation assay data for the 5 time points show that binding of α B-crystallin predominantly occurs within the first 10 s of desmin assembly. Rapid binding at 10 s occurs likely because hydrophobic surface residues of desmin IFs are available for binding of α B-crystallin shortly after assembly is initiated. Compared to co-assembly and binding at 10 s, the binding of α B-crystallin is reduced drastically upon subsequent addition at 1 min and 3 min and abolished completely after 10 min. The Coomassie-stained gel band density of α B-crystallin in pellet fraction was evaluated using ImageJ 1.32j. The mean values of three independent cosedimentation assays are presented as mean \pm SD. All samples were assembled for a total duration of 120 min. T: total, SN: supernatant, Su: sucrose, P: pellet. (c) Viscometry profile is shown for desmin assembled alone for 60 min (filled circle), desmin and α B-crystallin co-assembled for 60 min (filled square), and α B-crystallin added after 45 min of desmin assembly and the two proteins co-incubated for 15 min (filled triangle). When desmin and α B-crystallin were co-assembled, there was almost 50 % reduction in bulk viscosity as compared to desmin assembled on its own. This suggests binding of α B-crystallin to desmin and prevention of proper network formation. However, this effect was not observed, if α B-crystallin was added to desmin that was pre-assembled (for 45 min). (d) Electron micrographs are shown for (top): desmin and α B-crystallin co-assembled for 120 min, and (bottom): α B-crystallin added to desmin 60 min after initiation of assembly and the two proteins co-incubated for 60 min. EM data show that the oligomers of α B-crystallin are recruited to desmin when the two are co-assembled. Note that upon co-assembly, the filament backbone of desmin is almost totally obscured due to binding of α B-crystallin. In contrast, the desmin filaments are instantly recognizable if α B-crystallin is added subsequently to desmin after 60 min of assembly. No specific binding to α B-crystallin is observed in this case. All samples were fixed in 0.1% glutaraldehyde after completion of assembly. α B-crystallin in bracket denotes that it was added subsequently to pre-assembled desmin. All samples are dialyzed ON at 1.0 mM Tris-HCl, 0.2 mM EDTA, 0.02 mM EGTA, 1 mM DTT, pH of 7.4. Assembly was performed at 37°C by adding equal volume of 100 mM NaCl / 40 mM Tris-HCl pH 7.5. Scale bar: 100 nm.

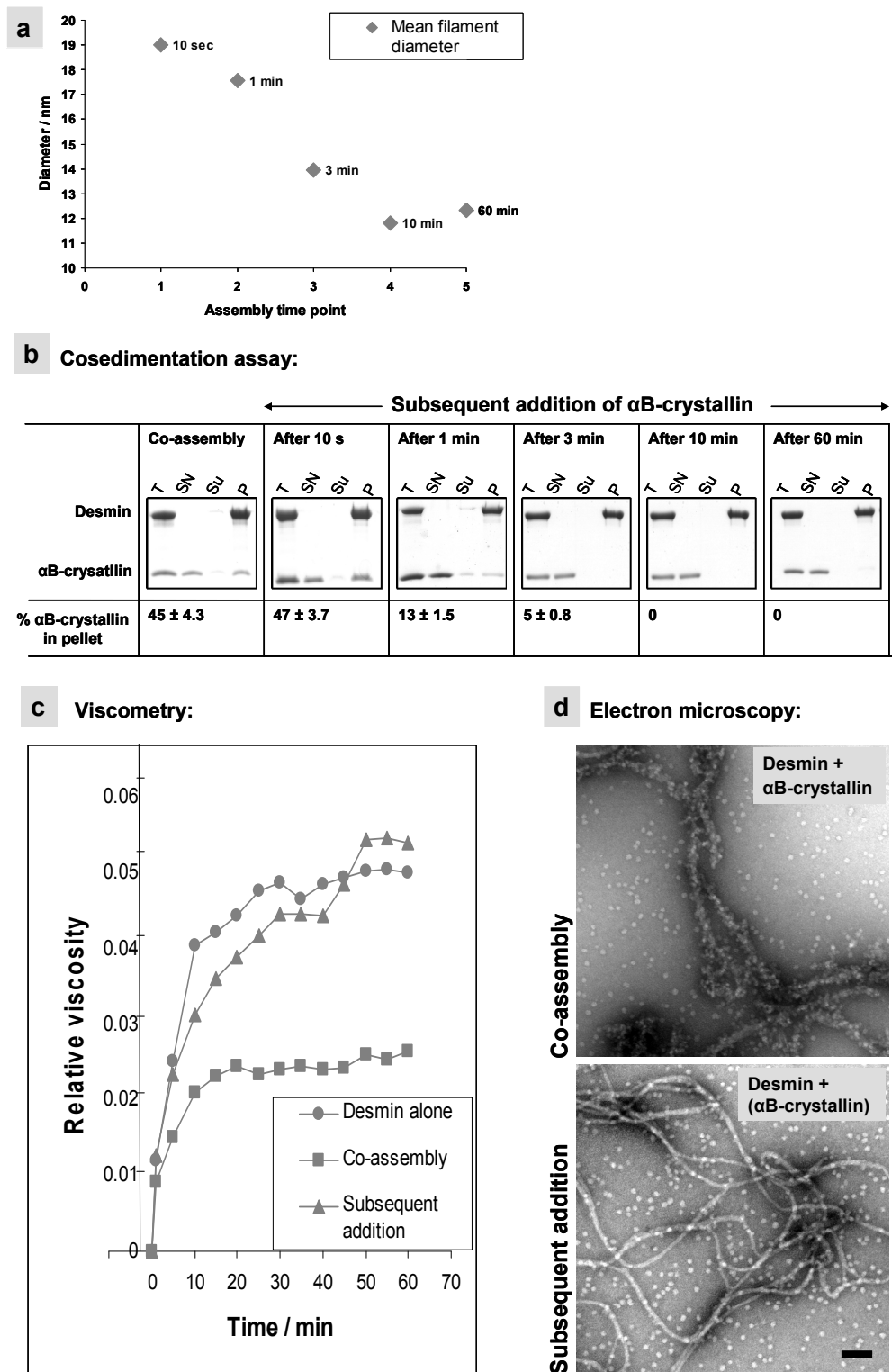


FIGURE 34 Binding of αB-crystallin to desmin is influenced by the assembly status of desmin

5.7 Desminopathy mutations influence the interaction of desmin with α B-crystallin

Several mechanisms have been proposed to explain the disease pathogenesis of the mutant CRYAB R120G associated with desmin-related myopathy and cataract. For example, *in vitro* experiments have confirmed that CRYAB R120G is a dominant negative mutation, whereby the mutant protein shows compromised polymeric structure when mixed with wild-type α B-crystallin [BOVA et al. 1999]. These structural changes coincide with a significant reduction in the *in vitro* chaperone activity of the R120G α B-crystallin protein, as assessed by temperature-induced protein aggregation assays [PERNG et al. 1999]. Yet another *in vitro* study has shown that this point mutation alters the binding characteristics of R120G α B-crystallin for desmin filaments, thus corroborating the observed disease pathology in DRM characterized by filament aggregation accompanied by α B-crystallin binding [PERNG et al. 2004]. So far, the mechanism of α B-crystallin-induced aggregation of desmin and vimentin leading to DRM and cataract respectively, has been investigated in detail, but the impact of desminopathy mutations on the interaction of desmin with α B-crystallin has not been analyzed.

To date, 11 desminopathy causing point mutations have been detected in the tail domain of desmin (*Supplementary FIGURE S10*; [GOLDFARB & DALAKAS 2009]). Mutations in the tail domain of desmin have been shown to have little impact on the assembly of mutant desmin protein, yet desmin-positive aggregates are seen in the muscle of patients harbouring these desminopathy mutations (please refer to **Section 4.4** [BÄR et al. 2007]). The phenotype exhibited by some of these tail mutants (e.g. DesR454W alone) is remarkable, because the tail domain, though evolutionarily highly conserved, is functionally not required for filament assembly [HERRMANN et al. 1996]. Few of these desmin tail mutants (DesI451M, DesE413K, DesK449T) also exhibit a dominant-negative effect on assembly of wild-type desmin when present in stoichiometric amounts during *in vitro* assembly. We have shown that the C-terminal domain of desmin modulates binding of α B-crystallin to desmin filaments (**Section 5.5**). Thus, we were interested to analyse the interaction of desminopathy-causing desmin tail mutants with α B-crystallin. To investigate their interaction, we focussed on two desmin tail mutants - DesR454W and DesI451M – that show abnormal filament properties either alone or as a mixture with desmin wild-type, respectively.

Samples were dialyzed ON in “modified Tris-buffer”. Co-assembly of desmin variants with α B-crystallin was performed at 37°C by adding an equal volume of “assembly buffer”. We also co-assembled DesWT, DesR454W and DesI451M with α B-crystallin at RT and 44°C. For cosedimentation assay, samples were centrifuged at 30,000 rpm, 20°C for 30 min. In cosedimentation assay, at any chosen temperature DesI451M, showed a weaker binding to α B-crystallin, whereas R454W showed a stronger binding compared to wild-type desmin (**FIGURE 35a, b**). At RT, the percentage of α B-crystallin recovered in the pellet for DesWT, DesI451M and DesR454W is 8%, 5% and 12%, respectively. At 37°C, the percentage of α B-crystallin recovered in the pellet for wild-type, DesI451M, and DesR454W proteins was measured to be 45%, 11%, and 84%, respectively. Interestingly, at 44°C, 100% of α B-crystallin was recovered in the pellet for Des R454W, whereas 80% and 32% α B-crystallin cosedimented with DesWT and DesI451M, respectively. For DesR454W, strong binding to α B-crystallin could be attributed to its “open” filament structure that was observed for this mutant when it was assembled alone at 10s, 5 min, 10 min and 60 min under our modified assembly conditions (data not shown). This open structure probably exposes hydrophobic patches on the filament surface and, thus, facilitates stronger binding to α B-crystallin. DesI451M showed no altered filament morphology when analyzed in EM. We investigated the binding of

DesR454W to α B-crystallin in more detail because of the distinct filament morphology of DesR454W under the buffer condition we used for assembly.

To assess if DesR454W can bind to α B-crystallin due to its inherent “open” structure even when α B-crystallin is added at 60 min to its pre-assembled filaments, we evaluated the kinetics of binding by performing EM and cosedimentation assay in parallel. DesR454W showed strong binding to α B-crystallin even after it had been pre-assembled for 1 h and then co-incubated with α B-crystallin for another 1 h at 37°C (**FIGURE 35c, e**). The same was observed for equimolar mixture of DesR454W with desmin wild-type (**FIGURE 35d, e**). EM and cosedimentation data suggest that the interaction between DesR454W and α B-crystallin occurs at all stages of DesR454W assembly. The mutant DesR454W has a dominant negative effect on the architecture and surface topology of wild-type filaments, as shown by the binding of the mixture to α B-crystallin even upon the subsequent addition of α B-crystallin at 60 min. To recapitulate briefly (**Section 5.6**), wild-type desmin that has been pre-assembled for 10 min or longer on its own, is incapable of binding to α B-crystallin, probably due to its mature surface.

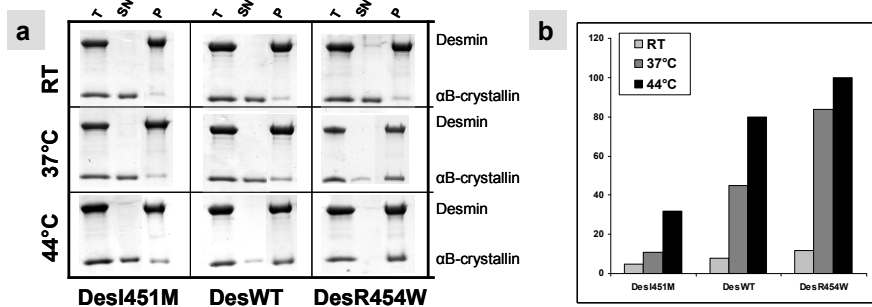
Next, to study if the stronger binding of α B-crystallin to DesR454W, as compared to DesWT, can also be reproduced in a cell, both mutant DesR454W or wild-type desmin were co-expressed with α B-crystallin in 3T3 cells by transfection. Our aim was to observe if any abnormal co-aggregation of R454W and α B-crystallin occurs in these cells. Of note, though 3T3 cells express endogenous α B-crystallin, the level of expression is comparatively low compared to cardiomyocytes (please refer to **Section 5.1: FIGURE 24**). Therefore, to obtain an expression-level of α B-crystallin comparable to those in cardiomyocytes, we transfected 3T3 cells with cDNA coding for wild-type α B-crystallin. Analysis of DesR454W or wild-type desmin co-transfected with α B-crystallin did not show any difference in morphology of the desmin filaments in immunofluorescence microscopy. We observed normal desmin filaments without aggregates of desmin and α B-crystallin for both DesWT and DesR454W (data not shown). Based on our *in vitro* data that suggest that the mutant DesR454W binds strongly to α B-crystallin likely due to its “open” filament, we next tested if this could also be true in cells by performing cytoskeletal extraction procedure on transfected cells. We proposed that the mutant DesR454W might be able to recruit more of the free cytosolic α B-crystallin to its exposed hydrophobic surface, and thus bind more strongly than wild-type desmin in 3T3 cells. If this happens to be true, then we expect to see more α B-crystallin in the insoluble IF protein-fraction for DesR454W than for wild-type through quantification of their respective supernatant and pellet fractions. Transfected cells were harvested and the supernatant and pellet fractions were further analyzed by Western blotting. To control for equal transfection efficiency, we probed the total lysate of both DesWT- and DesR454W-transfected cells against desmin antibodies as 3T3 cells do not express endogenous desmin. Similar transfection efficiency was obtained for both DesWT and DesR454W, as shown by comparable amount of desmin present in the pellets of both WT- and R454W-transfected cells (**FIGURE 35f**). However, for α B-crystallin we saw a significant difference in its distribution between supernatant and pellet fraction of cells transfected with WT and R454W (**FIGURE 35f, g**). In case of WT transfection, 76% and 24% α B-crystallin was distributed in supernatant and cytoskeletal-bound pellet fraction, respectively, whereas for R454W less α B-crystallin appeared in the supernatant (64%) and correspondingly more α B-crystallin was recovered in the pellet (36%). All in all, these transfection data suggest that DesR454W binds higher amount of cytosolic α B-crystallin than desmin wild-type. Probably, in desminopathy patients, mutant desmin variants recruit α B-crystallin to abnormal deposits of desmin in the myocyte by similar mechanism, i.e, by exhibiting “open” hydrophobic patches on their filament surface to which sHsps like α B-crystallin can bind rapidly.

FIGURE 35 Desminopathy mutants DesR454W and DesI451M exhibit altered binding to α B-crystallin

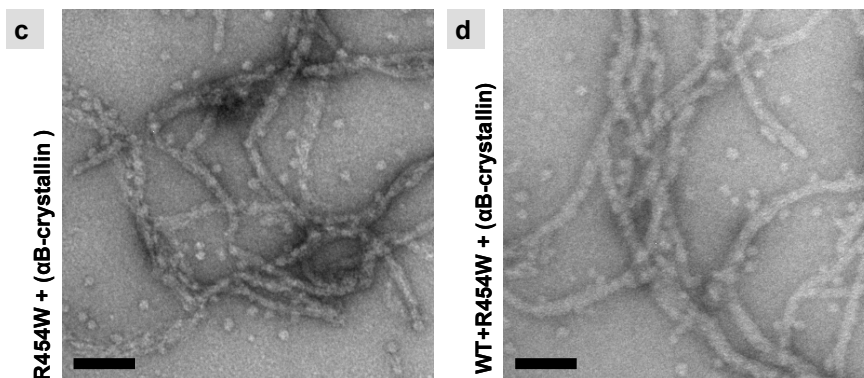
(Please refer to figure on next page)

(a-e) Samples were dialyzed ON in “modified Tris-buffer” (1.0 mM Tris-HCl, 0.2 mM EDTA, 0.02 mM EGTA, 1 mM DTT, pH 7.4). Co-assembly was performed at 37°C by adding equal volume of 100 mM NaCl / 40 mM Tris-HCl, pH 7.5. We also co-assembled DesWT, DesI451; and DesR454W at RT and 44°C. For cosedimentation assay, samples were centrifuged at 30,000 rpm, 20°C for 30 min. Gel band density of Coomassie-stained gels was evaluated using ImageJ 1.32j and plots were generated in Excel 2003. **(a, b)** In cosedimentation assay, at any given temperature DesI451M, showed a weaker binding to α B-crystallin, whereas DesR454W showed a stronger binding compared to wild-type desmin. In Excel plot, the ordinate depicts the percentage distribution of α B-crystallin in pellet. **(c, d)** EM images of negatively stained samples are shown. DesR454W shows binding to α B-crystallin even after it had been pre-assembled for 1 h and then co-incubated with α B-crystallin for another 1 h at 37°C, due to its “open” filament structure. The same was observed for equimolar mixture of DesR454W with desmin wild-type. All samples were fixed in 0.1% glutaraldehyde after assembly. Scale bar: 200 nm. **(e)** Cosedimentation data show that both DesR454W and its equimolar mixture with DesWT bind to α B-crystallin even after pre-assembly for 1 h and subsequent co-incubation with α B-crystallin for another 1 h at 37°C. DesWT shows binding to α B-crystallin upon co-assembly but no binding is seen if it has been pre-assembled for 1h and the incubated with α B-crystallin. **(f, g)** α B-crystallin is distributed differently between supernatant and pellet fraction of 3T3 cells co-transfected with WT/CRYAB and R454W/CRYAB. Similar transfection efficiency for both DesWT and DesR454W was obtained, as shown by comparable amount of desmin present in the pellets of DesWT- and DesR454W-transfected cells. Cells were harvested 2 days after transfection and both the supernatant and the pellet fractions of the cell lysate were analyzed by Western blot. Transfection experiments were performed in triplicate and for each transfection 2x 10 cm Petridish of confluent 3T3 cells were used. T: total, SN: supernatant, Su: sucrose, P: pellet.

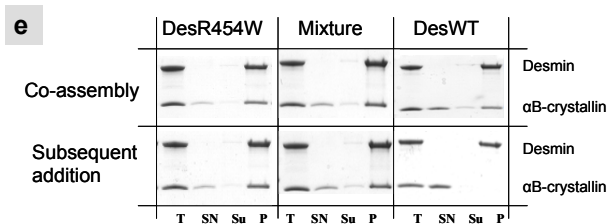
Cosedimentation assay:



Electron microscopy (α B-crystallin added subsequently):



Cosedimentation assay:



Transfection:

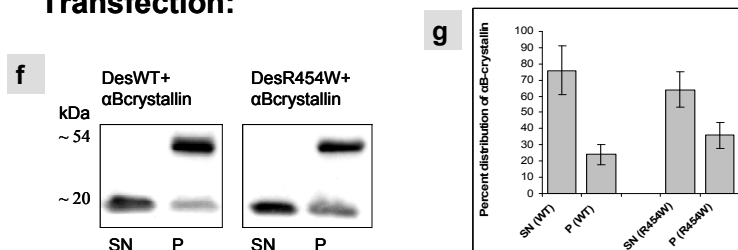


FIGURE 35 Desminopathy mutants DesR454W and Desl451M exhibit altered binding to α B-crystallin

Part III
Discussion, Conclusion & Outlook

Discussion

Microtubules (MTs), microfilaments (MFs) and intermediate filaments (IFs) form the three major cytoskeletal systems of a eukaryotic cell. Encoded by as many as 70 genes, the IF gene family represents the largest of the three groups [SZEVERENYI et al. 2008]. Besides their unique and complex tissue- and cell-specific distribution, several features distinguish IFs from MTs and MFs: (i) nucleotide-independent assembly, (ii) apolar fibrous structure that provides versatility to these proteins both structurally and functionally, (iii) existence of two parallel, yet spatially well separated IF systems - the cyto- and nucleoskeleton - in higher eukaryotes, and (iv) resistance to breakage by mechanical stress [HERRMANN et al. 2009]. The muscle-specific IF protein desmin possesses some intriguing properties that set it apart from the other members of type III IF protein with respect to its developmentally regulated expression pattern, polymorphic assembly behaviour, and mechanical properties [HERRMANN et al. 1999, KREPLAK et al. 2008]. IF genes are a primary target for point mutations that eventually lead to morphological and functional tissue damage. Mutations in desmin, that account for up to 2% of dilated cardiomyopathies, are categorized as a distinct subgroup of myofibrillar myopathies, known as desminopathy. In this thesis, the mechanism of desminopathy is investigated by studying the causal relationship between “intrinsically” modified desmin filament properties and “extrinsically” altered association of desmin to the small heat shock protein α B-crystallin (FIGURE 36).

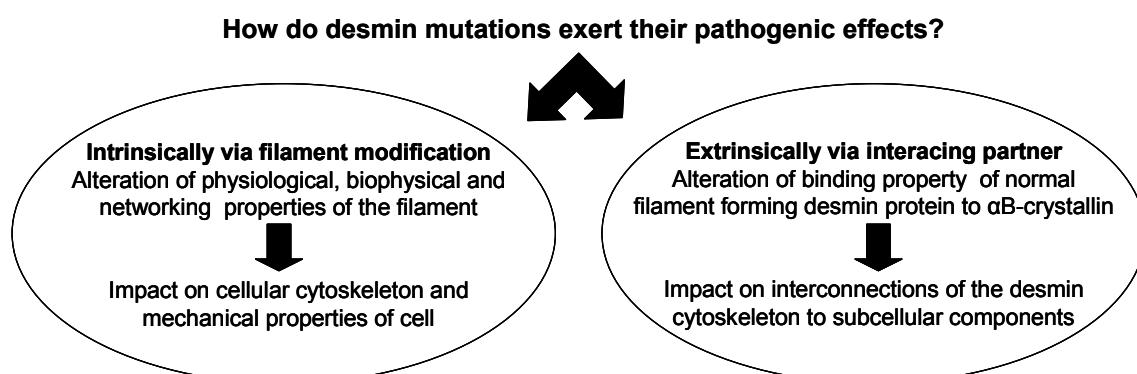


FIGURE 36 The objective of this dissertation is to understand the pathogenesis of desminopathy by analysis of “intrinsic” and “extrinsic” mechanisms that contribute to desminopathy

6.1 Modification of desmin filament properties by mutations

6.1.1 Impact of disease mutations in the head domain of desmin on assembly and network-forming properties

As a first objective of this thesis, we have characterized the filament-forming properties of desmin disease variants that arise due to mutations in the head, rod, or tail domain of desmin. In the case of head mutants, our investigations reveal that all but the two proteins, DesS13F and DesR16C, both harbouring mutations located in a highly conserved nonapeptide motif “SSYRRTFGG”, are assembly competent *in vitro*. These two mutants also exhibit the most severe effects on network-forming properties in transfected cells.

Like wild-type desmin, mutant head desmin variants form tetrameric species under low salt/high pH conditions. When compared to wild-type desmin, slightly higher *s*-values were obtained for four of the five mutants analyzed. However, in general, soluble tetrameric assembly precursors prevailed for all analyzed mutants along with minor higher order complexes. In this study, various assembly protocols were employed in order to follow the association behaviour of the mutant proteins. Even protocols that allow comparatively gentle renaturation and association of the recombinant protein did not prevent DesS13F and DesR16C from forming filamentous aggregates. The distinctly altered filaments formed by these two mutants, irrespective of a given renaturation protocol, thereby represent their inherent property. Upon co-assembly with wild-type desmin, most mutants formed apparently normal filaments. Mutant desmin variants located in the nonapeptide motif, i.e., DesS13F and DesR16C, formed comparatively thinner filaments, showing a readily distinguishable alteration of the filament's architecture. This variation in filament diameter corresponds to an altered number of subunits within each filament segment, as shown in the past for other desmin mutants by scanning transmission EM [BÄR et al. 2006].

Viscosity measurements were performed in order to analyze the bulk network properties of the polymerized filaments. Apart from DesS2I, the other four mutant desmin variants diverged considerably from the wild-type desmin phenotype as concluded from their time-dependent viscosity profile. This indicates a substantial impact of single point mutations in the desmin head domain on the viscosity of the filament network. Upon co-assembly with wild-type desmin, all mutant variants, but DesS46F, displayed an altered viscometric profile. Although some of the mixtures formed apparently normal filaments as visualized by EM, it can be stated that the bulk biophysical properties of most mutant proteins differed distinctly from those of wild-type desmin.

Different cell lines were employed to probe the capability of the mutant desmin variants to assemble into filamentous network in distinct cellular surroundings. Majority of the mutants were competent to form filaments in one or the other cell line used. Interestingly, DesS13F exhibited altered filament formation in SW13 and MEF Vim^{-/-} cells and disrupted the endogenous IF network in 3T3 and HL-1 cells to various extents. Hence, it can be speculated that under *in vivo* conditions the cell cannot compensate for the deleterious effect of this mutant on filament assembly and network formation. On the contrary, DesS2I showed a normal wild-type-like filament network in all four investigated cell lines, suggesting its ability to integrate and respond well to cellular cues. In case of DesR16C, DesS46F, and DesS46Y, around 12–15% of transfected cell population also showed proteinaceous deposits in MEF Vim^{-/-} and in HL-1 cells. Such variability with respect to the formation of desmin deposits has also been reported for desminopathy patients. In particular, variability was observed for mutant desmin protein expression,

turnover, and aggregation both in different tissues of individual patients and in corresponding tissues from different patients [CLEMEN et al. 2009].

Amino acid composition of the human desmin head domain

21 Ser residues are located in the “head” domain of human desmin. Most of them are potential phosphorylation sites (FIGURE 37). Phosphorylation has been shown to influence the structural organization of desmin and may even lead to disassembly of filaments under various physiological stimuli. Interestingly, most disease-causing mutations identified to date result from the substitution of Ser residues by hydrophobic residues (Ser2Iso, Ser13Phe, Ser46Tyr/Phe). This might have an impact on vital regulatory structural alterations of the desmin network that take place under cellular stress conditions. Moreover, the replacement of Ser by aromatic amino acids may interfere with a “matrix” of hydrophobic interactions exhibited by the aromatic residues. A “stacking-type” interaction of the aromatic rings may give rise to and stabilize a loop structure consisting of hydrophilic residues. All three mutations, S13F (FIGURE 37b), S46F, and S46Y (FIGURE 37c) would considerably change the loop pattern, particularly in the latter two cases, whereas the S13F mutation would introduce a bulky residue very close to the authentic tyrosine 14 and thereby change the chemical property of the entire evolutionary conserved nonapeptide motif (FIGURE 37a: boxed in wild-type desmin).

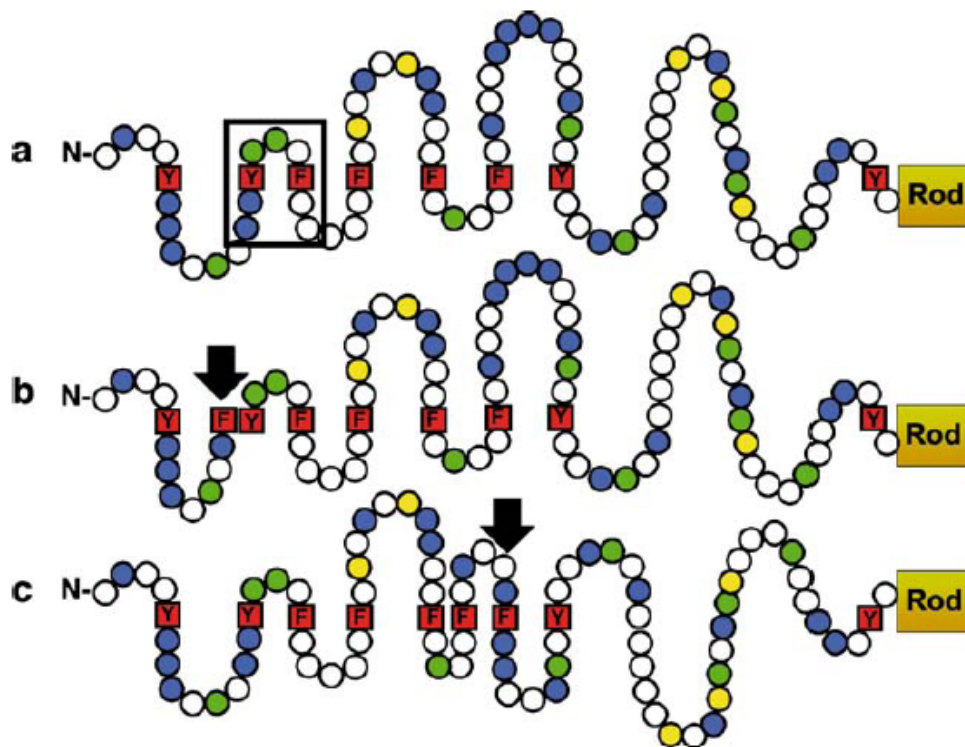


FIGURE 37 Amino acid composition of the human desmin amino-terminal head domain

(a) In case of wild-type desmin, 8 aromatic amino acid residues (red squares) interrupt the otherwise hydrophilic amino acid composition by forming a complex of benzene ring networks which are buried inward and are thought to stabilize the tertiary structure of the “head” domain. Black box depicts the conserved nonapeptide motif “SSYRRTFGG”. The mutations S13F (b) and S46F/Y (S46F, c) introduce additional aromatic residues that are expected to change the tertiary structure of the amino-terminal head domain. White circle: nonaromatic residue, blue circle: Ser residue, green circle: Arg residue, yellow circle: Leu residue, red square: aromatic residue.

Role of the nonapeptide motif “SSYRRXFGG” in assembly of type III IF proteins

The nonapeptide motif “SSYRRXFGG”, where X is variable, occurs within the otherwise rather heterogeneous head domain sequence of type III and IV IF proteins like desmin, vimentin, peripherin, internexin as well as NF-L and is evolutionarily conserved from amphibia to man. Previous studies have elaborated on the role of this motif “SSYRRTFGG” with respect to vimentin filament assembly. Deletion mutants from vimentin’s nonapeptide domain disturb its filament assembly and networking properties *in vitro* and in cells. In particular, the two central arginines and the flanking aromatic residues were shown to be important for proper filament assembly. Replacement of the arginine residues with serine resulted in aggregate formation. Substitution of the tyrosine and phenylalanine residues by Ser resulted in an assembly-deficient mutant phenotype. Interestingly, the deletion of the entire motif generated an extremely rapidly associating mutant protein, such that already after 1 min of assembly massive protein aggregations were observed. Moreover, this protein entered two assembly pathways: one pathway leading to the formation of normal filaments and the other one to large sheets of regularly associated fibers [SHARMA et al. 2009. & references therein].

Role of amino-terminal head domain in assembly of type III IF proteins

Various studies have shed light on the role of amino terminal sub-domain in assembly of type III IF proteins - desmin and vimentin. Data from *in vitro* assembly of headless vimentin and desmin indicate that an intact N-terminal domain of these IF proteins is a prerequisite for the formation of higher order filamentous structures. Partial or complete removal of the desmin- or vimentin-head by proteolysis or mutagenesis renders these IF proteins assembly-incompetent [GEISLER et al. 1982, TRAUB & VORGIAS 1983, KAUFMANN et al. 1985]. In another example, at 5 mM Tris-HCl, pH 8.4 headless vimentin only forms dimers, whereas tetramers are obtained for wild-type vimentin. Even under assembly conditions, headless vimentin dimers can only form tetramers and fail to mature further, suggesting that the removal of the head domain renders IF molecules soluble under physiological conditions, i.e., they do not associate significantly above tetramers [HERRMANN et al. 1996, MÜCKE et al. 2004]. It has been suggested that the arginine-rich head domain of type III IF proteins, which is basic in nature, interacts with the carboxy end of the rod domain which is acidic in nature, and this interaction may serve to position the dimers appropriately into A₁₁-type tetramers [PARRY et al. 2007]. Correspondingly, the introduction of negatively charged groups by phosphorylation of serine residues in the head domain causes the disassembly of filaments, as shown for vimentin and desmin, whereas phosphatase treatment of phosphorylated subunits restores their competence for assembly.

6.1.2 DesL377Δ22fs and loss of desmin expression in humans

A homozygous out-of-frame desmin deletion in exon 6 was identified in 2 siblings born from French consanguineous parents. This mutation leads to the synthesis of a shortened desmin that is truncated at the end of rod domain. In effect, this mutation causes total desmin depletion in muscle, as the mutant desmin does not accumulate in the patients. Our *in vitro* assembly studies indicate that the mutant protein DesL377Δ22fs possibly interacts with wild-type desmin at the dimer level and at the tetramer level, forms mature filaments in presence of wild-type desmin, yet it fails to form an extended cytoskeleton in all four cell lines that were investigated. As desmin positive aggregates were not detectable in the tested individuals that harbour this mutation, we suspected that the aberrantly folded mutant protein, as seen upon *in vitro* assembly on its own, might be rapidly degraded by the ubiquitin

proteasome system (UPS). The UPS successfully unfolds and degrades a vast variety of substrates in a robust and efficient manner [CIECHANOVER et al. 2000]. Soluble ubiquitinated misfolded proteins accumulate in a juxtannuclear compartment where proteasomes are concentrated. In contrast, terminally aggregated proteins are sequestered in a perivacuolar inclusion. In most cases modification by ubiquitin targets the substrate for degradation by the 26S proteasome. We could not detect the truncated desmin variant in primary myotubes of the heterozygous mother even when the proteasome degradation machinery was inhibited by epoxomicin or lactacystin.

The mutation L377 Δ 22fs generates a premature termination codon which fulfils the conditions for nonsense-mediated decay (NMD). Transcripts with premature termination codons are rapidly degraded by NMD, if the premature stop codon is situated 50–55 nucleotides 5' of a splicing-generated exon–exon junction. In eukaryotes, NMD is an indispensable surveillance pathway to prevent accumulation of potentially harmful truncated proteins and for proper regulation of alternatively spliced products [AMRANI et al. 2006]. We propose that the mutant transcript is most likely downregulated by NMD, hence no misfolded or aggregated protein is seen in the muscle of both the homozygous siblings and the heterozygous mother. To verify that this mRNA quality control mechanism is responsible for mutant desmin absence, our collaborators [Dr. Ana Ferreiro, Paris] quantified desmin mRNA and pre-mRNA in skeletal muscle from homozygous and heterozygous individuals using real-time qPCR. Remarkably, in the homozygous muscle, we found a major depletion of total desmin mRNA and total absence of wild type mRNA. Total mRNA in the muscle from heterozygous mother was reduced by at least 50% compared to control muscles [Manuscript in preparation: CARMIGNAC et al.]. These data indicate a NMD-mediated downregulation of L377 Δ 22fs.

Unexpectedly, vimentin was overexpressed in the muscle of affected homozygous patients. During myogenesis, vimentin is originally predominantly synthesized in the muscle precursor cells and is then gradually replaced by desmin in some kinds of muscle such that it is no longer detectable [HERRMANN et al. 1989]. Additionally, it has been shown that vimentin and desmin can copolymerize *in vivo* [QUINLAN & FRANKE 1982]. Overexpression of vimentin suggests that this protein could partially take over some of the functions of desmin IF in the myocyte of these patients. All in all, the findings with respect to DesL377 Δ 22fs expand the spectrum of MFM and suggest that not all desminopathies are associated with desmin-positive aggregates. In summary, the absence of desmin is – like in transgenic mice – not immediately lethal and is compatible with the generation of by and large normal muscle architecture.

6.1.3 Desmin tail mutants and filament property

In contrast to the head domain, the tail domain does not seem to be essential for assembly of cytoplasmic IFs and it appears to be primarily involved in regulating lateral interactions to control filament width [HERRMANN et al. 1996]. Accordingly, proteolytic removal of the last 27 residues from the tail domain of desmin still leads to the formation of filaments [KAUFMANN et al 1985]. The smallest IF protein known, i.e. cytokeratin 19, which is devoid of tail domain, forms normal IFs in the presence of a type II cytokeratin indicating that the tail is dispensable for filament formation [HATZFELD & FRANKE 1985]. Interestingly, recently it was reported that the R454W mutation, which did not show an obvious phenotype in transfected cells, seems to affect desmin assembly properties *in vivo*. In the cytoplasm of patient cells, a somewhat higher content of dimmers, than with wild-type desmin in control cells, was observed [LEVIN et al. 2010].

The theory raised previously that disease mutations render the mutant desmin protein assembly incompetent, consecutively causing the misfolded protein to segregate into large intracellular aggregates in myocytes of desminopathy patients harbouring these mutations, needs revision especially in the context of mutations residing in desmin's non- α -helical carboxy-terminal tail domain. These mutants are, by and large, assembly competent, as shown in this and past studies [BÄR et al. 2007]. As the tail is supposed to reside to a large part outside of the filament body, it is conceivable that mutations in the tail domain do not influence interactions within the filament (“intrinsic” properties) but those of the filament with cellular components (“extrinsic” properties). The modification of “intrinsic” biophysical properties was measured recently for three rod mutants whose single filaments were adsorbed to a solid support and then the single filaments were manipulated with the tip of a cantilever of AFM [KREPLAK & BÄR 2009]. Two of these mutants exhibited aberrant nanomechanical behaviour as measured by the change in torque of AFM cantilever that was monitored during stretch.

To analyze a causal relationship between the tail mutants and their effect on filament property, novel insights into the network forming properties and the viscoelastic behaviour of various tail mutants was gained by means of mechanical rheometry in cooperation with the group of Norbert Willenbacher at the Karlsruhe Institute of Technology [BÄR et al. 2010]. For the tail mutants, we compared how the filament assembly as observed *in vitro* and in transfected cells, correlates to bulk filament properties as measured rheologically. Of note, unlike MTs and MFs which break when subjected to shear stress, IFs made from vimentin and desmin have been shown to exhibit a pronounced increase in their elastic modulus, a behaviour known as “strain stiffening” [SCHOPFERER et al. 2009]. For DesR454W alone, the storage modulus decreased monotonically with increasing strain amplitude. This result for DesR454W corroborates with EM and transfection data as discussed (**Section 4.4**). All other mutant proteins, as well as their mixtures with wild-type desmin, showed significant strain stiffening

The idea of “intermediate filaments as mechanical integrators of cellular space”, proposed way back in 1980 by Elias Lazarides [LAZARIDES 1980], is now widely accepted and has been extended to the whole cytoskeleton. IF proteins supposedly provide cells with compliance to small deformations, yet strengthen cells when large stresses are applied. Hence, mutations that alter the flexible intracellular scaffolding of IF proteins may dispose cells to mechanical injury and cause human disorders, a typical example being epidermolysis bullosa simplex that occurs in humans most frequently by IF-disrupting mutations in the keratins [FUCHS & CLEVELAND 1998]. Recent disease mutations in human IF proteins indicate that the nanomechanical properties of cell-type-specific IFs are central to the pathogenesis of diseases as diverse as muscular dystrophy and premature ageing [HERRMANN et al. 2007]. However, the analysis of these various diseases suggests that IFs also have an important role in cell-type-specific physiological functions.

6.2 Desmin “crosstalks” with the small heat shock protein α B-crystallin

6.2.1 Interaction of desmin filaments with α B-crystallin

As a second objective of this thesis, we have addressed the question “if” and “how” the interaction between desmin disease mutants and α B-crystallin is altered and hence may take part in the pathomechanism of some of the desminopathies. First, we speculated that the tail domain of desmin mediates its interaction with other cellular proteins, because: (i) like other members of IF protein multi-gene family, a significant fraction of the end domains of desmin is disposed in outer positions on the

filament surface, where they can interact optimally either with one another or with other cellular entities to meet functional and/or structural obligations, (ii) a considerable body of evidence indicates that intrinsically unstructured regions of proteins play key roles in protein–protein interactions, and (iii) in contrast to the head domain, the removal of the tail domain does not inhibit desmin assembly. Thus, to identify potential binding partners of desmin we performed Y2H analysis, whereby, human cardiac, skeletal and smooth muscle libraries were screened using a bait construct coding for the last 67 amino acid residues of desmin (Des Δ N403). Des Δ N409 contains the “TYRKLLEGEE” motif from the C-terminal end of the rod domain which represents the domain boundary between rod and tail domain of desmin. Hence, we employed Des Δ N403 as bait to ensure proper folding of this fragment in yeast cells. From the sequencing analysis of positive clones, we identified CRYAB as a reproducible hit in as many as 60 clones and it showed a low score for “prey promiscuity”, whereas other preys like smoothelin and H1FO were identified in 7 and 2 clones, respectively. As an ATP-independent molecular chaperone, α B-crystallin is a ubiquitous component of the protein “quality control” network and mutations in CRYAB can also lead to MFM, therefore we found α B-crystallin to be an interesting interaction partner of desmin for further analysis. We showed by immunofluorescence staining that desmin and α B-crystallin co-localize in cardiomyocytes as well as in 3T3 cells at the subcellular level.

sHsps like α B-crystallin bind and maintain denaturing proteins in a folding-competent state and thereby, serve as a first line of defense against stress-induced cell damage. The mechanism, by which a sHsp interacts with IF proteins could represent an additional means by which at least some chaperones protect against protein aggregation and limit the onset of misfolding diseases.

Our data show that the binding of α B-crystallin to desmin occurs predominantly within the first 10 s after initiation of assembly. Of note, desmin occurs predominantly as ULF at 10 s under assembly conditions and these ULFs are considered to be “open” structures, hence they might provide an ideal platform for binding of α B-crystallin desmin. On the other hand, mature desmin filament fails to bind α B-crystallin. We speculate that once the filaments have a mature surface, then the binding of α B-crystallin is prevented due to “closed” and compact structure of the desmin filament. Additionally, these data show that, despite the decrease in diameter as desmin filament matures, the α B-crystallin is retained bound to the filament. Stable binding observed between desmin and α B-crystallin might be critical for cellular processes where the sHsps bind to their substrates in an energy-independent manner until ATP-dependent Hsps are recruited to prevent protein aggregation. Other groups have proposed from *in vitro* data, that sHsps associate with IF proteins to help prevent non-covalent filament-filament interactions resulting in cells [PERNG et al. 1999].

The substrate binding regions of ATP-dependent chaperones are well-defined, but interactions between sHsps and substrates are poorly understood [JAYA et al. 2009]. Defining the substrate-binding sites of α B-crystallin on desmin is a key to understanding its cellular functions and to harnessing its aggregation-prevention properties for controlling damage due to protein aggregation that ensues in the myocyte of desminopathy patients.

6.2.2 Domain of desmin modulating interaction with α B-crystallin

In desminopathy, α B-crystallin should recognize and bind the IF protein desmin prior to nucleation of aggregation, i.e. should detect the increased shift of destabilized desmin proteins toward the aggregation-prone non-native states. In order to determine the precise region on the desmin molecule that is necessary for its interaction with α B-crystallin, we performed *in vitro* investigations. Initial results

using EM and cosedimentation assays showed that of the three different buffer systems, “Tris-NaCl” buffer system is suitable to study the interaction of desmin and α B-crystallin. AUC data show that the oligomeric status of α B-crystallin does not vary significantly in different buffer systems at a pH value of 7.5 and the complex comprising ~22 subunits sediments at 17 S. As <10% of total α B-crystallin cosedimented with desmin in this buffer system, we optimized the pH and ionic strength of this buffer. We observed maximum binding of α B-crystallin to desmin when samples were dialyzed into 1.0 mM “Tris-HCl” pH 7.4 and assembled at a final ionic strength of 20.5 mM Tris-HCl / 50 mM NaCl, pH 7.1. On contrary, under similar conditions, we show that binding to α B-crystallin is severely reduced for a desmin fragment Des Δ C451 with <50% α B-crystallin recovered in its pellet upon cosedimentation, as compared to wild type desmin and ~2 oligomers of α B-crystallin associated with its filaments for a predefined area. For DesWT, approximately 7 oligomers of α B-crystallin associate with its filaments within the same area when observed in EM. Binding to α B-crystallin is almost completely suppressed for all other fragments that are shorter than 440 amino acids starting from the N-terminus, i.e. Des Δ C441, Des Δ C431 and Des Δ tail (Des Δ C403). For Des Δ tail, ~4% α B-crystallin was recovered in the pellet but no specific association was observed in EM. We speculate that the reduction of bound α B-crystallin occurs likely due to differences in hydrophobic surface properties and exposed residues of wild-type desmin and its deletion variants. The tail domain of IF proteins have certain conserved residues like the tripeptide motif “RDG”. We showed that there is no effect on binding of α B-crystallin to Des Δ RDG that is devoid of this conserved motif. Therefore, we propose that the prerequisite for binding of α B-crystallin to desmin is the 3-dimensional protein conformation which can be altered in a mutant, and not the linear amino sequence involving conserved motifs *per se*.

6.2.3 Evidence for binding of α B-crystallin to multiple desmin domains

Headless desmin (Δ N85) and its rod domain (Δ N85- Δ C409) were not used for cosedimentation assay to study association with α B-crystallin under “high salt” conditions because they cannot form *bona fide* filaments. But when we analyzed these fragments as well as DesWT and Des Δ T with respect to interaction with α B-crystallin in 1.0 mM “Tris-HCl” pH 7.4, both EM and AUC data pointed to the presence of a similar association between these proteins (please refer to **FIGURE 33**). Thus, under unphysiological salt condition, protofibrils of desmin can bind to α B-crystallin also via non-carboxy terminal domains. Unlike the ATP-dependent chaperones Hsp70 or Hsp90, which have distinct substrate binding regions, it is likely that sHsps like α B-crystallin rely on multiple contact sites distributed throughout the substrate protein to protect substrates from irreversible aggregation. Thus, binding sites for α B-crystallin could be present in the non- α -helical amino-terminal head, the central α -helical rod and in the non- α -helical carboxy-terminal tail domain of desmin. These binding domains are probably obscured in mature and “compact” wild-type desmin filament or in Des Δ tail due to their altered arrangement of protofibrils, hence disabling the binding of α B-crystallin to these entities.

We have proposed a model for binding of α B-crystallin under “low” (unphysiological) and “high” salt (physiological) conditions. Whereas α B-crystallin oligomers are recruited to exposed hydrophobic patches / residues of filamentous wild-type desmin or disease mutants under “high” salt (**FIGURE 38a**), under “low” salt condition the oligomers of α B-crystallin slide through the protofibril-like structure of desmin that originate under such buffer condition (**FIGURE 38b**). Of note, quaternary structure of α B-crystallin protein, as seen by cryo-EM, reveals spherical assemblies between 8 and 18 nm in diameter with a central cavity [HALEY et al. 2000]. Hence, it is likely that the diameter of the protofibrils is smaller

than 8 nm under “low” salt conditions such that these protofibrils fit into and can pass through the cavity of α B-crystallin complex (for comparison please refer to **FIGURE 32a**, **FIGURE 33a**).

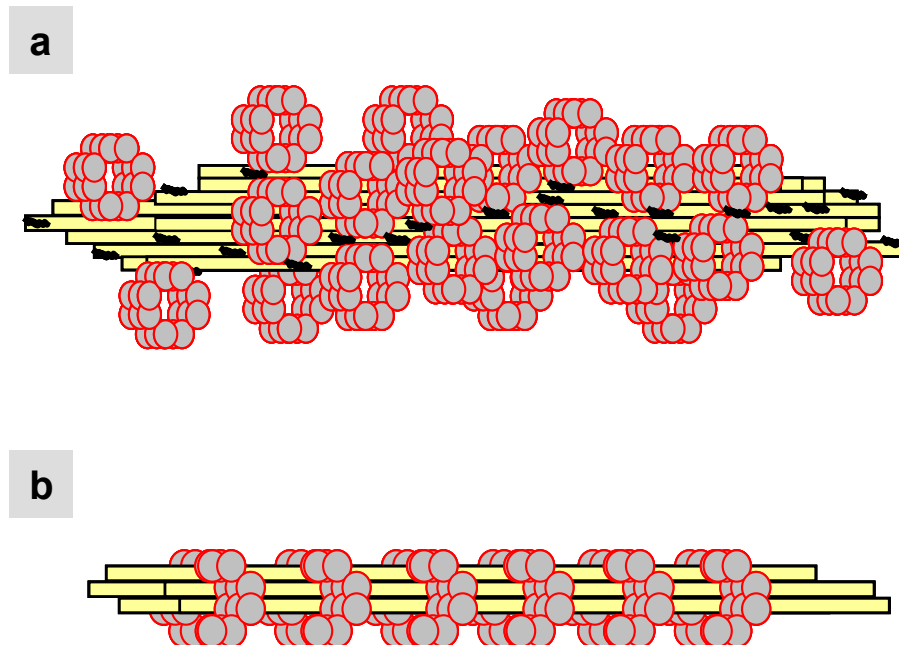


FIGURE 38 A Model depicting association of α B-crystallin to desmin under “high” and “low” salt conditions

(a) Whereas α B-crystallin-complex is recruited to exposed hydrophobic patches / residues (black wavy lines) of filamentous wild-type desmin or disease mutants under “high” salt, (b) under “low” salt condition the oligomers of α B-crystallin slide through the protofibril-like structures of desmin that originate under such buffer condition. Grey circle: subunit of α B-crystallin, yellow rod: subunit of desmin.

6.2.4 Desminopathy mutants show altered interaction with α B-crystallin

To analyze the interaction of α B-crystallin with desminopathy mutations, we chose two missense mutations – I451M and K449T - from the tail domain of desmin. These tail mutants show abnormal filament properties either alone or as a mixture with desmin wild-type, respectively. Analysis of the binding of the two tail mutants - DesI451M and DesR454W – to α B-crystallin by cosedimentation assay reveals weaker and stronger binding at all three temperatures (RT, 37°C and 44°C), respectively, compared to wild-type protein. We speculate that, much like ULFs, mutant DesR454W exhibits “open” filament architecture throughout its assembly and is, thus, able to recruit α B-crystallin to its exposed hydrophobic surface more robustly at all assembly time points compared to desmin wild-type as shown by EM. Even as equimolar mixture with desmin wild-type, binding to α B-crystallin is retained at all time-points of assembly for this mutant. This indicates that the mutant exerts dominant-negative effect on wild-type desmin in terms of altered filament nanoarchitecture.

The *in vitro* data for mutant DesR454W is complemented by *in vivo* data. The soluble and insoluble protein fractions of DesWT and DesR454W-transfected 3T3 cells were harvested and further analyzed by Western blotting. Despite similar transfection efficiencies for both DesWT and DesR454W, we observed a significant difference in the distribution of α B-crystallin between their supernatant and pellet fractions. DesR454W is capable of binding ~50% more cytosolic α B-crystallin than desmin wild-type in cells. Probably it recruits the free cytosolic α B-crystallin to its exposed hydrophobic surface more actively than DesWT. Presumably, this mutant causes a changed association of desmin with α B-crystallin in 3T3 cells. Our data suggest that the mutation R454W causes toxic gain-of-function, whereby the desmin mutant shows enhanced binding to α B-crystallin. One plausible explanation for aggregate formation in desminopathy could be this altered interaction of desmin with its associated proteins.

All in all, DesR454W is a dominant mutant that forms altered filaments both alone and in mixture with desmin wild-type (*in vitro*) and exhibits toxic gain of function, i.e. enhanced binding to α B-crystallin (both *in vitro* and in cells). Thus, these data extend the paradigm that “intrinsic” architecture is crucial to protein function. The weaker binding of DesI451M to α B-crystallin needs further investigation, but it is worth mentioning here that whereas the mutation R454W introduces a bulky aromatic tryptophan residue in the mutant protein by replacing the original negatively charged arginine residue, for I451M, one apolar residue is substituted by another apolar residue of lighter MW. Thus, it is reasonable to assume that, depending on the type of amino acid substitution, the exposed surface properties of resulting filaments of DesI451M and DesR454W are different and this also dictates their altered binding to α B-crystallin. Consequently, it is possible that altered binding to α B-crystallin may, in a feedback inhibition mode, interfere with the desmin assembly and disassembly process.

For the R120G mutant of α B-crystallin, it has been proposed that an enhanced protein–protein interaction between R120G α B-crystallin and lens vimentin promotes vimentin aggregation, and this eventually leads to cataract [SONG et al 2008]. In this study, GFP-tagged vimentin as donor and red fluorescence protein (RFP)-tagged α B-crystallin as acceptor were imaged by confocal fluorescence resonance energy transfer (FRET) microscopy after transfecting HeLa cells. Confocal fluorescence images showed that the cells expressing vimentin and R120G α B-crystallin contained large amounts of protein aggregates compared to wild-type α B-crystallin expressing cells. Besides R120G, there are two other myopathy-associated α B-crystallin mutations: Q151X and 464delCT. Both mutations lead to the formation of cytoplasmic aggregates in skeletal muscles, but they do not cause cataract. Perhaps, the effects of these two mutations in terms of interaction with desmin are the same as that of R120G mutation, but the effects on vimentin are different. The mechanism underlying such different effects is not known until today.

Interestingly, it was recently demonstrated that the expression of an assembly competent disease-causing DesE245D mutant in primary cultures of cardiac and skeletal myocytes destroys the actin thin filament architecture yielding filaments of variable lengths [CONOVER et al. 2009]. It was shown that the coil 1B region of desmin, where the mutation E245D is located, binds to the C-terminal end of the giant sarcomere actin-binding protein nebulin with high affinity. In case of mutant DesE245D, the binding of desmin to nebulin was enhanced by 4-fold in solid-phase binding assays. Expression of the DesE245D in myocytes displaced endogenous desmin and C-terminal nebulin from the Z-discs and caused a concomitant increase of intracellular aggregates, reminiscent of histopathological hallmark of desminopathies.

6.2.5 Defining the mechanism of chaperone action of sHsps

Protein aggregation resulting from stress, disease, or mutation poses a major threat to all cells. To avoid this, cells have developed mechanisms of protein “quality control” involving specific proteases and molecular chaperones to prevent or resolve protein aggregation [JAYA et al 2009]. The differential expression patterns of sHsps with regards to tissue types, for instance relatively high expression levels in eyes and muscles, suggest that sHsps have general as well as specialized functions in cells. Since upregulation of sHsps has been implicated in a wide range of diseases from cancer to cardiomyopathies, defining the mechanism of sHsp chaperone action has wide-ranging implications for understanding cellular stress and disease processes.

sHsps have an unusually high capacity to bind unfolding proteins and to facilitate subsequent substrate refolding by ATP-dependent chaperone systems. High capacity and absence of energy consumption make sHsp proteins an efficient defence mechanism under stressful conditions that promote indiscriminate unfolding of cellular proteins and where use of ATP-dependent chaperones might be wasteful of cell resources [MCHAOURAB et al. 2002]. Recently, upon analyzing the architecture and dynamics of complexes formed between an oligomeric Hsp18.1 and its substrate by mass spectrometry, over 300 different stoichiometries of interaction were observed. This demonstrates that an ensemble of structures underlies the protection these chaperones confer to unfolding proteins [STENGEL et al. 2010]. Accordingly, sHsps are one of the least well understood classes of molecular chaperones because of their inherent tendency to heterogeneity, both due to their stoichiometry of oligomerization and substrate binding.

At least five common interactive domains in human α B-crystallin participate in the recognition and selection mechanisms used by sHsps to distinguish between homologous subunits, unfolding substrates, and assembling filament proteins. The selective rather than specific nature of the interaction between sHsps and unfolded substrate proteins appears to be a function of the amount of unfolding and exposed hydrophobic surface of the substrates [GHOSH et al. 2006]. Evidence indicates that α B-crystallin may interact with another family member, Hsp27, in non-lenticular tissue just as it does with α A-crystallin in the lens. Thus, possible heterogeneous oligomerization of mutant R120G α B-crystallin with Hsp27 may stabilize the mutant, delaying the formation of aggregates and the symptoms associated with this subtype of desmin-related myopathy [FU & LIANG 2003]. Very little is known about the regulation of α B-crystallin under physiological conditions and about the parameters that influence its oligomerization and substrate binding. Therefore, further investigations are required in order to have a better understanding of these mechanisms.

Conclusion and Outlook

Although accumulation of aggregated desmin seems to be a consistent histopathological finding in desminopathy, it remains to be elucidated how the different desmin mutations identified in human patients lead to the dysfunction of myocyte at the molecular level.

In principle, both a loss of function caused by the insufficient assembly of “normal” desmin filaments and a dominant gain of gene function, which deviates from the “typical” function of a desmin molecule, may contribute to desminopathy. Our data demonstrate the impact of desmin mutations on its structural properties as well as the molecular interaction of desmin with α B-crystallin. This adds to our understanding of the molecular basis of desminopathy as we show that subtle alterations in the nanoarchitecture of desmin filament are sufficient to induce aberrant interaction with the associated protein α B-crystallin. Such a modified protein-protein interaction could be a plausible explanation for aggregate-formation in desminopathy.

Although various tissue-specific functions and interaction partners of the intermediate filament protein desmin are still to be defined, its principal hallmark, i.e. its coiled-coil architecture not only dictates its oligomerization, but evidently also plays a critical role in imparting filament stiffness and maintaining desmin’s ability to function as molecular sensor for pre-determined biological functions. One such function is the interaction of desmin with the molecular chaperone α B-crystallin that might be essential to the integrity of the cellular cytoskeleton. Mutations in desmin that perturb its inherent coiled-coil architecture may jeopardize both the structural and functional stability of the cellular machinery.

In case of desminopathy, much less information is available on the tissue expression levels of the mutant protein with respect to that of wild-type. Thus, the question remains: how much mutant desmin protein is sufficient to cause protein aggregation in skeletal or cardiac muscle of affected patients? Another challenging question is how the “crosstalk” between desmin cytoskeleton and the nucleoskeleton contributes to the overall structural integrity and “well-being” of cells, and how this might be “jeopardized” due to mutations arising in desmin. The fact that varying disease phenotypes (e.g. involvement of skeletal versus cardiac muscle) have been observed for different desmin mutations suggests that different mutations may act via separate molecular pathways.

The remarkable “phenotypic convergence” for desmin and α B-crystallin is reflected by the finding that mutations in either of the proteins can lead to myofibrillar myopathies. In a cellular system, it is likely that a “symbiosis” occurs between α B-crystallin and desmin in the “co-habitation” arrangement. The

filaments can retain their stability whilst α B-crystallin has a safe haven to associate with other cellular targets. To understand the molecular basis of desminopathy, the cytoplasmic regulatory mechanisms that govern the assembly-disassembly of desmin and α B-crystallin need further investigations.

Recently, a much unexpected finding by Capetanaki and colleagues shows that overexpression of α B-crystallin in Des^{-/-} mice completely rescues the desmin knock out phenotype [personal communication]. These data, thus, set the stage for detailed investigations on molecular association of the two proteins.

Eventually, a better understanding of the molecular basis of desminopathy may contribute to the development of new therapeutic approaches that aim at restoring normal cellular function by maintaining physiological desmin filament assembly and inhibiting the formation of pathological aggregates.

Part IV
Materials and Method

In vitro analyses

8.1 Cloning and mutagenesis

Point mutations were introduced into the full-length clone of human desmin cDNA by site-directed mutagenesis (Quickchange[®], Stratagene) according to the manufacturer's protocol [Herrmann et al. JMB 1999: 286, Bär et al. 2005] using appropriate primers (see appendix). Des Δ head (Δ N85) and Desrod (Δ N85- Δ C409) were generated as described [Dissertation Norbert Mücke 2009, Division of Biophysics of Macromolecules, DKFZ]. Des Δ tail (Δ C409) in pDS5 was generated as described [HERRMANN et al. 1999] (**FIGURE 39**). This construct was transferred into the vector p163/7 using primers containing EcoRI/XhoI restriction site. The deletion variant Des(ESA) Δ C244 in the α -helical rod domain was generated as described [BÄR et al. 2009]. Mutation L377 Δ 22fs was introduced into the full-length clone of the human desmin WT cDNA by PCR. The desmin C-terminal truncation constructs for interaction studies with α B-crystallin were generated using primers designed to introduce stop codon at the respective amino acid positions (**Section 5.5, Appendix A.1.2**).

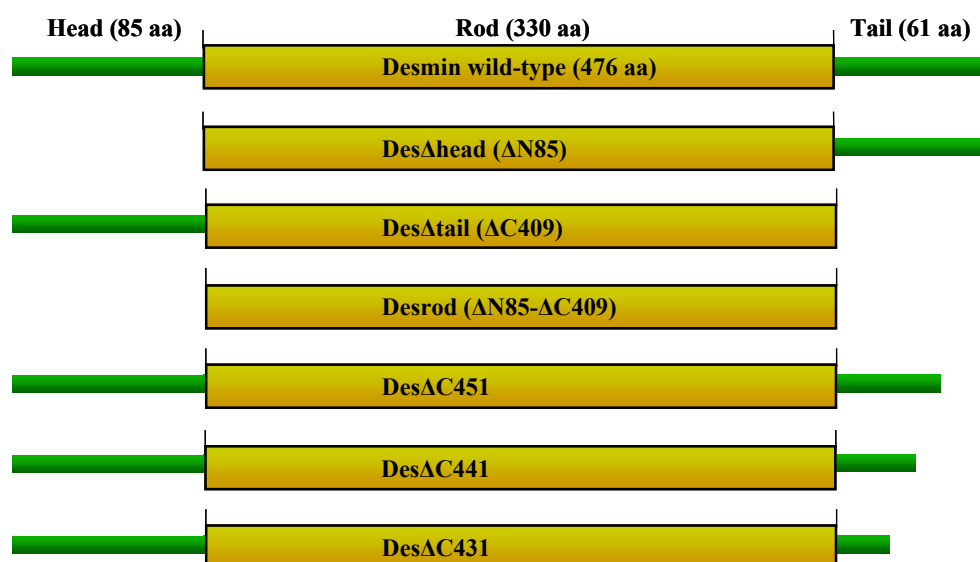


FIGURE 39 Schematic representation of desmin deletion constructs used in the current study

Following transformation into *E. coli* strain DH5 α , the appropriate clone was identified by DNA sequencing. For protein expression, cDNAs of desWT or point mutations and deletion constructs were subcloned into the T5 promoter-driven prokaryotic expression vector pDS5 using EcoRI/EcoRI restriction sites. This vector was modified slightly at its multiple cloning site, whereby the NcoI site was exchanged against the original NdeI site and a Shine-Dalgarno sequence was inserted after the unique EcoRI site. For cell transfections, human MHC promoter-driven eukaryotic expression vector p163/7 was used routinely [BÄR et al. 2006]. Of note, except for desmin head mutants, all other mutant variants used during this thesis expressed alanine at position 2. This modification was done to avoid rapid degradation of serine residue at this position in prokaryote expression systems [ROGERS et al. 1986].

For yeast-two-hybrid screening vector pGBT9 was restriction digested (EcoRI/BamHI) along with PCR-amplified desmin “tail” domain of desmin which was used as bait (primers, see appendix). The vector pGBT9 is suitable for expression of fusion proteins with the DNA-binding domain of GAL4, and carries the TRP1 marker for selection in yeast. The bait consisted of nucleotides coding for the last 67 aa residues of desmin’s amino-terminus starting at the motif TYRKLEEGEE. The screening was performed against libraries of the human heart, skeletal muscle and smooth muscle from aorta by Manfred Kögl (Core Facilities, DKFZ). DNA sequencing was performed by Andreas Hunziker (Core Facilities, DKFZ). Primers were synthesized by Wolfgang Weinig (Core Facilities, DKFZ) or ordered from Biospring (Frankfurt) and Sigma-Aldrich (Darmstadt).

8.2 Inclusion body and protein purification

8.2.1 Inclusion body purification

For protein expression and purification, wild-type or mutant desmin cDNAs were subcloned into the prokaryotic expression vector pDS5 as described previously [HERRMANN et al. 1999]. The clones were expressed in *E. coli* strain TG1 (Amersham Biosciences) or JM109 (Novagen) for protein purification. JM109 was the strain of choice due to considerably less degradation of exogenously expressed desmin in inclusion bodies of these bacteria. Inclusion body purification was carried out as mentioned ([HERRMANN et al. 2004]; **FIGURE 40**; Buffer compositions: *Appendix A.3.1*).

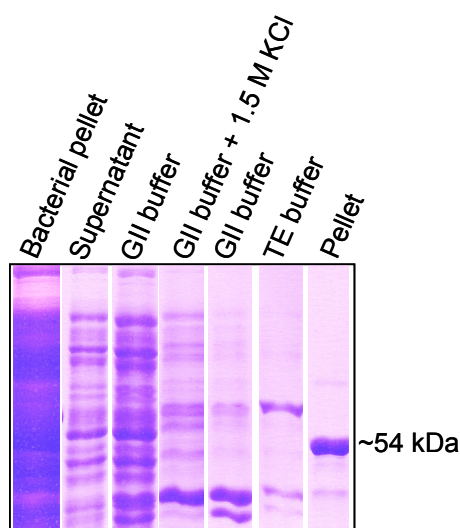


FIGURE 40 Inclusion body purification of recombinant desmin

Briefly, the harvested bacterial pellets were lysed in lysis and detergent buffers, respectively, in a dounce homogenizer. After eliminating the soluble proteins, DNA and RNA fragments post centrifugation, the pellet fraction consisting of inclusion bodies was washed with different buffers (GII, GII + 1.5 M KCl, GII, TE). Finally the pellet was dissolved in 9.5 M urea buffer and centrifuged at 35 k rpm for 1 h. The different fractions post bacterial cell lysis were loaded on 10% Laemmli gel and stained with Coomassie blue. Of note, the supernatant and the consecutive wash fractions (from GII buffer till TE buffer) are virtually devoid of desmin. The desmin-enriched pellet fraction is used as an input for DEAE column.

8.2.2 Desmin protein purification with ion exchanger

Purification of a given protein with anion and cation exchanger is based on the net protein charge, and hence it is pH dependent. Therefore, it is important to know the pI of the protein to be purified, which in case of desmin is 5.4. For the DEAE anion exchange resin a pH above the pI of desmin was chosen such that the protein would be negatively charged and vice versa for a CM cation-exchanger (Sepharose™ Fast Flow GE Healthcare) [HERRMANN et al. 2004]. Both the DEAE- and the CM-column buffers used for routine desmin purification had a pH of 7.5, for Des Δ head and Desrod, 30 mM sodium formate urea buffer at pH 4.0 was used instead (Buffer compositions: *Appendix A.3.2*). This is due to the fact that the head domain of desmin protein is rich in basic residues, thus its deletion changes the pI of desmin protein to < 5.4. Bound protein was eluted from the column with a linear salt gradient of 0-0.3 M KCl. Of the numerous protein fractions eluted from DEAE-column, peak fractions as observed in Bradford assay and SDS-PAGE were pooled for further purification through CM-column (**FIGURE 41a, b**). Eluted fractions from CM column were analyzed by SDS-PAGE. Fractions containing purified desmin were collected, aliquoted, and stored at -80 °C by adding 10 mM methyl ammonium chloride till further use. Protein concentrations were determined by Bradford assay using bovine serum albumin as standard. Purified proteins were checked for appropriate size (**FIGURE 41c**), degradation and stability by running protein samples on gel. Western blot was performed routinely for every purified protein with suitable anti-desmin antibody (**TABLE 5**).

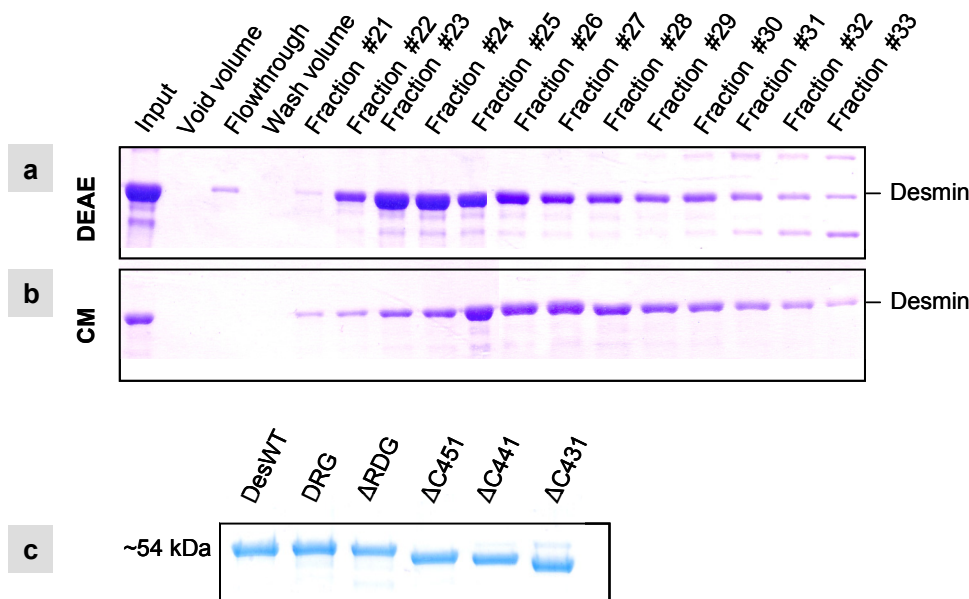


FIGURE 41 Purification of recombinant human desmin and protein quality control

Desmin wild-type was purified by (a) DEAE- and (b) CM-sepharose columns. From the DEAE column, fractions #22 - #29 were pooled and used for further purification by CM-column. The DEAE fractions #30 - #33 are discarded as, in addition to desmin, they also contain other bacterial proteins. The protein purified through CM-column is virtually devoid of other bacterial proteins. (c) Protein size is controlled for the generated C-terminal deletion constructs of desmin. The different proteins were loaded on 10% Laemmli gel and stained with colloidal Coomassie blue. DRG is a construct where the conserved RDG residue in tail domain has been flipped to DRG, hence it runs at same size as DesWT. The shorter size of deletion variants Δ C451, Δ C441 Δ C431 is distinctly visible on the stained gel.

8.3 Protein dialysis

For all different dialysis methods, protein concentration was adjusted to 1 µg/µl by diluting the sample in 8 M urea buffer if required. For standard assessment of assembly competence and for measuring viscometric properties of desmin variants, samples were dialyzed step-wise from 8 M urea buffer into “Tris-buffer” (5 mM Tris-HCl, 1 mM EDTA, 0.1 mM EGTA, 1 mM DTT, pH 8.4) ON. as employed in the past for various desmin mutants [BÄR et al. PNAS, BÄR et al HMG]. Half the volume of urea buffer was replaced with equal volume of “Tris-buffer” in a stepwise manner every 20 min starting from 8M urea→ 4M urea → 2M urea → 1M urea (Buffer compositions: *Appendix A.3.5*). This step-wise dialysis ensured that the denatured protein gradually reverts to soluble tetramer-octamer units. For experiments involving mixtures of wild-type and mutant protein, equal amounts of the two proteins were combined prior to dialysis in 8 M urea so as to allow heterodimer formation upon dialysis into “Tris buffer”. The following day, protein concentration of the samples was measured by Bradford assay before assembling the protein for electron microscopy, viscometry or diameter measurement.

8.4 Protein assembly for EM and viscometry

Purified desmin protein is reconstituted *in vitro* for characterization by different assays. Three different assembly methods are employed as mentioned below:

- i. For routine assessment, after dialysis in “Tris-buffer” the protein concentration was adjusted to 0.4 mg/ml prior to assembly for electron microscopy. The head mutant proteins DesS13F and DesR16C were also assembled at a lower protein concentration of 0.1 mg/ml. For viscometric analyses, all head mutant proteins were assembled at 0.1 mg/ml. Assembly was initiated by rapid addition of equal volumes of “assembly buffer” (100 mM NaCl, 40 mM Tris-HCl, pH 7.0) at 37°C.
- ii. Alternatively, samples were dialyzed into “Tris-buffer” as in method 1 and adjusted to a protein concentration of 0.2 mg/ml post dialysis. Assembly was initiated by further dialysis of samples into “filament buffer” (50 mM NaCl, 20 mM Tris-HCl, pH 7.5) for 1 h at 37°C. This method enables a slower change to higher salt and lower pH conditions, which in turn allows the formation of more uniform and homogeneous filament species compared to method 1. This method was employed to check assembly competence under “milder” conditions and for diameter measurement of mature filaments of head mutant proteins.
- iii. In a third variation, head mutant protein samples were dialyzed initially at a concentration of 0.2 mg/ml in 8 M urea for 2 h at RT and then directly into “filament buffer” at 37°C for 5, 30, 60 or 120 min, respectively. Thereby, o.n. dialysis in “Tris-buffer” was omitted.

For electron microscopy, protein samples were fixed in 0.1% glutaraldehyde-and were mounted upon glow-discharged formvar-carbon coated 200-mesh copper grids (spi® Supplies, West Chester, PA USA) or self-coated grids after assembly. These grids were negatively stained with 0.2% uranyl acetate for 20 s. The specimens were observed in a Zeiss 900 transmission electron microscope (Carl Zeiss, Germany) with use of an accelerating voltage of 80 kV. Images were acquired at various magnifications between 21000-112000x on a CCD-camera. These images were further processed in Adobe Photoshop 7 (Adobe systems).

Viscosity measurements were carried out with an Ostwald viscometer (Cannon-Nanning, Semi-Viscometer, Zematra BV, Netherlands) [Bär et al. HMG 2005]. For diameter measurements protein samples were dialyzed and assembled on a single day for comparison. The EM images were processed

using ImageJ 1.32j (<http://rsb.info.nih.gov/ij>). At least 100 filament-width measurements were carried out per sample. Data are reported as mean \pm SD. Student's t test was used to analyze the statistical significance of the filament diameters determined for the desmin disease variants, their mixtures with wild-type desmin, and DesWT. All reported p values were two-sided and considered to be statistically significant at $p < 0.05$. Statistical evaluations were performed using Excel 2003 (Microsoft®, Seattle, USA).

8.5 Cosedimentation assay and gel quantification

To study interaction of desmin with α B-crystallin, equimolar ratio of the two proteins was maintained for all assays, whereby desmin at a concentration of 0.3 $\mu\text{g}/\mu\text{l}$ and α B-crystallin at 0.12 $\mu\text{g}/\mu\text{l}$ was used. Human recombinant α B-crystallin protein was kindly provided by Dr Roy Quinlan (School of Biological and Biomedical Sciences, Durham University) and was purified as described [PERNG et al. 1999]. Starting with imidazole buffer [PERNG et al. 1999], later phosphate [MÜCKE et al. 2004] and "Tris-buffer" systems were analyzed to study interaction of the two proteins. The "Tris-buffer" conditions were further optimized to maintain the physiological filament morphology and width while simultaneously enhancing the interaction of desmin and CRYAB. Eventually, I settled for a "modified Tris-buffer" (1 mM Tris pH 7.4, 0.2 mM EDTA, 0.02 mM EGTA, 1 mM DTT) as the interaction between desmin and α B-crystallin was maximized under these conditions and, simultaneously, the physiological filament properties were maintained (see appendix A.3.5). Whereas desmin was dialysed step-wise from urea buffer into "modified Tris-buffer", α B-crystallin was directly dialysed into the latter. As routine, co-assembly was initiated in a Beckman ultracentrifuge tube (#344090) by rapid addition of equal volume of "assembly buffer" (100 mM NaCl, 40 mM Tris-HCl, pH 7.0) to equimolar desmin and α B-crystallin protein sample assembled at RT, 37°C or 44°C for 1 h such that the final salt / pH conditions were 50 mM NaCl, 20.5 mM Tris-HCl, pH 7.1. After co-incubation for 1 h at indicated temperature, samples were centrifuged at 30,000 rpm for 30 min at 20°C in a Beckman centrifuge with swing-out TLS 55 rotor (Beckman Coulter) in order to pellet the assembled desmin filament and any filament-associated α B-crystallin (**FIGURE 42**).

Protein samples were assembled directly onto 0.85 M sucrose cushion to prevent any loss of assembled desmin filament because of adhesion to pipette tips while transferring the assembled protein sample. During initial optimization of cosedimentation assay, 100 μl protein sample was layered onto 300 μl of 0.85 M sucrose cushion and after sedimentation this sucrose fraction was pipetted out in volumes of 50 μl , resulting in 6 different sucrose fractions being loaded on the tricine gel altogether. The top 100 μl sample after centrifugation was pipetted out as the supernatant fraction, followed by 300 μl sucrose and 100 μl pellet. The pellet was dissolved in equal volume of 10 M urea and sample buffer to obtain a final volume of 100 μl . Later on, once the cosedimentation assay was optimized, 100 μl protein sample was layered onto 200 μl of 0.85 M sucrose cushion and just one pooled sucrose fraction was loaded onto the gel. The pellets were dissolved as before in a total of 100 μl . Representative amounts of supernatant, sucrose and pellet fractions were loaded on 15% tricine gels and stained with Coomassie blue overnight. Once the domain of desmin to which α B-crystallin binds had been narrowed down, a 16 aa peptide SEVHTKKTVMIKTIET corresponding to this region was synthesized for peptide competition assay. This peptide synthesis was carried out by Peptide Specialty Laboratories GmbH, Heidelberg. All cosedimentation assays were performed in triplicates to make statistical evaluations. For quantification, all gels were stained overnight in Colloidal Coomassie. Destaining was performed for 1 h in destaining solution followed by fixation in fixation buffer (Buffer compositions: *Appendix A.3.4*). The gels were scanned in Adobe Photoshop CS3 and the saved images were quantified with ImageJ 1.41. The values

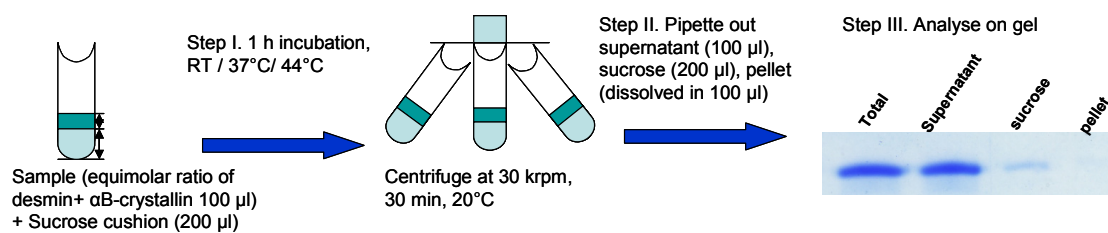


FIGURE 42 Flowchart for cosedimentation assay

The protein sample is layered onto a 0.85-M sucrose cushion in assembly buffer and after 1 h centrifuged at 80,000 g for 30 min. The supernatant and pellet fractions are analyzed by SDS-PAGE and are visualized by Coomassie blue staining. The proportion of GFAP distributed between pellet and supernatant fractions was measured using ImageJ software.

obtained from quantification of individual bands were imported in excel to obtain graphs for the distribution of proteins in sucrose, supernatant and pellet fractions.

8.6 Analytical ultracentrifuge

Analytical ultracentrifugation (AUC) is a rigorous method for characterization of soluble molecular complexes in the native state and as they exist in solution. AUC is considered to be a universal choice to study interactions between two solute molecules. Aggregation between molecules will lead to a change in molecular weight, so that a detailed study of changes in molecular weight as a function of the concentrations of the components can illuminate the type of reaction (e.g., reversible or nonreversible), the stoichiometry, and the strength of binding.

The application of a centrifugal force causes the depletion of macromolecules at the meniscus and the formation of a concentration boundary that moves toward the bottom of the centrifuge cell as a function of time. Sedimentation coefficient of a macromolecule s is a function of its molar mass. The s -values are commonly reported in Svedberg (S) units, which correspond to 10^{-13} seconds. All AUC experiments were performed with an Optima™ XL-A analytical ultracentrifuge. There are two basic types of experiment with the analytical ultracentrifuge: sedimentation velocity and sedimentation equilibrium. In sedimentation velocity, the rate of movement of boundary of sedimenting solute is measured. This leads to the determination of the sedimentation coefficient s , which depends directly on the mass of the particles. Sedimentation velocity experiments were carried out at 20 °C and 40,000 rpm. Sedimentation equilibrium experiments provide the means of determining the molecular weight of the complex as it exists in solution independent of the shape of the particle. Sedimentation equilibrium runs were carried out at 20 °C by first pre-sedimenting the sample for two hours. For desmin, scans were recorded at 7000 rpm and at 10,000 rpm every four hours until no change could be detected between successive runs; this usually took 20 hours [MÜCKE et al. 2004]. For α B-crystallin, the scans were recorded at 5000 rpm. The distribution of centrifugally accelerated particles is measured by absorption optics. The absorbance optical system of the Optima™ XL-A is a high-intensity xenon flash lamp that allows the use of wavelengths between 190 and 800 nm. Recombinant protein samples were dialyzed step-wise from 8 M urea into "Tris-buffer" or into the buffer of choice overnight at a concentration of 0.5–1.0 mg/ml using regenerated cellulose dialysis tubing (Spectra/Por®, MWCO 50,000; Roth, Germany). Dialysis-steps in urea were omitted for α B-crystallin. $s^*(20,w)$ indicates sedimentation coefficient of a macromolecule corrected for the viscosity and density of the solvent, relative to that of water at 20°C (20°C, water). The $g(s^*)$ distribution is determined by extrapolating the distribution back to time zero, accounting for the

radial dilution effects. Thus the total area under the $g(s^*)$ curve represents the loading concentration of any one species in a mixture. The dc/dt (dc : differential concentration, dt : differential time) method calculates a differential apparent sedimentation coefficient distribution $g(s^*)$. $g(s^*)$ distribution can be computed with the software Dcdt+ developed by J. Philo (<http://www.jphilo.mailway.com/dcdt+.htm>) [LEBOWITZ et al. 2002]. Data analysis was performed as described [MÜCKE et al. 2004].

8.7 Oxidative cross-linking

In order to detect if the mutant and wild-type proteins are capable of interacting at dimer level, oxidative crosslinking of the two proteins was performed. The mutant, wild-type and their equimolar mixtures were dialyzed step-wise from 8 M urea into “Tris buffer” ON and the following day in freshly prepared “Tris buffer” without DTT in order to remove the reductant. Cross-linking was done at a protein concentration of 0.4 mg/ml in Tris-buffer using with 50 μM H_2O_2 / 5 μM CuCl_2 for 1 h at RT [ROGERS et al. 1996]. The cross-linked products were analyzed by SDS-PAGE whereby the reductant DTT was omitted from the protein sample buffer.

Analyses in cells

9.1 Cell lines and cell culture

For transfection studies, we used four different cell lines, two of them were completely devoid of cytoplasmic IFs: the human adrenocortical carcinoma cell line SW13 and mouse embryonic fibroblasts derived from vimentin knockout mice ((MEF Vim^{-/-}; [COLUCCI-GUYON et al. 1994]). The latter was kindly provided by Dr. Robert Goldman (Northwestern University) and Dr. Thomas Magin (University of Bonn). In addition, two murine cell lines expressing cytoplasmic type III IFs were used to assess if mutant desmin variants are capable of integrating into a pre-existing IF cytoskeleton: fibroblast cells (3T3) expressing endogenous vimentin, and HL-1 cells derived from a AT-1 mouse atrial cardiomyocyte tumor lineage expressing endogenous desmin [CLAYCOMB et al. 1998]. SW13 and 3T3 cells were maintained in Dulbecco's Modified Eagle Medium (DMEM, Gibco, #41965) with 10% fetal calf serum (FCS) and 2 mM L-glutamine. MEF Vim^{-/-} cells were maintained in the same medium with 20% FCS. HL-1 cells were maintained in Claycomb medium (JRH Biosciences) supplemented with 10% FBS (Sigma-Aldrich F2442), 100 µg /ml penicillin/streptomycin (Life Technologies 15140-122), 0.1 mM norepinephrine (Sigma A-0937) and 2 mM L-glutamine (Life Technologies 25030-081). 10 mM norepinephrine stock was made in 30 mM L-ascorbic acid (Sigma A-7631). For HL-1 cells Petridish and coverslips were coated with fibronectin (Sigma-Aldrich F3667) and incubated for 2 h at 37°C prior to splitting the cells. In general, no penicillin and streptomycin was added to the medium to control sterile, contamination-free handling of the cells, except in case of cells obtained from external labs that were kept in quarantine. Isolated rat cardiomyocytes for co-staining desmin and αB-crystallin were kindly provided by Dr. Sven Pleger (Dept. of Cardiology, University Hospital Heidelberg)

9.2 Transfection and staining

For transfection studies, full-length clones of WT or mutant desmin were inserted into the unique EcoRI site of the eukaryotic expression vector p163/7. We additionally employed a full-length cDNA of human lamin B1 (LMNB1) cloned into the eukaryotic expression vector pEYFP-C1 (ClonTech, La Jolla, CA, USA). This LMNB1 construct was kindly provided by Dr. Stephanie Geiger from our lab. For DNA purification, these clones were expressed in E. coli strain DH5α. Cells were plated on glass coverslips placed in six-well plates for 1-2 days, grown to ~30% confluence and then transiently transfected with Eugene 6® according to the manufacturer's protocol (Roche Diagnostics, Germany). 48 h after transfection, cells

were processed for immuno-cytochemistry. Briefly, cells were fixed in methanol for 5 min followed by permeabilisation in acetone for 1 min at -20°C. Specimens were blocked in 10% donkey serum in phosphate-buffered saline (PBS) for 30 min. The coverslips were incubated with appropriate antibodies (**TABLE X**) for 60 min at RT. After thoroughly rinsing in PBS, either a Cy3,Cy5 (dilution 1:300, Dianova, Germany) or Alexa Fluor® 488, Alexa Fluor® 568 secondary antibodies (dilution 1:100, Invitrogen, Germany) were applied simultaneously for 30 min together with the nuclear stain DAPI (4,6-diamidino-2-phenylindole, dilution 1:1000, Roche Diagnostics, Germany). The coverslips were finally mounted on glass slides in Fluoromount G® (Southern Biotechnology Associates, USA).

HL-1 cells were co-transfected with mutant desmin and EYFP-LMN1 to distinguish the transfected cells from endogenously desmin-expressing cells upon staining for desmin. These cells were fixed in paraformaldehyde to achieve better fluorescence of EYFP-tagged LMN1. Briefly, cells grown on glass coverslips were rinsed with PBS / 1 mM MgCl₂ in the Petridish. The cells were fixed for 7 min with precooled 4% formaldehyde on ice in fumehood and washed thrice with PBS 5 min each. Then the cells were permeabilized in ice-cold PBS / 0.1% NP-40 for 5 min and washed in 3x PBS 5 min each.

9.3 Microscopy and image processing

Cells were viewed by confocal laser scanning (DM IRE2, Leica Microsystems, Germany) or inverted fluorescence microscopy (Olympus IX71, DeltaVision® Core, Applied Precision Inc., Issaquah, USA). Cells were imaged on a DeltaVision microscope system (Applied Precision). This system consists of an inverted microscope IX70 (Olympus) with a 1.35 NA 100 objective and FITC, Rhodamine, and Cy5 filter sets, a Photometrics CH350 12-bit camera (Photometrics) with a KAF1400 chip, and a UNIX-based Silicon Graphics O2 workstation with SoftWoRx software installed yielding cubic voxels. Images were deconvolved with the SoftWoRx software package (Applied Precision) using Decon3d. Images were processed further using softwares Adobe Photoshop and ImageJ 1.32j.

9.4 Proteasome-inhibition in myoblasts

To evaluate potential degradation of mutant desmin protein which might be particularly prone to proteasomal degradation due to protein misfolding by the ubiquitin-proteasome system, we established primary muscle cell cultures from the heterozygous mother M (cell cultures from the deceased patients P1 and P2 being unavailable) and from a control healthy muscle. Myoblasts were grown in Ham's Nutrient-Mix-F-10 supplemented with 20% fetal calf serum (Life Technologies). Myotube formation was induced by switching to differentiation medium (DMEM with 10 µg / ml insulin and 2% horse serum). Cells were maintained in differentiation medium for two weeks before the treatment with proteasome inhibitors lactacystin or epoxomicin was initiated. Lactacystin and epoxomicin inhibit three ATP-dependent activities of the 20S or 26S subunit of the proteasome, namely: chymotrypsin-like, trypsin-like and peptidylglutamyl peptide hydrolyzing activities. These proteasome inhibitors are also known to induce accumulation of p53 in cells upon treatment. Triplicate cultures of primary myotubes from heterozygous mother and a healthy control were grown independently and treated with lactacystin (60 µM, Biomol International LP, USA) for up to 7 h or epoxomicin (10 µM, Biomol International Inc., USA) for up to 22 h at 37 °C, 5% CO₂. As controls, both heterozygous mother and healthy cells were also treated with same volume of solvent (water or DMSO) in which the proteasome-inhibitors had been dissolved respectively. In the end, cells were trypsinized, thoroughly suspended in equal volume of fetal calf serum and counted in Neubauer-counting chamber. The cells were centrifuged and the pellets were

further suspended in 1x Laemmli protein sample buffer to obtain equal cell density per sample. Lysates were pushed several times through a no. 26G needle to shear DNA. Equal volumes of treated and control total cells extracts (1 μ L corresponding to 10^4 cells) were loaded on 10% Laemmli gels for Western blotting. To check if the proteasome machinery was duly blocked, the same blots were also probed with the monoclonal anti-p53 antibody (undiluted, Progen). Densitometric evaluations of the blots were performed using ImageJ 1.32j (<http://rsb.info.nih.gov/ij>).

The primary antibodies used for immunoblotting and their respective dilutions are listed in **Table 5**. HRP-conjugated goat anti-mouse or anti-rabbit antibody (1/5000, Jackson ImmunoResearch Laboratories Inc.) was used as secondary antibody. As per requirements, some primary and all secondary antibody staining procedures were carried out in 10 mM Tris-HCl pH 8.0, 150 mM NaCl and 0.05% Tween-20 (TBST) with 5% milk powder at room temperature

TABLE 5 Overview of primary antibodies for immunofluorescence or Western blotting

Antibody	Epitope	Dilution in immunofluorescence	Dilution in WB	Source
anti-desmin ms monoAb DK8, DK26	CIAFLKESA in N-terminus of human desmin	Undiluted	Undiluted	generated in collaboration with H. Zentgraf, DKFZ
anti-desmin ms monoAb D33	C-terminus of human desmin	1:50	1:500	Calbiochem, # IF11
anti-desmin rb monoAb Y66	C-terminus of human desmin	1:100	1:5000	Epitomics, #1466-1
anti-desmin rb polyAb	C-terminus of human desmin	1:20	1:100	SIGMA, #D8281
anti-desmin rb polyAb	C-terminus of human desmin	1:100	1:5000	PROGEN, #10570
anti-desmin ms monoAb D9	C-terminus of human desmin	1:100	1:2000	PROGEN, #10519
anti-vimentin ms monoAb VIM 3B4		Undiluted	1:50	CYMBUS, #CBL 202
anti- α B-crystallin ms monoAb		1:5000	1:50000	Stressgen, #SPA-222
anti- α B-crystallin rb polyAb	aa 1-175 of human α B-crystallin	1:200	1:2000	Santa Cruz #sc-22744

Bibliography

- Aebi U., Cohn J., Buhle L. & Gerace L. (1986) The nuclear lamina is a meshwork of intermediate-type filaments. *Nature*, **323 (6088)**: 560-564.
- Arbustini E., Pasotti M., Pilotto A., Pellegrini C., Grasso M., Previtali S., Repetto A., Bellini O., Azan G., Scaffino M., Campana C., Piccolo G., Viganò M. & Tavazzi L. (2006) Desmin accumulation restrictive cardiomyopathy and atrioventricular block associated with desmin gene defects. *Eur J Heart Fail*, **8 (5)**: 477-483.
- Arrigo AP., Simon S., Gibert B., Kretz-Remy C., Nivon M., Czekalla A., Guillet D., Moulin M., Diaz-Latoud C. & Vicart P. (2007) Hsp27 (HspB1) and alphaB-crystallin (HspB5) as therapeutic targets. *FEBS Lett*, **581 (19)**: 3665-3674.
- Amrani N, Dong S., He F, Ganesan R., Ghosh S., Kervestin S., Li C, Mangus DA., Spatrack P. & Jacobson A. (2006) Aberrant termination triggers nonsense-mediated mRNA decay. *Biochem Soc Trans*. **34**: 39-42.
- Bär H., Strelkov SV., Sjöberg G., Aebi U. & Herrmann H. (2004) The biology of desmin filaments: how do mutations affect their structure, assembly, and organisation? *J Struct Biol*, **148 (2)**: 137-152.
- Bär H., Mücke N., Kostareva A., Sjöberg G., Aebi U. & Herrmann H. (2005) Severe muscle disease-causing desmin mutations interfere with *in vitro* filament assembly at distinct stages. *Proc Natl Acad Sci U S A*, **102 (42)**: 15099-15104.
- Bär H., Kostareva A., Sjöberg G., Sejersen T., Katus HA. & Herrmann H. (2006) Forced expression of desmin and desmin mutants in cultured cells: impact of myopathic missense mutations in the central coiled-coil domain on network formation. *Exp Cell Res*, **312 (9)**: 1554-1565.
- Bär H., Mücke N., Ringler P., Müller SA., Kreplak L., Katus HA., Aebi U. & Herrmann H. (2006) Impact of disease mutations on the desmin filament assembly process. *J Mol Biol*, **360 (5)**: 1031-1042.
- Bär H., Mücke N., Katus HA., Aebi U. & Herrmann H. (2007) Assembly defects of desmin disease mutants carrying deletions in the alpha-helical rod domain are rescued by wild type protein. *J Struct Biol*, **158 (1)**: 107-115.
- Bär H., Goudeau B., Wälde S., Casteras-Simon M., Mücke N., Shatunov A., Goldberg YP., Clarke C., Holton JL., Eymard B., Katus HA., Fardeau M., Goldfarb L., Vicart P. & Herrmann H. (2007) Conspicuous involvement of desmin tail mutations in diverse cardiac and skeletal myopathies. *Hum Mutat*, **28 (4)**: 374-386.
- Bär H., Sharma S., Kleiner H., Mücke N., Zentgraf H., Katus HA., Aebi U. & Herrmann H. (2009) Interference of amino-terminal desmin fragments with desmin filament formation. *Cell Motil Cytoskeleton*, **66 (11)**: 986-999.
- Bär H, Schopferer M, Sharma S, Hochstein B, Mücke N, Herrmann H & Willenbacher N. Mutations in desmin's carboxy-terminal "tail" domain severely modify filament and network mechanics. *J Mol Biol*. 2010 Apr 16;397(5):1188-98.
- Basha E., Lee GJ., Demeler B. & Vierling E. (2004) Chaperone activity of cytosolic small heat shock proteins from wheat. *Eur J Biochem*, **271 (8)**: 1426-1436.
- Bennardini F., Wrzosek A. & Chiesi M. (1992) Alpha B-crystallin in cardiac tissue. Association with actin and desmin filaments. *Circ Res*, **71 (2)**: 288-294.
- Bova MP., Yaron O., Huang Q., Ding L., Haley DA., Stewart PL. & Horwitz J. (1999) Mutation R120G in alphaB-crystallin, which is linked to a desmin-related myopathy, results in an irregular structure and defective chaperone-like function. *Proc Natl Acad Sci U S A*, **96 (11)**: 6137-6142.

- Boyle DL., Takemoto L., Brady JP. & Wawrousek EF. (2003) Morphological characterization of the Alpha A- and Alpha B-crystallin double knockout mouse lens. *BMC Ophthalmol*, **3**: 3.
- Brady JP., Garland D., Duglas-Tabor Y., Robison WG Jr., Groome A. & Wawrousek EF. (1997) Targeted disruption of the mouse alpha A-crystallin gene induces cataract and cytoplasmic inclusion bodies containing the small heat shock protein alpha B-crystallin. *Proc Natl Acad Sci U S A*, **94** (3): 884-889.
- Capetanaki Y. & Milner DJ. (1998) Desmin cytoskeleton in muscle integrity and function. *Subcell Biochem*, **31**: 463-495.
- Ciechanover A., Orian A. & Schwartz AL. (2000) Ubiquitin-mediated proteolysis: biological regulation via destruction. *Bioessays*, **22** (5): 442-451.
- Ciocca DR. & Calderwood SK. (2005) Heat shock proteins in cancer: diagnostic, prognostic, predictive, and treatment implications. *Cell Stress Chaperones*, **10** (2): 86-103.
- Claeys KG., van der Ven PF., Behin A., Stojkovic T., Eymard B., Dubourg O., Laforêt P., Faulkner G., Richard P., Vicart P., Romero NB., Stoltenburg G., Udd B., Fardeau M., Voit T. & Fürst DO. (2009) Differential involvement of sarcomeric proteins in myofibrillar myopathies: a morphological and immunohistochemical study. *Acta Neuropathol*, **117** (3): 293-307.
- Claycomb WC., Lanson NA Jr., Stallworth BS., Egeland DB., Delcarpio JB., Bahinski A. & Izzo NJ Jr. (1998) HL-1 cells: a cardiac muscle cell line that contracts and retains phenotypic characteristics of the adult cardiomyocyte. *Proc Natl Acad Sci U S A*, **95** (6): 2979-2984.
- Clemen CS, Fischer D, Reimann J, Eichinger L, Müller CR, Müller HD, Goebel HH & Schröder R. (2009) How much mutant protein is needed to cause a protein aggregate myopathy in vivo? Lessons from an exceptional desminopathy. *Hum Mutat*, **30**(3): E490-499.
- Colucci-Guyon E, Portier MM, Dunia I, Paulin D, Pournin S, Babinet C. (1994) Mice lacking vimentin develop and reproduce without an obvious phenotype. *Cell*, **79** (4): 679-694.
- Conover GM, Henderson SN & Gregorio CC. (2009) A myopathy-linked desmin mutation perturbs striated muscle actin filament architecture. *Mol Biol Cell*, **20** (3): 834-45.
- Datta SA. & Rao CM. (2000) Packing-induced conformational and functional changes in the subunits of alpha - crystallin. *J Biol Chem*, **275** (52): 41004-41010.
- Djabali K., de Néchaud B., Landon F. & Portier MM. (1997) AlphaB-crystallin interacts with intermediate filaments in response to stress. *J Cell Sci*, **110**: 2759-2769.
- Döring V. & Stick R. (1990) Gene structure of nuclear lamin LIII of *Xenopus laevis*; a model for the evolution of IF proteins from a lamin-like ancestor. *EMBO J*, **9** (12): 4073-4081.
- Ehrnsperger M., Gräber S., Gaestel M. & Buchner J. (1997) Binding of non-native protein to Hsp25 during heat shock creates a reservoir of folding intermediates for reactivation. *EMBO J*, **16** (2): 221-9.
- Eriksson JE., Dechat T., Grin B., Helfand B., Mendez M., Pallari HM. & Goldman RD. (2009) Introducing intermediate filaments: from discovery to disease. *J Clin Invest*, **119** (7): 1763-1771.
- Franke WW., Schmid E., Osborn M. & Weber K. (1978) Different intermediate-sized filaments distinguished by immunofluorescence microscopy. *Proc Natl Acad Sci USA*, **75** (10): 5034-5038.
- Fu L. & Liang JJ. (2003) Alteration of protein-protein interactions of congenital cataract crystallin mutants. *Invest Ophthalmol Vis Sci*, **44** (3): 1155-9.
- Fuchs E. & Weber K. (1994) Intermediate filaments: structure, dynamics, function, and disease. *Annu Rev Biochem*, **63**: 345-382.
- Fuchs E. & Yang Y. (1999) Crossroads on Cytoskeletal Highways. *Cell*, **98**: 547-550.
- Geisler N., Kaufmann E. & Weber K. (1982) Proteinchemical characterization of three structurally distinct domains along the protofilament unit of desmin 10 nm filaments. *Cell*, **30** (1): 277-286.

- Ghosh JG, Clark JI. (2005) Insights into the domains required for dimerization and assembly of human alphaB crystallin. *Protein Sci*, **14** (3): 684-695.
- Ghosh JG., Shenoy AK Jr. & Clark JI. (2006) N- and C-Terminal motifs in human alphaB crystallin play an important role in the recognition, selection, and solubilization of substrates. *Biochemistry*, **45** (46): 13847-13854.
- Ghosh JG., Houck SA. & Clark JI. (2007) Interactive sequences in the stress protein and molecular chaperone human alphaB crystallin recognize and modulate the assembly of filaments. *Int J Biochem Cell Biol*, **39** (10): 1804-1815.
- Ghosh JG., Houck SA. & Clark JI. (2007) Interactive domains in the molecular chaperone human alphaB crystallin modulate microtubule assembly and disassembly. *PLoS One*, **2** (6): e498.
- Ghosh JG, Houck SA, Clark JI. (2008) Interactive sequences in the molecular chaperone, human alphaB crystallin modulate the fibrillation of amyloidogenic proteins. *Int J Biochem Cell Biol*, **40** (5): 954-967.
- Goebel HH. (1995) Desmin-related neuromuscular disorders. *Muscle Nerve*, **18** (11): 1306-1320.
- Goldfarb LG., Park KY., Cervenáková L., Gorokhova S., Lee HS., Vasconcelos O., Nagle JW., Semino-Mora C., Sivakumar K. & Dalakas MC. (1998) Missense mutations in desmin associated with familial cardiac and skeletal myopathy. *Nat Genet*, **19** (4): 402-403.
- Goldfarb LG., Vicart P., Goebel HH. & Dalakas MC. (2004) Desmin myopathy. *Brain*, **127** (4): 723-734.
- Goldfarb LG. & Dalakas MC. (2009) Tragedy in a heartbeat: malfunctioning desmin causes skeletal and cardiac muscle disease. *J Clin Invest*. **119** (7): 1806-1813.
- Granger BL. & Lazarides E. (1980) Synemin: a new high molecular weight protein associated with desmin and vimentin filaments in muscle. *Cell*, **22** (3): 727-738.
- Green KJ., Böhringer M., Gocken T. & Jones JC. (2005) Intermediate filament associated proteins. *Adv Protein Chem*, **70**: 143-202.
- Haley DA., Horwitz J. & Stewart PL. (1998) The small heat-shock protein, alphaB-crystallin, has a variable quaternary structure. *J Mol Biol*, **277**(1): 27-35.
- Haley DA., Bova MP., Huang QL., Mchaourab HS. & Stewart PL. (2000) Small heat-shock protein structures reveal a continuum from symmetric to variable assemblies. *J Mol Biol*, **298** (2): 261-272.
- Haslbeck M., Franzmann T., Weinfurtner D. & Buchner J. (2005) Some like it hot: the structure and function of small heat-shock proteins. *Nat Struct Mol Biol*, **12** (10): 842-6.
- Hatzfeld M. & Franke WW. (1985) Pair formation and promiscuity of cytokeratins: formation in vitro of heterotypic complexes and intermediate-sized filaments by homologous and heterologous recombinations of purified polypeptides. *J Cell Biol*, **101**: 1826-1841.
- Herrmann H., Hofmann I. & Franke WW. (1992) Identification of a nonapeptide motif in the vimentin head domain involved in intermediate filament assembly. *J Mol Biol*, **223** (3): 637-650.
- Herrmann H., Häner M., Brettel M., Müller SA., Goldie KN., Fedtke B., Lustig A., Franke WW. & Aebi U. (1996) Structure and assembly properties of the intermediate filament protein vimentin: the role of its head, rod and tail domains. *J Mol Biol*, **264** (5): 933-953.
- Herrmann H., Häner M., Brettel M., Ku NO. & Aebi U. (1999) Characterization of distinct early assembly units of different intermediate filament proteins. *J Mol Biol*, **286** (5): 1403-1420.
- Herrmann H. & Aebi U. (2000) Intermediate filaments and their associates: multi-talented structural elements specifying cytoarchitecture and cytodynamics. *Curr Opin Cell Biol*, **12** (1): 79-90.
- Herrmann H., Strelkov SV., Feja B., Rogers KR., Brettel M., Lustig A., Häner M., Parry DA., Steinert PM., Burkhard P. & Aebi U. (2000) The intermediate filament protein consensus motif of helix 2B: its atomic structure and contribution to assembly. *J Mol Biol*, **298** (5): 817-832.
- Herrmann H. & Aebi U. (2004) INTERMEDIATE FILAMENTS: Molecular Structure, Assembly Mechanism, and Integration Into Functionally Distinct Intracellular Scaffolds. *Annu Rev Biochem*, **73**: 749-789.

- Herrmann H, Kreplak L & Aebi U. (2004) Isolation, characterization, and in vitro assembly of intermediate filaments. *Methods Cell Biol.* **78** : 3-24.
- Herrmann H., Bär H., Kreplak L., Strelkov SV. & Aebi U. (2007) Intermediate filaments: from cell architecture to nanomechanics. *Nat Rev Mol Cell Biol*, **8** (7): 562-573.
- Herrmann H., Strelkov SV., Burkhard P. & Aebi U. (2009) Intermediate filaments: primary determinants of cell architecture and plasticity. *J Clin Invest*, **119** (7): 1772-1783.
- Hijikata T., Murakami T., Imamura M., Fujimaki N. & Ishikawa H. (1999) Plectin is a linker of intermediate filaments to Z-discs in skeletal muscle fibers. *J Cell Sci*, **112**: 867-876.
- Horwitz J. (1992) Alpha-crystallin can function as a molecular chaperone. *Proc Natl Acad Sci U S A*, **89** (21): 10449-10453.
- Horwitz J. (2003) Alpha-crystallin. *Exp Eye Res*, **76** (2): 145-153.
- Inada H., Goto H., Tanabe K., Nishi Y., Kaibuchi K. & Inagaki M. (1998) Rho-associated kinase phosphorylates desmin, the myogenic intermediate filament protein, at unique amino-terminal sites. *Biochem Biophys Res Commun*, **253** (1): 21-25.
- Ishikawa H., Bischoff R. & Holtzer H. (1968) Mitosis and intermediate-sized filaments in developing skeletal muscle. *J Cell Biol*, **38** (3): 538-555.
- Iwaki T., Kume-Iwaki A., Liem RK. & Goldman JE. (1989) Alpha B-crystallin is expressed in non-lenticular tissues and accumulates in Alexander's disease brain. *Cell*, **57** (1): 71-78.
- Ito H., Kamei K., Iwamoto I., Inaguma Y., Nohara D. & Kato K. (2001) Phosphorylation-induced change of the oligomerization state of alpha B-crystallin. *J Biol Chem*, **276** (7): 5346-5352.
- Jaya N., Garcia V. & Vierling E. (2009) Substrate binding site flexibility of the small heat shock protein molecular chaperones. *Proc Natl Acad Sci U S A*, **106** (37): 15604-15609.
- Kappé G., Franck E., Verschuure P., Boelens WC., Leunissen JA. & de Jong WW. (2003) The human genome encodes 10 alpha-crystallin-related small heat shock proteins: HspB1-10. *Cell Stress Chaperones*, **8** (1): 53-61.
- Kato K., Shinohara H., Goto S., Inaguma Y., Morishita R. & Asano T. (1992) Copurification of small heat shock protein with alpha B crystallin from human skeletal muscle. *J Biol Chem*. **267** (11): 7718-7725.
- Kaufmann E., Weber K. & Geisler N. (1985) Intermediate filament forming ability of desmin derivatives lacking either the amino-terminal 67 or the carboxy-terminal 27 residues. *J Mol Biol*, **185** (4): 733-742.
- Kim KK., Kim R. & Kim SH. (1998) Crystal structure of a small heat-shock protein *Nature*, **394** (6693): 595-599.
- Kim S. & Coulombe PA. (2007) Intermediate filament scaffolds fulfill mechanical, organizational, and signaling functions in the cytoplasm. *Genes Dev*, **21**: 1581-1597.
- Kirmse R., Portet S., Mücke N., Aebi U., Herrmann H. & Langowski J. (2007) A quantitative kinetic model for the in vitro assembly of intermediate filaments from tetrameric vimentin. *J Biol Chem*, **282** (25): 18563-18572.
- Klemenz R., Fröhli E., Steiger RH., Schäfer R. & Aoyama A. (1991) Alpha B-crystallin is a small heat shock protein. *Proc Natl Acad Sci U S A*. **88** (9): 3652-3656.
- Konieczny P., Fuchs P., Reipert S., Kunz WS., Zeöld A., Fischer I., Paulin D., Schröder R. & Wiche G. (2008) Myofiber integrity depends on desmin network targeting to Z-disks and costameres via distinct plectin isoforms. *J Cell Biol*, **181** (4): 667-681.
- Kreplak L., Richter K., Aebi U. & Herrmann H. (2008) Electron microscopy of intermediate filaments: teaming up with atomic force and confocal laser scanning microscopy. *Methods Cell Biol*, **88**: 273-297.
- Kreplak L. & Bär H. (2009). Severe myopathy mutations modify the nanomechanics of desmin intermediate filaments. *J Mol Biol*, **385** (4): 1043-1051.
- Lazarides E. (1980) Intermediate filaments as mechanical integrators of cellular space. *Nature*, **283** (5744): 249-256.

- Levin J, Bulst S, Thirion C, Schmidt F, Bötzel K, Krause S, Pertl C, Kretzschmar H, Walter MC, Giese A & Lochmüller H. (2010) Divergent molecular effects of desmin mutations on protein assembly in myofibrillar myopathy. *J Neuropathol Exp Neurol*, **69** (4): 415-424.
- Li Z., Colucci-Guyon E., Pinçon-Raymond M., Mericskay M., Pournin S., Paulin D. & Babinet C. (1996) Cardiovascular lesions and skeletal myopathy in mice lacking desmin. *Dev Biol*, **175** (2): 362-366.
- Li Z., Mericskay M., Agbulut O., Butler-Browne G., Carlsson L., Thornell LE., Babinet C. & Paulin D. (1997) Desmin is essential for the tensile strength and integrity of myofibrils but not for myogenic commitment, differentiation, and fusion of skeletal muscle. *J Cell Biol*, **139** (1): 129-144.
- Magin TM., Hatzfeld M. & Franke WW. (1987) Analysis of cytokeratin domains by cloning and expression of intact and deleted polypeptides in *Escherichia coli*. *EMBO J*, **6** (9): 2607-2615.
- Maloyan A., Sanbe A., Osinska H., Westfall M., Robinson D., Imahashi K., Murphy E. & Robbins J. (2005) Mitochondrial dysfunction and apoptosis underlie the pathogenic process in alpha-B-crystallin desmin-related cardiomyopathy. *Circulation*, **112** (22): 3451-3461.
- Mchaourab HS., Godar JA. & Stewart PL. (2009) Structure and mechanism of protein stability sensors: chaperone activity of small heat shock proteins. *Biochemistry*, **48** (18): 3828-3837.
- Mchaourab HS., Dodson EK. & Koteiche HA. (2002) Mechanism of chaperone function in small heat shock proteins. Two-mode binding of the excited states of T4 lysozyme mutants by alphaA-crystallin. *J Biol Chem*, **277** (43): 40557-40566
- Milner DJ., Weitzer G., Tran D., Bradley A. & Capetanaki Y. (1996) Disruption of muscle architecture and myocardial degeneration in mice lacking desmin. *J Cell Biol*, **134** (5): 1255-1270.
- Mücke N., Wedig T., Bürer A., Marekov LN., Steinert PM., Langowski J., Aebi U. & Herrmann H. (2004) Molecular and biophysical characterization of assembly-starter units of human vimentin. *J Mol Biol*, **340** (1): 97-114.
- Omary MB. (2009) "IF-pathies": a broad spectrum of intermediate filament-associated diseases. *J Clin Invest*, **119** (7): 1756-1762.
- Parry DA. & Steinert PM. (1999) Intermediate filaments: molecular architecture, assembly, dynamics and polymorphism. *Q Rev Biophys*, **32** (2): 99-187.
- Parry DA. (2005) Microdissection of the sequence and structure of intermediate filament chains. *Adv Protein Chem*, **70**: 113-142.
- Parry DA., Strelkov SV., Burkhard P., Aebi U. & Herrmann H. (2007) Towards a molecular description of intermediate filament structure and assembly. *Exp Cell Res*, **313** (10): 2204-2216.
- Paulin D. & Li Z. (2004) Desmin: a major intermediate filament protein essential for the structural integrity and function of muscle. *Exp Cell Res*, **301** (1): 1-7.
- Perng MD., Muchowski PJ., van Den IJssel P., Wu GJ., Hutcheson AM., Clark JI. & Quinlan RA. (1999) The cardiomyopathy and lens cataract mutation in alphaB-crystallin alters its protein structure, chaperone activity, and interaction with intermediate filaments in vitro. *J Biol Chem*. **274** (47): 33235-33243.
- Perng MD., Wen SF., van den IJssel P., Prescott AR. & Quinlan RA. (2004) Desmin aggregate formation by R120G alphaB-crystallin is caused by altered filament interactions and is dependent upon network status in cells. *Mol Biol Cell*, **15** (5): 2335-2346.
- Perng MD., Su M., Wen SF., Li R., Gibbon T., Prescott AR., Brenner M. & Quinlan RA. (2006) The Alexander disease-causing glial fibrillary acidic protein mutant, R416W, accumulates into Rosenthal fibers by a pathway that involves filament aggregation and the association of alpha B-crystallin and HSP27. *Am J Hum Genet*. **79** (2): 197-213.
- Pollard TD. & Borisy GG. (2003) Cellular motility driven by assembly and disassembly of actin filaments. *Cell*, **112** (4): 453-465.
- Price MG. (1984) Molecular analysis of intermediate filament cytoskeleton--a putative load-bearing structure. *Am J Physiol*, **246** (4): H566-H572.

- Quinlan RA. & Franke WW. (1982) Heteropolymer filaments of vimentin and desmin in vascular smooth muscle tissue and cultured baby hamster kidney cells demonstrated by chemical crosslinking. *Proc Natl Acad Sci U S A*. **79** (11): 3452-3456.
- Rogers S., Wells R. & Rechsteiner M. (1986) Amino acid sequences common to rapidly degraded proteins: the PEST hypothesis. *Science*, **234**(4774) : 364-368.
- Rogers KR., Herrmann H. & Franke WW. (1996) Characterization of disulfide crosslink formation of human vimentin at the dimer, tetramer, and intermediate filament levels. *J Struct Biol*, **117** (1): 55-69.
- Schaffeld M., Herrmann H., Schultess J. & Markl J. (2001) Vimentin and desmin of a cartilaginous fish, the shark *Scyliorhinus stellaris*: sequence, expression patterns and in vitro assembly. *Eur J Cell Biol*, **80** (11): 692-702.
- Schlesinger MJ. (1990) Heat shock proteins. *J Biol Chem*, **265** (21): 12111-12114.
- Schopferer M., Bär H., Hochstein B., Sharma S., Mücke N., Herrmann H. & Willenbacher N. (2009) Desmin and vimentin intermediate filament networks: their viscoelastic properties investigated by mechanical rheometry. *J Mol Biol*, **388** (1): 133-143.
- Schröder R., Goudeau B., Simon MC., Fischer D., Eggermann T., Clemen CS., Li Z., Reimann J., Xue Z., Rudnik-Schöneborn S., Zerres K., van der Ven PF., Fürst DO., Kunz WS. & Vicart P. (2003) On noxious desmin: functional effects of a novel heterozygous desmin insertion mutation on the extrasarcomeric desmin cytoskeleton and mitochondria. *Hum Mol Genet*, **12** (6): 657-669. Erratum in: *Hum Mol Genet*, 2007;**16** (23): 2989-2990.
- Schröder R. & Schoser B. (2009) Myofibrillar myopathies: a clinical and myopathological guide. *Brain Pathol*, **19** (3): 483-492.
- Selcen D., Ohno K. & Engel AG. (2004) Myofibrillar myopathy: clinical, morphological and genetic studies in 63 patients. **127** (2): 439-451.
- Sharma S., Mücke N., Katus HA., Herrmann H. & Bär H. (2009) Disease mutations in the "head" domain of the extra-sarcomeric protein desmin distinctly alter its assembly and network-forming properties. *J Mol Med*, **87** (12): 1207-1219.
- Shashidharamurthy R., Koteiche HA., Dong J. & McHaourab HS. (2005) Mechanism of chaperone function in small heat shock proteins: dissociation of the HSP27 oligomer is required for recognition and binding of destabilized T4 lysozyme. *J Biol Chem*, **280** (7): 5281-5289.
- Simon S., Fontaine JM., Martin JL., Sun X., Hoppe AD., Welsh MJ., Benndorf R. & Vicart P. (2007) Myopathy-associated alphaB-crystallin mutants: abnormal phosphorylation, intracellular location, and interactions with other small heat shock proteins. *J Biol Chem*. **282** (47): 34276-34287.
- Song S, Hanson MJ, Liu BF, Chylack LT & Liang JJ. (2008) Protein-protein interactions between lens vimentin and alphaB-crystallin using FRET acceptor photobleaching. *Mol Vis*. **14**: 1282-1287.
- Stengel F., Baldwin AJ., Painter AJ., Jaya N., Basha E., Kay LE., Vierling E., Robinson CV. & Benesch JL. (2010) Quaternary dynamics and plasticity underlie small heat shock protein chaperone function. *Proc Natl Acad Sci U S A*, **107** (5): 2007-2012.
- Strelkov SV., Herrmann H., Geisler N., Lustig A., Ivaninskii S., Zimbelmann R., Burkhard P. & Aepli U. (2001) Divide-and-conquer crystallographic approach towards an atomic structure of intermediate filaments. *J Mol Biol*, **306** (4): 773-781.
- Sun Y. & MacRae TH. (2005) Characterization of novel sequence motifs within N- and C-terminal extensions of p26, a small heat shock protein from *Artemia franciscana*. *FEBS J*, **272** (20): 5230-5243.
- Szeverenyi I, Cassidy AJ, Chung CW, Lee BT, Common JE, Ogg SC, Chen H, Sim SY, Goh WL, Ng KW, Simpson JA, Chee LL, Eng GH, Li B, Lunny DP, Chuon D, Venkatesh A, Khoo KH, McLean WH, Lim YP & Lane EB.(2008) The Human Intermediate Filament Database: comprehensive information on a gene family involved in many human diseases. *Hum Mutat*. **29** (3): 351-60.
- Taylor MR., Slavov D., Ku L., Di Lenarda A., Sinagra G., Carniel E., Haubold K., Boucek MM., Ferguson D., Graw SL., Zhu X., Cavanaugh J., Sucharov CC., Long CS., Bristow MR., Lavori P., Mestroni L.; Familial Cardiomyopathy Registry;

- & BEST DNA Bank. (2007) Prevalence of Desmin Mutations in Dilated Cardiomyopathy. *Circulation*, **115 (10)**: 1244-1251.
- Traub P. & Vorgias CE. (1983) Involvement of the N-terminal polypeptide of vimentin in the formation of intermediate filaments. *J Cell Sci*, **63**: 43-67.
- van Montfort RL, Basha E., Friedrich KL., Slingsby C. & Vierling E. (2001) Crystal structure and assembly of a eukaryotic small heat shock protein. *Nat Struct Biol*, **8 (12)**: 1025-1030.
- Vicart P., Caron A., Guicheney P., Li Z., Prévost MC., Faure A., Chateau D., Chapon F., Tomé F., Dupret JM., Paulin D. & Fardeau M. (1998) A missense mutation in the alphaB-crystallin chaperone gene causes a desmin-related myopathy. *Nat Genet*, **20 (1)**: 92-95.
- Wadhwa R., Ryu J., Gao R., Choi IK., Morrow G., Kaur K., Kim I., Kaul SC., Yun CO. & Tanguay RM. (2010) Proliferative functions of Drosophila small mitochondrial heat shock protein 22 in human cells. *J Biol Chem*, **285 (6)**: 3833-3839.
- Waterman-Storer CM. & Salmon ED. (1997) Microtubule dynamics: treadmilling comes around again. *Curr Biol*, **7 (6)**: R369-372.
- Waudby CA., Knowles TP., Devlin GL., Skepper JN., Ecroyd H., Carver JA., Welland ME., Christodoulou J., Dobson CM. & Meehan S. (2010) The interaction of alphaB-crystallin with mature alpha-synuclein amyloid fibrils inhibits their elongation. *Biophys J*, **98 (5)**: 843-851.
- Wiche G. (1998) Role of plectin in cytoskeleton organization and dynamics. *J Cell Sci*, **111**: 2477-2486.
- Wickert U., Mücke N., Wedig T., Müller SA., Aebi U. & Herrmann H. (2005) Characterization of the in vitro co-assembly process of the intermediate filament proteins vimentin and desmin: mixed polymers at all stages of assembly. *Eur J Cell Biol*, **84 (2-3)**: 379-391.

Appendix A

A.1 Primer sequence

A.1.1 Desmin head mutants

Primer	Sequence
Forward A2S	5' G GAG AAA TTA ACC ATG TCC CAG GCC TAC TCG TCC 3'
Reverse A2S	5' GGA CGA GTA GGC CTG GGA CAT GGT TAA TTT CTC C 3'
Forward A2I	5' G GAG AAA TTA ACC ATG ATC CAG GCC TAC TCG TCC 3'
Reverse A2I	5' GGA CGA GTA GGC CTG GAT CAT GGT TAA TTT CTC C 3'
Forward S13F	5' CAG CGC GTG TCC TTC TAC CGC CGC ACC TTC 3'
Reverse S13F	5' GAA GGT GCG GCG GTA GAA GGA CAC GCG CTG 3'
Forward R16C	5' C GTG TCC TCC TAC CGC TGC ACC TTC GGC GGG GC 3'
Reverse R16C	5' GGC CCC GCC GAA GGT GCA GCG GTA GGA GGA CAC G 3'
Forward S46F	5' GGC TCT AAG GGC TCC TAC AGC TCG GTG ACG TCC 3'
Reverse S46F	5' GGA CGT CAC CGA GCT GTA GGA GCC CTT AGA GCC 3'
Forward S46Y	5' GGC TCT AAG GGC TCC TTC AGC TCG GTG ACG TCC 3'
Reverse S46Y	5' GGA CGT CAC CGA GCT GAA GGA GCC CTT AGA GCC 3'

A.1.2 Desmin tail deletion constructs

Forward DRG	5' ACC ATC GAG ACA GAT CGG GGG GAG GTC GTC 3'
Reverse DRG	5' GAC GAC CTC CCC CCG ATC TGT CTC GAT GGT 3'
Forward Δ RDG	5' AAG ACC ATC GAG ACA GAG GTC GTC AGT GAG GCC 3'
Reverse Δ RDG	5' GGC CTC ACT GAC GAC CTC TGT CTC GAT GGT CTT 3'
Forward Δ C451	5' GAT CAA GAC CAT CTA AAC ACG GGA TGG GGA 3'
Reverse Δ C451	5' CTC CCC ATC CCG TGT TTA GAT GGT CTT GAT 3'
Forward Δ C441	5' GT TCT GAG GTC CAT TGA AAG AAG ACG GTG 3'
Reverse Δ C441	5' CAC C GT CTT CTT TCA ATG GAC CTC AGA AC 3'
Forward Δ C431	5' C TTC CGA GAA ACC TGA CCT GAG CAA AGG 3'
Reverse Δ C431	5' CCT TTG CTC AGG TCA GGT TTC TCG GAA G 3'

A.1.3 Desmin mutant L377 Δ 22fs

In pDS5 vector (NcoI/BamHI):

Forward 5'GAG AGA CCA TGG ATG GCC CAG GCC TAC TCG TCC AGC CAG CGC GTG TCC TCC TAC CGC CGC ACC TTC GGC 3'

Reverse 5' GAG AGA GGA TCC TCA CGT TGA GCA GGT CCT GGT ACT CGC GCA GAG GTG CCG GAT TTC CTC CTC CAG GCG-3'

In p163/7 vector (EcoRI/Xho1):

Forward 5'GAG AGA GAA TTC ATG GCC CAG GCC TAC TCG TCC AGC CAG CGC GTG TCC TCC TAC CGC CGC ACC TTC GGC 3'

Reverse 5'GAG AGA CTC GAG TCA CGT TGA GCA GGT CCT GGT ACT CGC GCA GAG GTG CCG GAT TTC CTC CTC CAG GCG 3'

A.1.4 Yeast two-hybrid screening using tail domain of desmin as bait

In pGBT9 vector (EcoRI/BamHI):

Forward 5'GAG AGA GAA TTC ACC TAC CGG AAG CTG CTG 3'

Reverse 5' GAG AGA GGA TCC TTA GAG CAC TTC ATG CTG 3'

A.1.5 Transfer of Des Δ tail from pDS5 into p163/7 (EcoRI/XhoI)

Forward 5'GAG AGA GAA TTC ATT AAA GAG GAG AAA TT 3'

Reverse 5'GAG AGA CTC GAG TTA GAT CCG GCT CTC CTC 3'

A.1.6 Desmin tail mutants

Primer	Sequence
Forward K449T	5'G AAG ACG GTG ATG ATC ACG ACC ATC GAG ACA CCG 3'
Reverse K449T	5' CCG TGT CTC GAT GGT CGT GAT CAT CAC CGT CTT C3'
Forward V469M	5' CAG CAG CAT GAA ATG CTC TAA AGA CAG AGA CC 3'
Reverse V469M	5' GG TCA CTG TCT TTA GAG CAT TTC ATG CTG CTG 3'
Primer	Sequence
Forward T453I	5' G ATC AAG ACC ATC GAG ATA CGG GAT GGG GAG GTC 3'
Reverse T453I	5' GAC CTC CCC ATC CCG TAT CTC GAT GGT CTT GAT C 3'
Forward V459I	5' CGG GAT GGG GAG GTC ATC AGT GAG GCC ACA CAG C 3'
Reverse V459I	5' G CTG TGT GGC CTC ACT GAT GAC CTC CCC ATC CCG 3'

A.2 Peptide synthesis for peptide competition assay

desC438-C453 [16 AA]

SEVHTKKTVMIKTIET

A.3 Buffers

A.3.1 Inclusion body purification

Lysis buffer:

50 mM Tris-HCl pH8.0, 25 % (w/v) saccharose, EDTA 1 mM

Detergent buffer:

20 mM Tris-HCl pH 7.5, 200 mM NaCl, 2 mM EDTA, 1 % (v/v) NP-40, 1% (w/v) sodium desoxycholate

GII buffer:

10 mM Tris-HCl pH 8.0, 0.5% (w/v) Triton X-100

GII + 1.5 M KCl buffer:

10 mM Tris-HCl pH 8.0, 0.5% (w/v) Triton X-100, 1.5 M KCl

9.5 M urea buffer:

9.5 M urea, 10 mM Tris-HCl pH 7.5, 5 mM EDTA, 4 mM PMSF, 1 mM DTT

A.3.2 Protein purification

Standard column buffer:

8 M urea , 5 mM Tris-HCl pH 7.5, 1 mM EDTA, 0.1 mM EGTA, 1 mM DTT

Sodium formate buffer (for headless and rod desmin constructs):

8 M urea , 30 mM sodium formate pH 4.0, 1 mM EDTA, 0.1 mM EGTA, 1 mM DTT

A.3.3 Tricine buffer

Tricine gel buffer: 3 M Tris-HCl pH 8.45, 1.5 g SDS, *a.d.* 500 ml H₂O

Tricine running buffer: 1000 ml: Tris 12.11 g, Tricin 17.7 g, SDS 1g

A.3.4 Gel staining/destaining/ fixation

Staining solutions:

CBB R-250 0.2%, Isopropanol 40%, Acetic acid 7% or

CBB G-250 0.02%, 5% Al₂(SO₄)₃·6H₂O, 10 % EtOH (96%), 2.4 % orthophosphoric acid (85%)

Destaining solution:

For CBB G-250 dye (colloidal): 10% EtOH, 2% phosphoric acid

For CBB R-250 dye: Isopropanol 20%, acetic acid 7.5%

Fixation buffer

Acetic acid 60%

A.3.5 Buffers for dialysis and protein assembly

For characterization of desmin disease mutants

Tris buffer for dialysis:

5 mM Tris-HCl pH 8.4, 1 mM EDTA, 0.1 mM EGTA and 1 mM DTT

8 M urea buffer for dialysis:

For 200 ml volume: 160 ml 10 M urea, 40 ml of Tris, 1 mM DTT, pH adjusted to that of Tris/phosphate/imidazole buffer

Assembly buffer 2X:

100 mM NaCl, 40 mM Tris-HCl, pH 7.0

Filament buffer:

50 mM NaCl, 20 mM Tris-HCl, pH 7.5

For cosedimentation / chaperone assay

“Modified Tris-buffer”:

1 mM Tris-HCl pH 7.4, 0.2 mM EDTA, 0.02 mM EGTA, 1 mM DTT

2 mM phosphate dialysis buffer:

1l: 70 ml 20 mM Na₂HPO₄, 2mM NaH₂PO₄ to adjust pH to 7.5, 1 mM DTT

Buffer system for assembly with imidazole:

Dialysis in 10 mM Tris-HCl, pH 8.0, 1 mM DTT, 0.2 mM PMSF

Assembly buffer 2X: 200 mM imidazole-HCl, 2 mM DTT, 0.4 mM PMSF (final pH 6.8)

Assembly buffer PO₄-KCl: 100 mM KCl, 2 mM PO₄, pH 7.5

A.4 Abbreviations and chemical formulas

A	
aa	Amino acid
Ab	Antibody
ATP	Adenosine triphosphate
AUC	Analytical ultracentrifuge
C	
CBB	Coomassie brilliant blue
cDNA	Complementary DNA
CM	Carboxy methyl
CRYAB	α B-crystallin
C-terminus	Carboxy-terminus
D	
3-D	3 dimensional
DAPI	4,6 diamidino-2-phenylindole
DEAE	Diethylaminoethyl
Des	Desmin
Des Δ head	Desmin headless
Des Δ tail	Desmin tailless
DesWT	Desmin wild-type
DMEM	Dulbecco's modified Eagle's medium
DMSO	Dimethyl sulfoxide
DNA	Deoxyribonucleic acid
DNase	Deoxyribonuclease
DTT	Dithiothreitol
E	
EDTA	Ethylenediaminetetraacetic acid
EGTA	Ethylene glycol tetraacetic acid
EM	Electron microscopy
E. coli	Escherichia coli
EtOH	Ethanol
EYFP	Enhanced yellow fluorescent protein
F	
FCS	Fetal calf serum
FITC	Fluorescein isothiocyanate
G	
G	Gauge
H	
H ₂ O ₂	Hydrogen peroxide
HEPES	2-(4-(2-Hydroxyethyl)-1-piperazinyl)-ethane sulfonic acid
I	
IF	Intermediate filaments
IgG	ImmunoglobulinG
K	
KCl	Potassium chloride
L	
LMNB1	Lamin B1
M	
MHC	Major histocompatibility complex
MgCl ₂	Magnesium chloride
monoAb	Monoclonal antibody
ms	Mouse
MW	Molecular weight
MWCO	Molecular weight cut off
N	
n	Number
NaCl	Sodium chloride
NA	Nuclear aperture
NMR	Nuclear magnetic resonance

NP-40	Nonidet-P40
N-terminus	Amino-terminus
O	
ON	Overnight
P	
PBS	Phosphate buffered saline
PCR	Polymerase chain reaction
pI	Isoelectric point
PMSF	Phenylmethylsulphonyl fluoride
polyAb	Polyclonal antibody
Q	
qPCR	quantitative polymerase chain reaction
R	
Rb	Rabbit
rpm	Revolutions per minute
RNA	Ribonucleic acid
RT	Room temperature
S	
sHsp	Small heat shock protein
SD	Standard deviation
SDS/SDS-PAGE	Sodium dodecyl sulfate / polyacrylamide gel electrophoresis
s	Sedimentation coefficient
S	Svedberg unit (10^{-13} seconds)
STEM	Scanning transmission electron microscopy
T	
TE	Tris-EDTA
Tris / Tris-HCl	Tris(hydroxymethyl)aminomethane hydrogen chloride
U	
UTR	Untranslated region
UV	Ultra-violet
V	
v/v	Volume per volume
W	
w/v	Weight per volume
WT	Wild-type
Y	
Y2H	Yeast two-hybrid

A.5 Prefixes, units and symbols

A.5.1 Prefixes

c	Centi, 10^{-2}
k	Kilo, 10^3
m	Milli, 10^{-3}
μ	Micro, 10^{-6}
n	Nano, 10^{-9}

A.5.2 Units and symbols

bp	Base pair
Da, kDa	Dalton, kiloDalton
$^{\circ}\text{C}$	Degree Celsius
g, mg, μg	Gram, milligram, microgram
h	Hour
kV	kilo Volt
l, ml, μl	Liter, milliliter, microliter
m, cm	Meter, centimeter
M	Molar
min	Minute
n	Number of measurements
r	Radius
s	Second

A.6 Amino acids

Amino acid	three-letter code	single-letter code
Alanine	Ala	A
Arginine	Arg	R
Aspartic acid	Asp	D
Cysteine	Cys	C
Glutamic acid	Glu	E
Glutamine	Gln	Q
Glycine	Gly	G
Histidine	His	H
Isoleucine	Ile	I
Leucine	Leu	L
Lysine	Lys	K
Methionine	Met	M
Phenylalanine	Phe	F
Proline	Pro	P
Serine	Ser	S
Threonine	Thr	T
Tryptophan	Trp	W
Tyrosine	Tyr	Y
Valine	Val	V

Supplementary
S

Supplementary figure 1

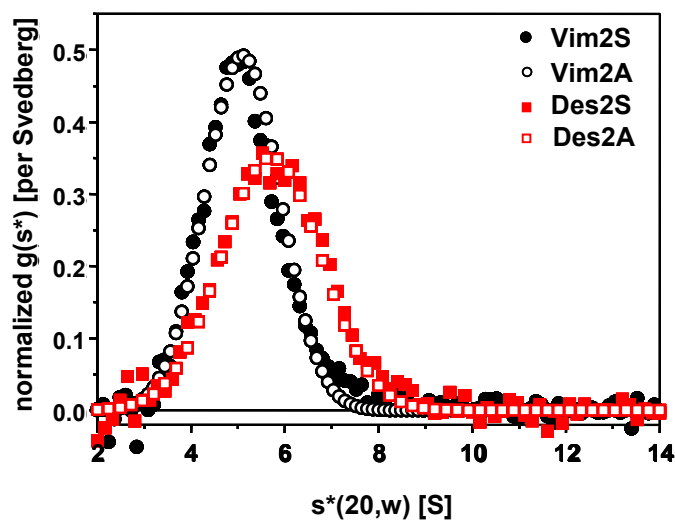


FIGURE S1 Analytical ultracentrifugation analysis of soluble assembly entities of wild-type desmin and vimentin

All runs in AUC were performed after step-wise renaturation of samples from 8 M urea into “Tris-buffer” (5 mM Tris-HCl, 1 mM EDTA, 0.1 mM EGTA, 1 mM DTT, pH 8.4). Similar sedimentation curves were obtained for both 2S and 2A desmin or 2S and 2A vimentin. This indicates that exchange of amino acid *Ser* with *Ala* at position 2 does not alter the biophysical properties of soluble assembly precursors for either desmin or vimentin. $s^*(20,w)$ indicates sedimentation coefficient that has been corrected for the viscosity and density of solvent, relative to that of water at 20°C. To make direct comparisons, area normalization was done for different concentrations. Data analysis was performed using the software DCDT+. Vim: vimentin, Des: desmin

FIGURE S2 Assembly of desmin head mutant proteins in “assembly buffer” leads to aggregates for DesS13F and irregular filaments for DesS2I as well as DesS46F

(Please refer to figure on next page)

Electron micrographs of negatively stained samples of head mutant proteins DesS2I, DesS13F and DesS46F are shown at three assembly time points. Assembly was performed at 37°C by addition of an equal volume of “assembly buffer” (100 mM NaCl, 40 mM Tris-HCl, pH 7.0 at 37°C) and stopped by adding 0.1% glutaraldehyde at 10 s, 5 min and 60 min, respectively. (a, g) At 10 s, uniformly distributed ULFs are seen for DesS2I and DesS46F. (d) In contrast, for mutant protein DesS13F separate clusters of ULF-like structures are seen. (b, e, h) At 5 min, the differences in the structure of DesS2I, DesS46F versus DesS13F are particularly noticeable. DesS13F forms highly cohesive filamentous aggregates. Mutant proteins DesS2I and DesS46F form slightly irregular filaments at this time point. (c, f, i) The phenotypes seen at 5 min remain similar for all three mutant s at 60 min. Scale bar: 100 nm.

FIGURE S3 Assembly of desmin head mutant proteins in “filament buffer” leads to aggregates for DesR16C and irregular filaments for DesS46F, DesS46Y

(Please refer to figure on next page)

Electron micrographs of negatively stained assembled samples of desmin head mutant proteins DesR16C, DesS46F and DesS46Y are shown. Proteins were dialyzed in “Tris-buffer” and assembly was initiated by further dialysis of samples into “filament buffer” containing 50 mM NaCl, 20 mM Tris-HCl, pH 7.5 at 37°C for 1h. Assembly was stopped by adding 0.1% glutaraldehyde. (a) Bundles of filamentous aggregates are seen for DesR16C, whereas (b, c) irregular protein filaments are observed for DesS46F and DesS46Y. Scale bar: 100 nm.

Supplementary figure 2

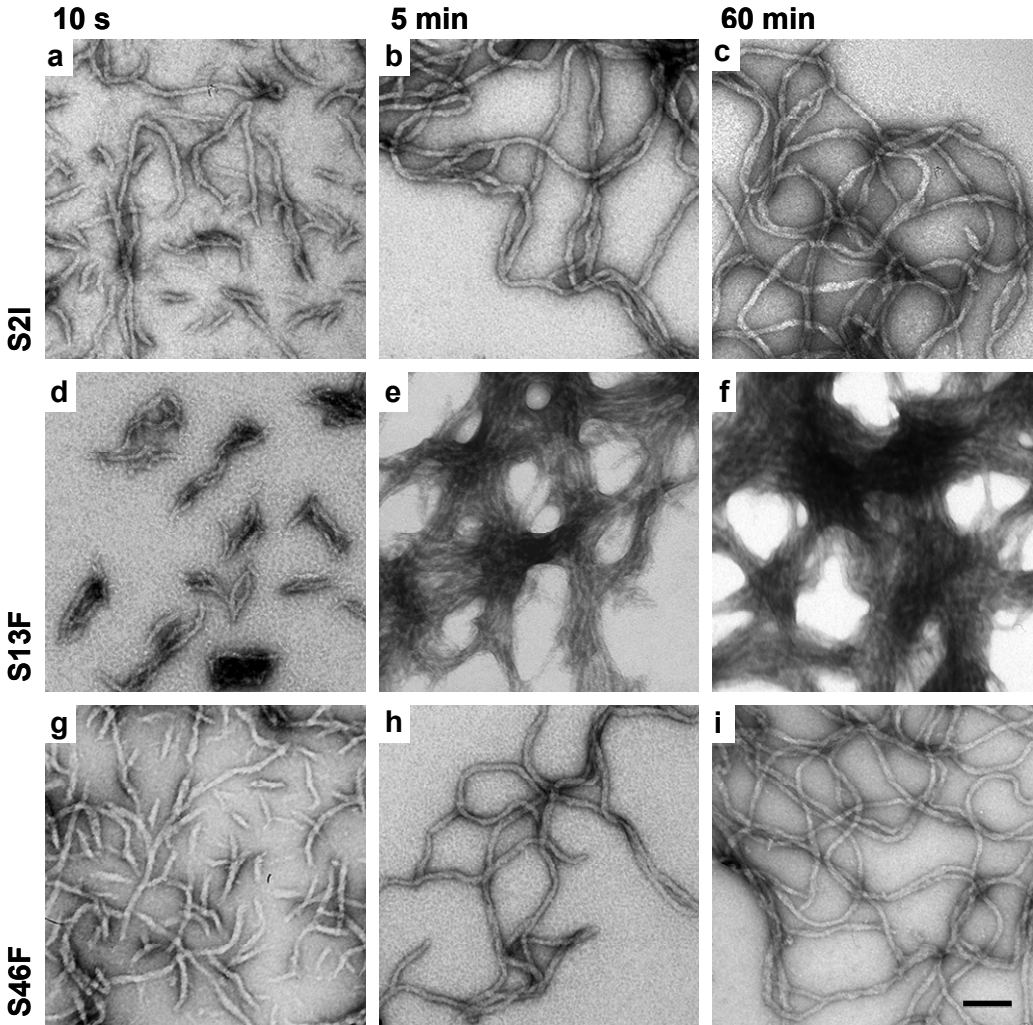


FIGURE S2 Assembly of desmin head mutant proteins in “assembly buffer” leads to aggregates for DesS13F and irregular filaments for DesS2I as well as DesS46F

Supplementary figure 3

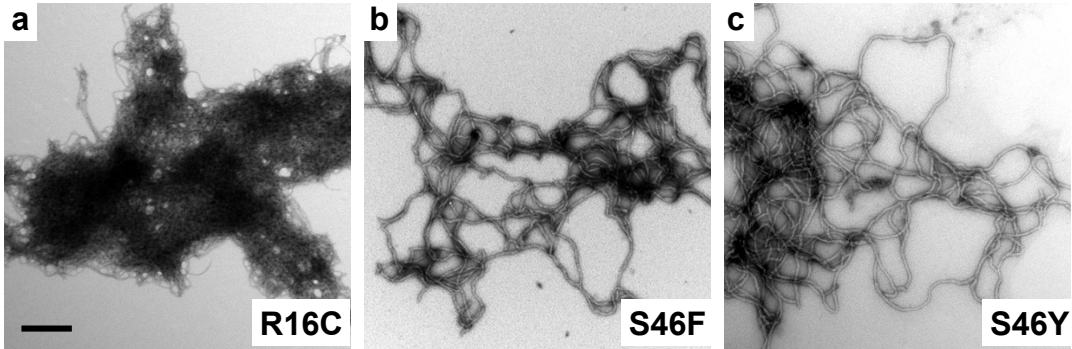


FIGURE S3 Assembly of desmin head mutant proteins in “filament buffer” leads to aggregates for DesR16C and irregular filaments for DesS46F, DesS46Y

Supplementary figure 4

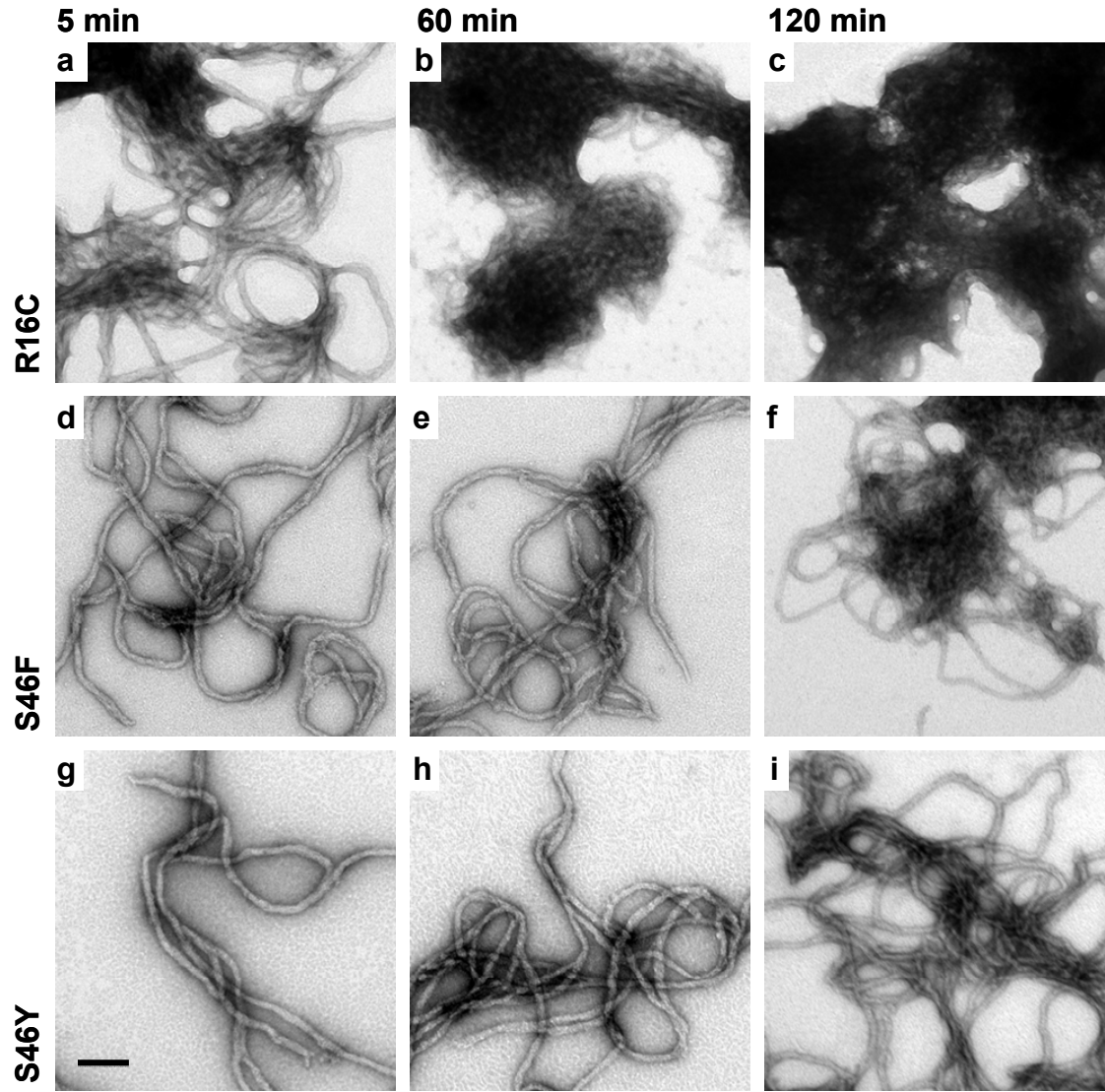


FIGURE S4 Assembly of desmin head mutant proteins from 8 M urea into “filament buffer”

Electron micrographs of negatively stained samples of head mutant proteins DesR16C, DesS46F and DesS46Y are shown for three assembly time points. Samples were dialyzed directly out of 8 M urea into “filament buffer” containing 50 mM NaCl, 20 mM Tris-HCl, pH 7.5 at 37°C for three different time points: 5 min, 60 min and 120 min. (a-c) Bundled, yet individually distinguishable filaments are seen for S13F at 5 min, whereas aggregate formation occurs at assembly time points of 60 and 120 min (d-i) For DesS46F and DesS46Y, regular filaments are observed at 5 min and 60 min whereas entangled filaments are seen at 120 min. Scale bar: 100 nm.

Supplementary figure 5

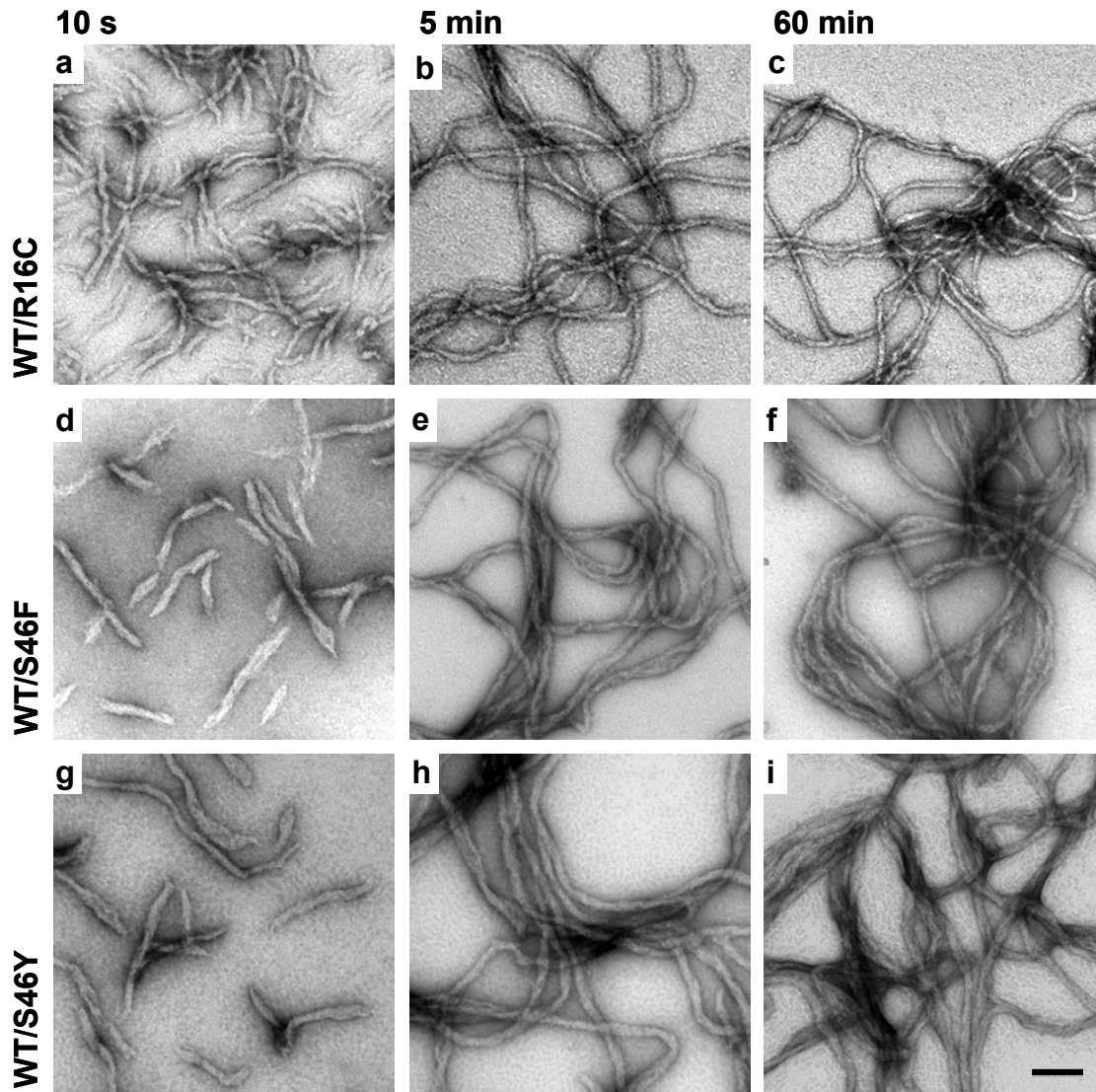


FIGURE S5 Co-assembly of desmin head mutant proteins with wild-type desmin

Electron micrographs of negatively stained samples of equimolar mixture of desmin wild-type (WT) with head mutant proteins DesR16C, DesS46F and DesS46Y are shown for three assembly time points. Assembly was performed at 37°C by addition of equal volume of “assembly buffer” (100 mM NaCl, 40 mM Tris-HCl, pH 7.0 at 37°C) and stopped by adding 0.1% glutaraldehyde at 10 s, 5 min and 60 min, respectively. (a-c) Equimolar mixture of desmin head mutant DesR16C and wild-type protein forms extended filamentous networks, yet these co-polymers appear visibly thinner. (d-i). Mixture of desmin head mutant DesD46F or DesS46Y and wild-type protein also form extended filamentous networks. Scale Bar: 100 nm.

Supplementary figure 6

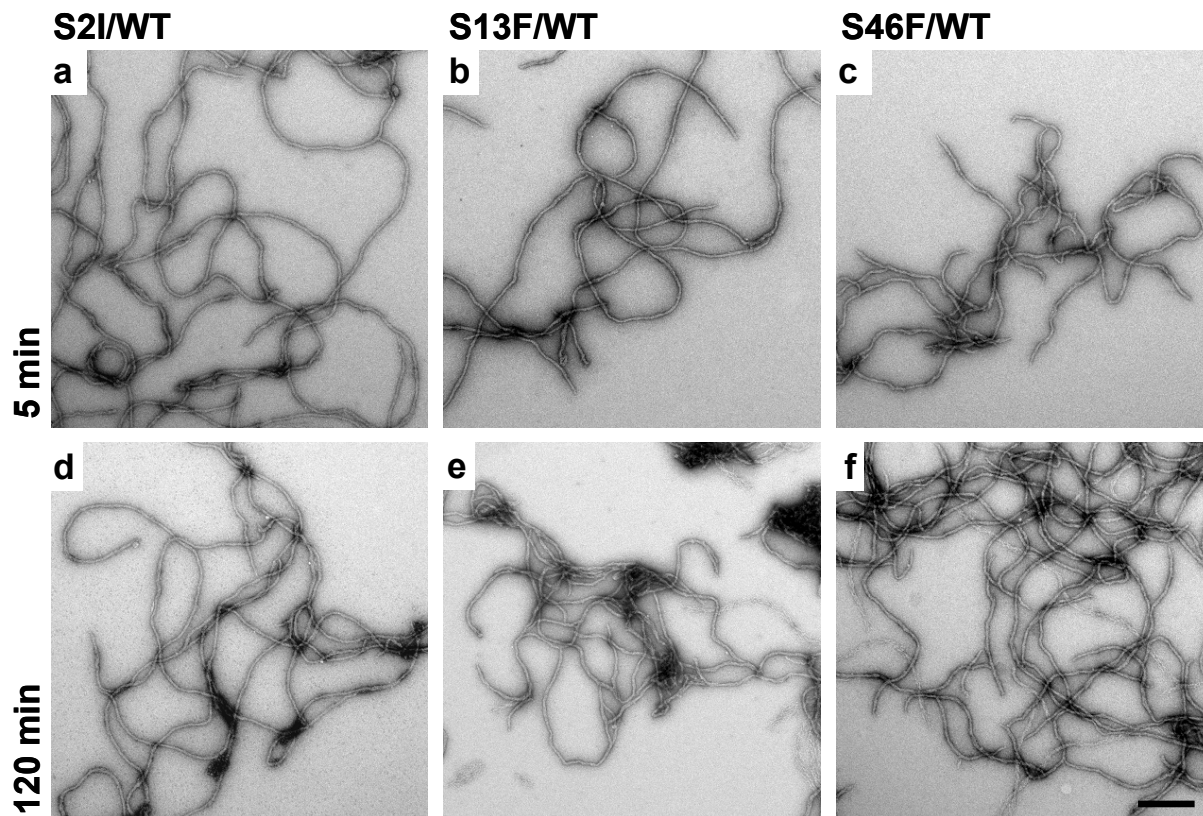


FIGURE S6 Co-assembly of desmin head mutant proteins with wild-type desmin

The mixtures were dialyzed directly out of 8 M urea into “filament-buffer” and assembled for 5 min and 120 min, respectively. No bundling of filaments was observed for any of the mixtures, as exemplified for (a, d) DesS2I, (b,e) DesS13F, and (c,f) Des46F. Scale Bar: 100 nm.

Supplementary figure 7

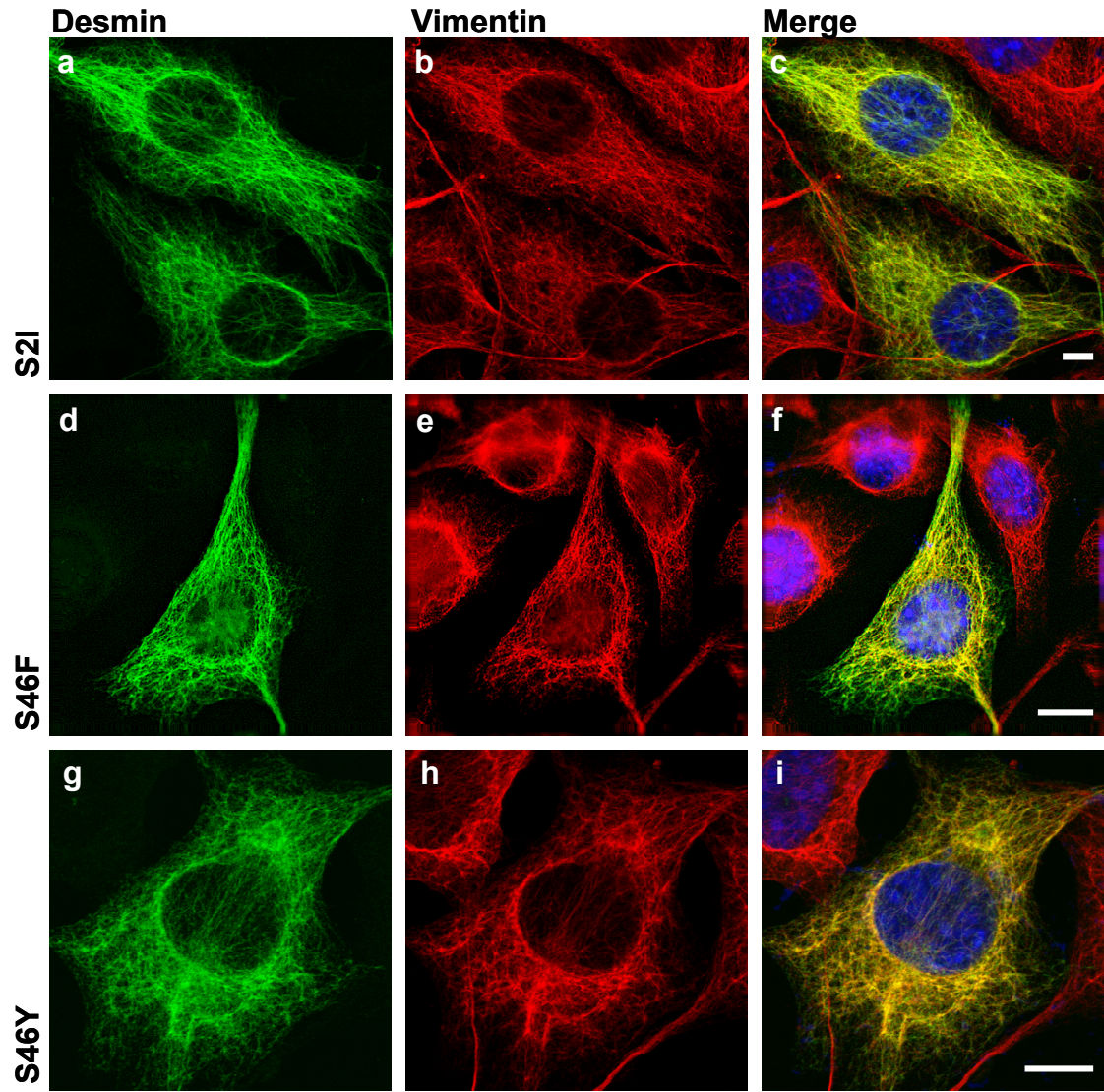


FIGURE S7 Desmin head mutants DesS2I, DesS46F and DesS46Y display normal filaments in 3T3 cells

Murine 3T3 fibroblast cells express endogenous vimentin but no desmin. In cells transfected with (a-c) S2I, (d-f) S46F and (g-i) S46Y extended desmin cytoskeleton is observed. Note that for all desmin head mutants (green), thorough co-localization with endogenous vimentin (red) is observed. Co-localization of desmin and vimentin is depicted in yellow for the merged image. Green: desmin, red: vimentin, blue: nuclear DAPI stain. Scale bar: 10 μ m.

Supplementary figure 8

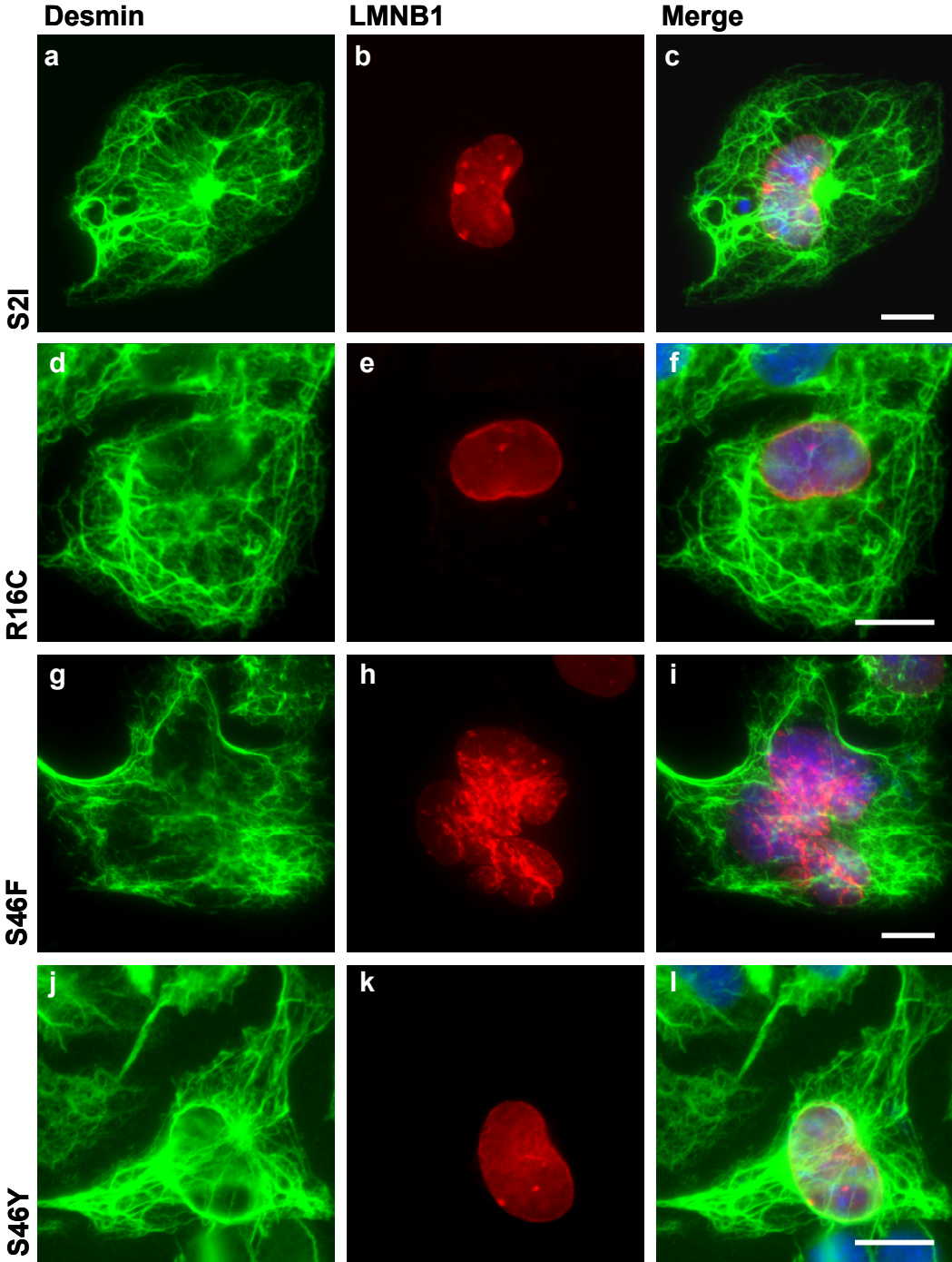


FIGURE S8 Expression of desmin head mutants in HL-1 cells

In HL-1 cells, the co-polymeric situation with endogenous wild-type desmin can be investigated. The transfected cells can be identified by LMNB1-EYFP fluorescence due to co-transfection of both desmin and lamin B1. Here, a seemingly normal filamentous network was observed for all five desmin head mutants in majority of the transfected cells. Green: desmin, red: LMNB1-EYFP, blue: nuclear DAPI stain. Scale bar: 10 μ m

Supplementary figure 9

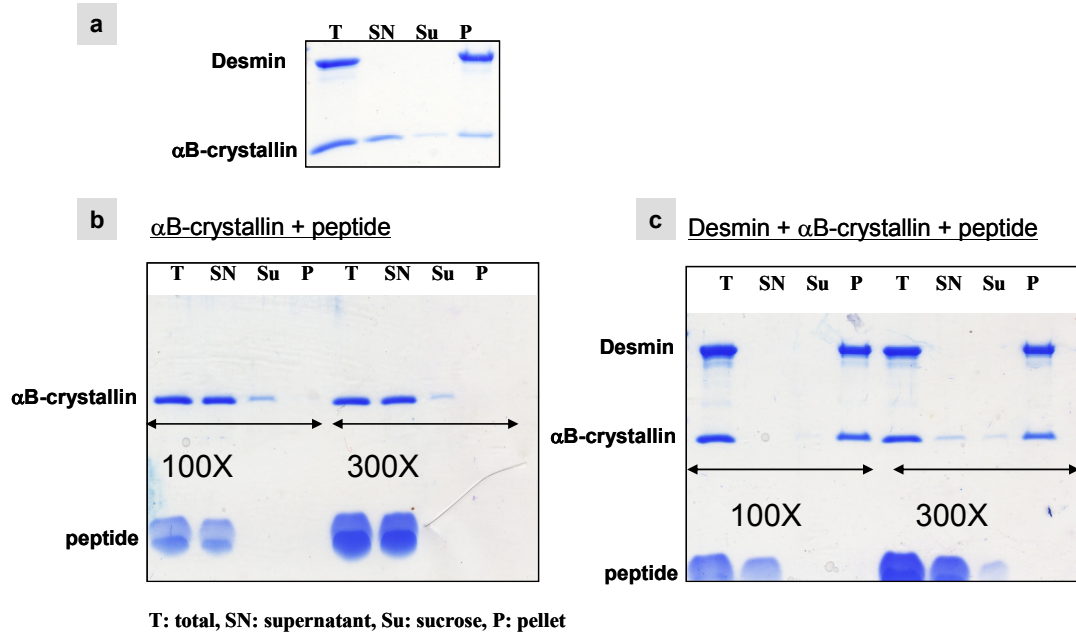
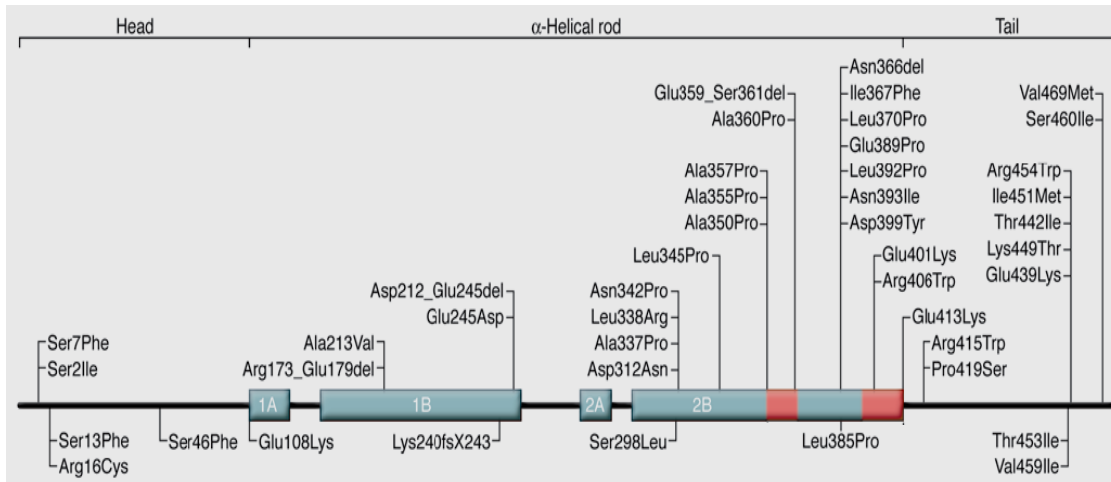


FIGURE S9 Competition binding assay with peptide SEVHTKKTVMIKTIET

(a-c) Coomassie-stained gels of total, supernatant, sucrose and pellet fraction obtained after cosedimentation assay are depicted. EM and cosedimentation assay indicated that binding between desmin and αB-crystallin most likely occurs between the amino acid residues 442-453 of desmin. Hence, we generated a peptide fragment SEVHTKKTVMIKTIET representing aa 438-453 of desmin and performed a competition-based binding assay. For cosedimentation assay, desmin, αB-crystallin and the 16 aa long peptide were co-incubated in “assembly buffer” for 1 h at 37°C after separate dialysis of desmin and αB-crystallin in “modified Tris-buffer” ON. The peptide was not dialyzed, but dissolved directly in “modified Tris-buffer”. (a) For desmin and αB-crystallin co-assembled for 1 h, we observe in cosedimentation assay that around 40-45% of total αB-crystallin is recovered in the pellet with desmin. Thus, for competition binding assay with peptide SEVHTKKTVMIKTIET, we expected that due to selective binding of αB-crystallin to this peptide, which represents the potential binding region of αB-crystallin to desmin, more αB-crystallin will appear in the supernatant (as it is not bound to desmin) and no /less αB-crystallin will be recovered in the pellet fraction upon cosedimentation assay. This is because the peptide, which is present in excess, will compete for binding to αB-crystallin, thus preventing αB-crystallin’s binding to desmin. (b, c) Contrary to our expectation, at a 100-fold or 300-fold excess, all of αB-crystallin was recovered in the pellet. We speculate that, this peptide probably interacts with wild-type desmin and alters its surface properties such that, αB-crystallin can bind to desmin more strongly than in the absence of the peptide.

Supplementary figure 10



[Source: GOLDFARB & DALAKAS 2009]

FIGURE S10 Human desmin mutations

Thus far, the number of known disease-causing DES mutations has reached 45: 40 are missense mutations, 3 are small in-frame deletions of between one and seven amino acids, 1 is an exon-skipping mutation, and 1 is an insertion of a single nucleotide resulting in premature translation termination. Thirteen of the mutations are recurrent, appearing in more than one unrelated family. Five mutations are in the head domain, one is in the 1A helical segment, five are in the 1B segment, 23 reside in the 2B helical segment, and 11 are in the tail domain. No mutations have thus far been identified in the 2A helical segment.

Thesis Declaration

“I, hereby, declare than I am the sole author of this dissertation and that I have not made use of any sources or help apart from those cited.”

Date: 26.08.10

Place: Heidelberg

Signature